AWARD NUMBER: W81XWH-17-1-0092

TITLE: Investigation of a Novel PARP Inhibitor PET Tracer in Ovarian Carcinoma

PRINCIPAL INVESTIGATOR: Fiona Simpkins

CONTRACTING ORGANIZATION: University of Pennsylvania, Philadelphia, PA

REPORT DATE: September 2022

TYPE OF REPORT: Final

PREPARED FOR: U.S. Army Medical Research and Development Command
Fort Detrick, Maryland 21702-5012

DISTRIBUTION STATEMENT: Approved for Public Release;
Distribution Unlimited

The views, opinions and/or findings contained in this report are those of the author(s) and should not be construed as an official Department of the Army position, policy or decision unless so designated by other documentation.

REPORT DOCUMENTATION PAGE

Form Approved
OMB No. 0704-0188

Public reporting burden for this collection of information is estimated to average 1 hour per response, including the time for reviewing instructions, searching existing data sources, gathering and maintaining the data needed, and completing and reviewing this collection of information. Send comments regarding this burden estimate or any other aspect of this collection of information, including suggestions for reducing this burden to Department of Defense, Washington Headquarters Services, Directorate for Information Operations and Reports (0704-0188), 1215 Jefferson Davis Highway, Suite 1204, Arlington, VA 22202-4302. Respondents should be aware that notwithstanding any other provision of law, no person shall be subject to any penalty for failing to comply with a collection of information if it does not display a currently valid OMB control number. **PLEASE DO NOT RETURN YOUR FORM TO THE ABOVE ADDRESS.**

1. REPORT DATE	2. REPORT TYPE	3. DATES COVERED
September 2022	Final	01Jun2017-31May2022

4. TITLE AND SUBTITLE

Investigation of a Novel PARP Inhibitor PET Tracer in Ovarian Carcinoma

5a. CONTRACT NUMBER
W81XWH-17-1-0092

5b. GRANT NUMBER

5c. PROGRAM ELEMENT NUMBER

6. AUTHOR(S)
Fiona Simpkins

E-Mail: fiona.simpkins@pennmedicine.upenn.edu

5d. PROJECT NUMBER

5e. TASK NUMBER

5f. WORK UNIT NUMBER

7. PERFORMING ORGANIZATION NAME(S) AND ADDRESS(ES)

The Trustees of the University of Pennsylvania
Department of Obstetrics and Gynecology
1210 BRB II/III 421 Curie Boulevard
Philadelphia, PA 19104-6160

8. PERFORMING ORGANIZATION REPORT NUMBER

9. SPONSORING / MONITORING AGENCY NAME(S) AND ADDRESS(ES)

U.S. Army Medical Research and Development Command
Fort Detrick, Maryland 21702-5012

10. SPONSOR/MONITOR'S ACRONYM(S)

11. SPONSOR/MONITOR'S REPORT NUMBER(S)

12. DISTRIBUTION / AVAILABILITY STATEMENT

Approved for Public Release; Distribution Unlimited

13. SUPPLEMENTARY NOTES

14. ABSTRACT

Epithelial ovarian carcinomas are amongst the most deadly gynecologic cancers due to their insidious onset, lack of efficient screening methods, and late presentation. Approximately 10% of epithelial ovarian carcinomas have germline mutations in Breast Cancer Susceptibility Genes 1/2 (BRCA1/2) which are genes responsible for encoding primary DNA-repair proteins necessary for homologous recombination (HR). Furthermore, approximately 50-60% of non-BRCA1/2 related ovarian carcinomas have functional defects in HR (HRD) and behave phenotypically like BRCA1/2-related tumors due to genetic/epigenetic events. There is now substantial data that DNA-damaging chemotherapy +/- poly (ADP-ribose) polymerase-1 (PARP) inhibitors may be highly effective in BRCA-related cancers by exploiting the inherent HRD. However, clinical trials of PARPi in unselected ovarian cancer patients, alone or combined with other DNA damaging agents, have shown mixed response rates. A potential explanation for the disappointing results is the lack of an effective biomarker for functional HRD to predict benefit from PARPi or DNA-damaging agents.

15. SUBJECT TERMS
None listed.

16. SECURITY CLASSIFICATION OF:			17. LIMITATION OF ABSTRACT	18. NUMBER OF PAGES	19a. NAME OF RESPONSIBLE PERSON
a. REPORT	b. ABSTRACT	c. THIS PAGE			USAMRDC
Unclassified	Unclassified	Unclassified	Unclassified	58	19b. TELEPHONE NUMBER *(include area code)*

TABLE OF CONTENTS

Section	Page
Introduction	2
Keywords	2
Accomplishments	3
Impact	13
Changes / Problems	15
Products	17
Participants & other collaborating organizations	20
Special Report Requirements	23
Appendices	24

INTRODUCTION

Despite recent advances in targeted therapies, ovarian carcinoma remains a deadly malignancy. Poly(ADP-ribose) polymerase (PARP) inhibitors (PARPi) are a newer class of agents that are FDA approved for the treatment of high grade serous ovarian cancer (HGSOC) in the maintenance and recurrent setting. However, despite defined selection criteria predominately based on known genetic associations, response to PARPi remains variable with not all patients responding to or benefitting from treatment with these agents. A biomarker to better select patients for this targeted therapy and predict response represents an unmet clinical need. Our group of investigators has developed a PET companion diagnostic, [^{18}F]FluorThanatrace ([FTT), as a potential biomarker of response for patients under consideration for PARP inhibitor treatment. As a radiolabeled PARPi, FTT enables non-invasive visualization and measurement of PARP-1 expression, the drug target of PARPi. The purpose of our work was to test whether this companion diagnostic can ultimately guide oncologists in selecting ovarian cancer patients that will benefit from PARPi treatment, providing a new tool to advance precision medicine. In this proposal, we evaluated our companion diagnostic as a biomarker to predict response to PARP inhibitor therapy. We conducted a prospective clinical trial imaging ovarian carcinoma patients with FTT-PET before and soon after PARPi therapy. Subjects were followed until disease progression, with FTT uptake measures—both at baseline and post-PARPi—correlated with response. This work provided us with the valuable information to justify additional trials to utilize FTT to further study this radiotracer as a biomarker to select patients for PARPi therapy and expand current indications for PARPi.

KEYWORDS:

PARP inhibitor, BRCA1, BRCA2, Ovarian Carcinoma, Companion Diagnostic, PET imaging, Drug Target Engagement, DNA repair, Homologous Recombination, and Cancer Therapy

ACCOMPLISHMENTS

What were the major goals of the project?

The approved SOW is pasted below. An additional column has been added to demonstrate the time these goals were completed.

Tasks (Major Goals)	Expected completion (months)	Actual completion (months)
Major task 1: Protocol preparation and IRB submission/approval		
Preparation of regulatory documents and research protocol for clinical trial, proposed 1-3 months	1-3	2
Cross Reference current held eIND for [18F]FTT, proposed 1-3 months	1-3	2
Finalize consent form and human subjects protocol, proposed 1-3 months	1-3	3
Submit amendments, deviations, adverse even recordings as needed, proposed as needed	As needed	As needed
IRB protocol submission, proposed 1-3 months	1-3	3
Milestone achieved: local IRB approval, proposed 4 months	4	5
Milestone achieved: approval by HRPO	6	10
Major task 2: coordinate study staff for clinical trials		
Coordination of study implementation (clinical trial, pathology acquisition, sampling storage, etc)	5-6	5
Coordinate cross departmental processes for data management	5-6	5
Major task 3: Participant recruitment, imaging, tissue analysis		
Coordinate with sites for clinical recruitment, imaging timepoints, tissue acquisition	5-6	5
Milestone achieved: first patient consented, screened, and enrolled	7-10	10

Begin subject recruitment	7-30	10
Participants complete imaging studies over 9-12 weeks (3 imaging scans)	7-30	10
Imaging analysis: identify up to 5 lesions in each patient on both and measure uptake	9-33	10
Follow patients for RECIST criteria	9-33	18
Major task 4: Data analysis		18
Perform analysis according to specifications	33-36	50
Work with data core on dissemination of findings (abstracts, publications, DOD)	33-36	50
Milestone achieved: Report results from clinical study and data analyses	33-36	58

What was accomplished under these goals?

The work funded by this grant led to the publication of three manuscripts in high-impact journals. We first established FTT as a non-invasive measure of PARP-1 expression in ovarian cancer and demonstrated the necessity of PARP-1 in the efficacy of PARPi (*1*). Next, through detailed PET kinetic analysis, we developed clinically accessible imaging protocols to facilitate human PET imaging (*2*). Then, we demonstrated the potential of FTT to serve as a biomarker to predict response to PARPi (*3*). These publications are listed below and attached in the appendix. Additional abstracts/conference presentations are listed at the end of the document:

1. Makvandi M, Pantel A, Schwartz L, et al. A PET imaging agent for evaluating PARP-1 expression in ovarian cancer. J Clin Invest. 2018;128:2116-2126.

2. Young AJ, Pantel AR, Viswanath V, et al. Kinetic and Static Analysis of Poly-(Adenosine Diphosphate-Ribose) Polymerase-1-Targeted (18)F-Fluorthanatrace PET Images of Ovarian Cancer. J Nucl Med. 2022;63:44-50.

3. Pantel AR, Gitto SB, Makvandi M, et al. [18F]FluorThanatrace ([18F]FTT) PET Imaging of PARP-Inhibitor Drug-Target Engagement as a Biomarker of Response in Ovarian Cancer, a Pilot Study. Clin Cancer Res. 2023;29:1515-1527.

Over the course of the award, we have consented 36 subjects and imaged 34 subjects, of which 16 patients were imaged pre- and post-PARPi. The specific aims of the original OCRP research are summarized below:

Specific Aim 1: To determine analytic validity of [^{18}F]FTT PET/CT, including the range of tumor FTT uptake in patients with ovarian carcinoma undergoing [^{18}F]FTT PET/CT imaging and correlation of tumor uptake of [^{18}F]FTT with in vitro assays of PARP-1 expression in tumor tissue both pre- and post-neoadjuvant chemotherapy.

Specific Aim 2: To test [^{18}F]FTT PET/CT as a predictive assay for response to neoadjuvant carboplatin/paclitaxel +/- veliparib.

Specific Aim 3: To measure early (pharmacodynamic) change in PARP-1 expression using serial [^{18}F]FTT PET/CT imaging in patients receiving neoadjuvant carboplatin/paclitaxel +/- veliparib, and explore associations between the early change in [^{18}F]FTT uptake and subsequent response.

We have made significant progress on each of these aims over the course of the grant, including validating the biologic target of the radiotracer (Aim 1), analyzing radiotracer kinetics to develop clinically accessible protocols, and demonstrating the biomarker potential to predict response to PARPi therapy (Aim 2 and 3). This latter accomplishment has provided encourages early results to establish FTT, a radiolabeled PARPi, to predict response to PARPi therapy, creating a paired biomarker-drug with the same molecular target. This evolution in our research aims aligns with advances in the treatment of OVCA, with the increasing use of PARPi targeted therapy. At the time of the original proposal, only the PARPi olaparib was FDA approved in the treatment in advanced OVCA, and only for BRCA+ patients. Since that time, two additional PARPi have been approved (niraparib and rucaparib) and indications have expanded, now including patients with *BRCA1/2* deficiencies, homologous recombination deficient (HRD) tumors, and even those without known genetic deficiencies or HRD tumors (e.g. HR-proficient OVCAs) (*4*). In addition, the carboplatin/paclitaxel +/- veliparib proposed in the original proposal trial closed earlier than expected. These notable clinical evolutions that occurred close at the start of the grant proposal while we were working on Aim 1, and we decided to pivot our studies towards the use of approved PARPi, primarily olaparib, and therapy combining PARPi with other DNA damage response (DDR) targeted agents, specifically patients participating in Dr. Simpkins multicenter SPORE CAPRI trial combining PARPi with ATR inhibitors (ATRi), especially in PARPi-resistant cancers

that had progress on standard PARPi-containing regimens. We have utilized FTT as a biomarker to guide PARPi focusing on these emerging indications. The evolution of clinical treatment paradigms also led us to study (outside of the scope of the DOD project, but guided by the DOD project results) the predictive value of combined PARPi/ATRi in PDX models, including PARPi-resistant PDX model. We had notable success, including a manuscript published in *The Journal of Clinical Investigation* validating FTT as a maker of PARP1-expression in ovarian cancer (*1*). More recently, we had two presentations at the 2022 Society of Nuclear Medicine and Molecular Imaging and a manuscript published in *Clinical Cancer Research (CCR)* (*3*) showing the value of serial FTT after a short course of PARPi in predicting response both in pre-clinical models and early patient studies. A favorable editorial accompanied this work in *CCR (5)*.

We highlight specific notable research accomplishments below. The full scope of our work is detailed in the three publications attached to this final report:

PARP-1 expression is required for PARPi efficacy (*1*): In the development of a PARPi PET biomarker, we first established that necessity of drug-target expression, PARP-1, in drug efficacy. Using CRISPR/Cas9 genome editing, we deleted PARP-1 in two PARPi-sensitive OVCA cell lines, one with a *BRCA1* mutation (UWB1.289) and another with BRCA1 promoter methylation (and OVCAR8) (**Figure 1A**). Cell viability assays demonstrated PARP-1 expression for maximum efficacy. Additionally, PARP-1 knockout (KO) cell lines were equally resistant to PARPi as *BRCA1* restored cells (**Figure 1B**) (*1*). This pre-clinical data provides impetus to measure PARP-1 expression with a radiotracer to predict PARPi efficacy.

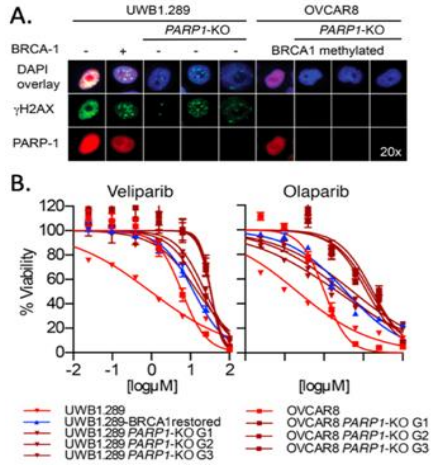

Figure 1: PARPi response is dependent on PARP1 expression. A) Immunofluorescence confirmed PARP-1 was absent in PARP1-KO polyclonal populations and reduced in BRCA1-restored cells. **B)** Cell viability assays demonstrated that PARP-1 was required maximum efficacy; PARPi resistance was seen with loss of PARP-1. Published in (1).

First-in-human studies: biodistribution, dosimetry, and target validation (*1*): A first-in-human clinical trial at Penn imaged 20 patients with OVCA with two imaging cohorts. Organ doses from the biodistribution cohort were comparable to other commonly used radiotracer. A wide range of FTT was seen in known OVCA lesions, ranging from background (SUV_{max} of 2) to markedly

elevated (SUV_{max} of 12) (**Figure 2).** FTT was seen in the bowel owing to excretion of the tracer (also seen in Figure 2), but uptake correlating to the known lesion was discernable. Additionally, minimal FTT in the urine enabled visualization of lesions in the pelvis.

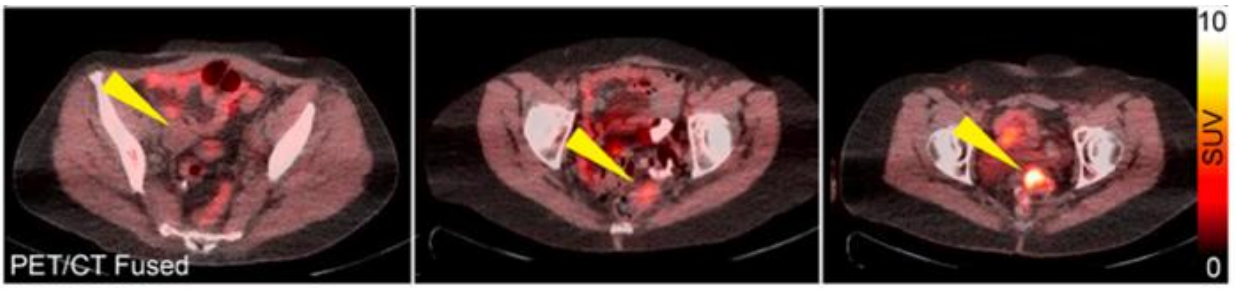

Figure 2: A spectrum of FTT uptake is seen in sites of ovarian cancer. Yellow arrows demonstrate sites of disease with SUV_{max} ranging from 2 (left) to 12 (right). Published in (1).

To validate FTT as a measure of PARP-1 expression, surgical tissue excised from 7 patients was used to correlate FTT uptake on PET with tissue markers of PARP-1 expression. A significant positive correlation was seen between FTT SUV_{max} at 90 minutes and immunohistochemistry (IHC), validating the tracer as a non-invasive measure of PARP-1 expression (**Figure 3A)**, the intended molecular target.

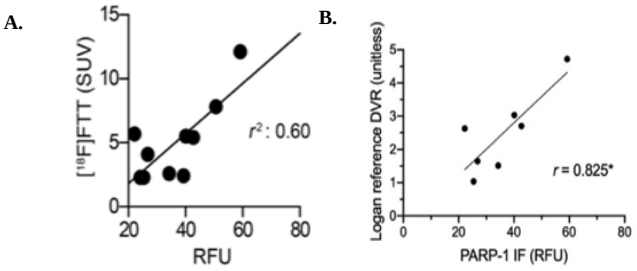

Figure 3: FTT-PET uptake measures correlate with tissue PARP-1 expression. Both SUVmax obtained from static images at 1.5 hours (published in (2)) and Logan reference DVR from dynamic imaging (published in (5)) correlated with PARP-1 expression as measured by immunofluorescence in excised surgical tissue, validating FTT as a measure of PARP-1 expression.

Kinetic analysis of dynamic FTT-PET to optimize clinical imaging protocols (*2*): FTT uptake was best described by reversible models, with variable uptake at later time points. Kinetic analysis of dynamic imaging cohort supported tumor SUV_{max} at 55-60 min after injection and later (noting results in **Figure 3A** obtained at 1.5 hours post-injection) and Logan reference tissue distribution volume ratio (DVR), a kinetic measure of radiotracer uptake, from at least 60 min appear to be robust noninvasive measures of PARP-1 binding (**Figure 3B).** From this analysis, we have modified the imaging protocol for FTT in patients with OVCA. We now image 60 minutes after injection from the skull base to thigh; dynamic images have been eliminated given that we have shown that both dynamic and static measures can measure PARP-1 expression in tumor. Recruitment has improved secondary to this change as subjects can better tolerate the shorter image

acquisition. Additionally, less total scan time has enabled more flexible scheduling. This protocol now matches that for FDG, the most commonly used radiotracer in oncologic PET, facilitating clinical translation.

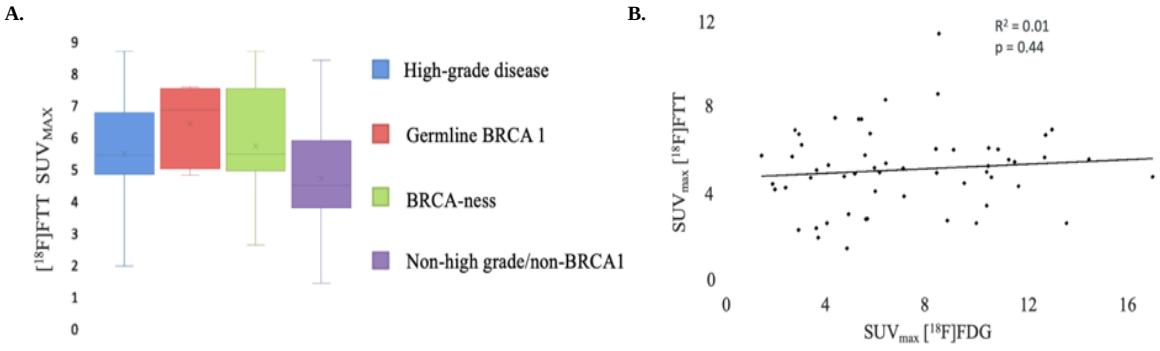

Figure 4: FTT uptake across tumor grades and genetic predictors of PARP-1 expression, without correlation with FDG uptake. (A) A wide range of FTT uptake was seen across tumor grades and BRCA/HRD status with significant overlap. (B) No correlation was seen between FDG uptake and FTT, reflecting their unique molecular targets. Up to six lesions per patients were selected for this analysis.

Wide range of FTT uptake across OVCA patients, without correlation with FDG-PET (*6*): A wide range of FTT uptake was seen in the first 20 OVCA patients we imaged, indicative of a wide range of PARP-1 tissue expression. This wide range persisted when patients were stratified by grade of disease and BRCA/HRD status (**Figure 4A**). Given that BRCA/HRD status is used to select patients for PARPi therapy, this range of uptake suggests that patients with markedly different levels of drug-target expression may be treated with PARPi, possibly explaining variability in response. Additionally, variable uptake in the non-high grade/non-BRCA1 group, including some with relatively high uptake, suggests that some patients in this group may particularly benefit from targeted therapy. This patient population is included in **Aim 1** of this proposal. Concomitant FDG scans were obtained in these initial subjects. No correlation was seen between FDG uptake, a measure of tissue glycolysis, and FTT uptake, as expected based on their unique molecular targets (**Figure 4B**). This further supports that FTT-PET provides orthogonal information to currently available imaging methods, providing additional impetus for continued study. This work is nearly ready for submission to the *Journal of Nuclear Medicine*.

FTT-PET as a biomarker for response to PARPi therapy - Preclinical Studies (*3*): As a validated non-invasive imaging biomarker of regional PARP-1 expression, we next studied FTT as a biomarker to predict response to PARPi in patient-derived xenograft (PDX) tumors models. Of

note, this research was not directly funded by this grant, but the insights from this grant led to this study, which, in turn, helped provide insight into our human work. Here, we specifically investigated the change in FTT uptake after PARPi treatment, as a measure of drug-target engagement, in predicting response. We focused on PARP-resistant tumors, aligning with an ongoing clinical trial at Penn (described below) and a pressing clinical need. A representative PDX model treated with PARPi, an ATR inhibitor (ATRi), and a combination of the two is shown in **Figure 5A**. In two PARPi-resistant PDX models, a positive correlation between the percent decrease in FTT tumor-to-background muscle (T/M) uptake and percent change in tumor size was seen when treated with PARPi alone and PARPi/ATRi combination therapy (data for one PDX shown in **Figure 5B**). Greater decreases in T/M (PARPi/ATRi and PARPi) correlated with better response to the corresponding agents (**Figure 5C**). We further demonstrated through reverse phase protein array studies that ATRi therapy leads to decreased expression of PARPi, providing a biologic mechanism to our FTT-PET studies. These pre-clinical studies supported translating this drug combination into humans, with preliminary data acquired and shown below. This will be more fully explored in **Aim 2** of this this proposed expansion, with particular attention to the biomarker potential of FTT in guiding combination therapies.

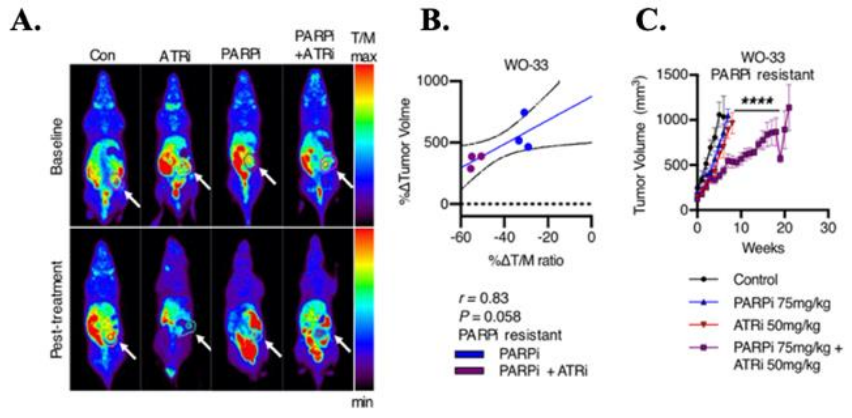

Figure 5: Preclinical PDX studies demonstrate signal abrogation in FTT uptake after PARPi therapy correlate with response. A) Representative imaging pre- and post-therapy. B) Percent change in tumor-to-muscle ratio in the WO-33 PDX model (PARPi resistant) correlates with change in tumor volume (Spearman correlation statistics shown). C) In this same PARPi-resistant model, the combination PARPi-ATRi therapy significantly blunted tumor growth compared to all other treatments. Published in (3).

FTT-PET as a biomarker for response to PARPi therapy – Early Clinical Studies (*3*): In a concomitant imaging trial, we translated our pre-clinical studies into humans. Sixteen patients with high-grade serous OVCA beginning PARPi therapy were imaged with FTT at baseline in a Phase

II trial; 13 of these patients had follow-up FTT imaging ~ one week after PARPi initiation, analogous to the paradigm studied in the PDX models. The subjects were then followed until disease progression, with the tumor marker CA-125 also followed (**Figure 6A**). Progression-free survival (PFS) (range 3-23 months, median of 5.5 months / mean of 8.5 months) and patient characteristics are shown in **Figure 6B**. The presence of genetic mutations would suggest PARPi efficacy, but as demonstrated PFD varied widely, suggesting additional biomarkers of PARPi response would be useful. As expected

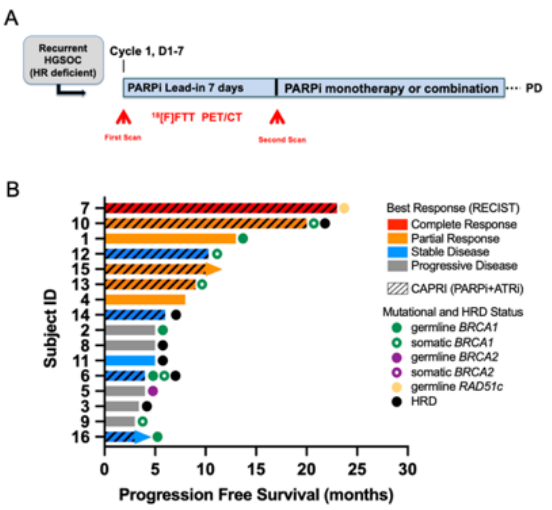

Figure 6: Clinical trial design and subject characteristics/PFS. Published in (3).

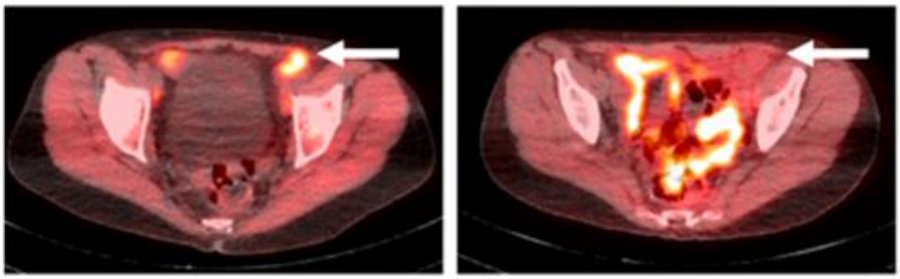

Figure 7: Representative subject imaged with FTT prior to and after the PARPi olaparib. Baseline imaging (A) demonstrated uptake in a left external iliac lymph node. Imaging 8 days after starting olaparib, uptake in that lymph node is at background representing drug-target engagement. This subject had a 20 month PFS, greater than the mean. Published in (3).

based on the underlying biology and in keeping with the pre-clinical studies, post-PARPi imaging demonstrated decreased FTT lesioned uptake compared to baseline, indicative of drug target engagement. That is, with pharmacologic doses of PARPi, FTT is blocked from binding to PARPi, with the degree of uptake related to pharmacologic effect of the PARPi. An example subject study is demonstrated in **Figure 7**.

The percent difference in uptake post-PARPi compared to baseline (△SUV) demonstrated a significant correlation with PFS, suggesting the potential for FTT to serve as a biomarker for PARPi therapy (**Figure 8A**). As drug target engagement increased, indicated by larger decreases in △SUV, PFS increased. In fact, using an △SUV threshold of 50% dichotomized the patients: decline in SUV >50% was necessary for >6-month PFS in these subjects. Similarly, △SUV demonstrated predictive capacity for CA-125 response. Baseline FTT uptake did not significantly correlate with either of these response metrics (see **Figure 8B** for PFS data).

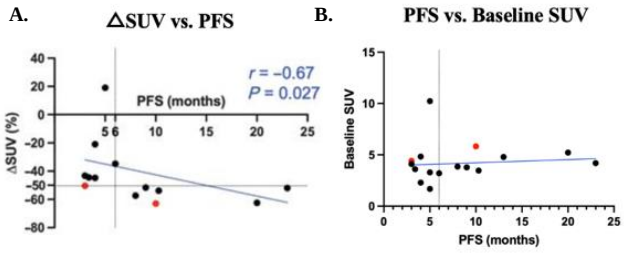

Figure 8: FTT SUV as a predictor of PFS. A) △SUV, the difference of FTT uptake after PARPi compared to baseline (with images obtained ~one week apart) demonstrated a significant correlation with PFS. B) Baseline uptake only did not demonstrate a correlation with PFS. Published in (3).

These encouraging results provided the impetus for future grants further studying FTT as a biomarker for PARPi therapy: an DOD Ovarian Cancer Research Program Teal Expansion Award and a DOD Clinical Translational Research Award. In the expansion application, we sought to further leverage [^{18}F]FTT to more precisely treat ovarian cancer patient with PARPi and expand the current indications for this class of therapies. Our specific aims are as follows, all of which directly follow from hypothesis generated from the first funding period:

Aim 1: Evaluate FTT as a biomarker of PARPi treatment response in patients with HGSOC.

Aim 2: Correlate FTT with tumor response after the initiation of a new combination, PARP-1 selective PARPi (AZD5305) with ATRi in PARPi-resistant patients in a clinical trial.

Aim 3: Evaluate mechanistic contribution of single-agent PARPi and ATRi on FTT uptake and correlate with response using our PDX HGSOC library.

What opportunities for training and professional development has the project provided?

This project has provided training opportunities for Nuclear Medicine junior faculty members Austin Pantel MD, MSTR, and Mehran Makvandi PharmD to participate and help lead a clinical

imaging trial. Dr. Pantel was co-first author of the published manuscript in *Clinical Cancer Research*. Sarah Gitto, PhD, a recent Penn recruit and Instructor of Pathology and Laboratory medicine, served as the other co-first author. The data analysis and writing of the manuscript facilitated a strong collaboration between these early investigators which has continued with new grant submissions emphasizing cross-department collaboration. Writing the manuscript and grants has provided both Dr. Pantel and Dr. Gitto ample opportunities to learn from senior, seasoned investigators, most notably Dr. Fiona Simpkins, the PI of this project. These two young investigators have also benefited from discussions with statistical collaborators. Dr. Makvandi has moved onto industry to continue research in radionuclide therapy.

This provided invaluable professional development in the following areas: team building, project management, inter-department collaboration, and hypothesis driven clinical research. The investigators also benefited from discussing this research with others at the conferences described below. The success from this work has been leveraged for a Teal Expansion Grant Application and Clinical Translational Research Award, utilizing the same team.

How were the results disseminated to communities of interest?

In addition, to the manuscripts described, Dr. Pantel has presented this work in several settings. Most recently, he had an oral presentation at the Society of Nuclear Medicine and Molecular Imaging (SNMMI) Annual Meeting in Vancouver, Canada in June 2022. Dr. Joanna Weeks also presented at this meeting(*6*). He has previously presented at the SNMMI Annual Meeting in 2017 and at a Basser Center for BRCA symposium in 2019. Dr. Makvandi previously presented this work at the AACR Annual Meeting in 2017 and a Basser Center for BRCA symposium in 2018. Dr. Gitto has presented this work at the 2023 AACR Annual meeting. These presentations/abstracts are listed below in section 6, products.

A press release was also issued by Penn to increase awareness of the manuscript published in the Journal of Clinical Investigation (*1*):
https://www.pennmedicine.org/news/news-releases/2018/april/parp-1-may-be-key-to-effectiveness-of-parp-inhibitors-and-now-researchers-can-image-it

IMPACT

What was the impact on the development of the principal discipline(s) of the project?

Three major milestones achieved as a result of this project have a direct impact on the future direction of research with FTT to establish this radiotracer as a biomarker for PARPi therapy:

1. FTT was validated as a non-invasive in vivo measure of PARP-1 expression through correlation with tissue samples from ovarian cancer patients (*1*). As a PET radiotracer, FTT can measure PARP-1 expression non-invasively through imaging, precluding the need for biopsy (which can often be difficult or impossible for many sites, and is not feasible across all sites of a patient's disease). As PARP-1 is the drug target of PARPi, this milestone provides the foundation for future studies with FTT to serve as a biomarker for PARPi therapy.
2. Clinically accessible imaging protocols for FTT-PET were developed (*2*). In the development of a new radiotracer, dynamic imaging must be first performed to understand radiotracer kinetics so that abbreviated protocols could later be developed. In the development of FTT-PET, we first images patients continuously for 1 hour after radiotracer injection, with up to two static whole-body scans to follow. Through detailed kinetic analysis, including correlation with tissue measures (#1 above), we established a more clinically accessible protocol (imaging at 1 hour post injection). This is clearly more tolerable for patients (a 150minute scan versus 60 minutes). This has eliminated a barrier to imaging and has helped with recruitment to the studies. Future studies use this abbreviated protocol (though without a loss of useable data).
3. Early studies demonstrated potential for [^{18}F]FTT-PET as a biomarker to guide PARPi therapy (*3*). We have demonstrated that change in FTT uptake after a short course of PARPi correlated to response in patients with DNA-repair deficiencies. We have designed additional studies to provide definite proof of this hypothesis, as well as expand to other patient populations.

We have submitted a Teal Expansion Grant Application and Clinical Translational Research Award utilizing the same team to further our work in this space. We do note that the manuscript

published in *Clinical Cancer Research* represents the first study demonstrating the biomarker potential of a PARPi (*3*).

What was the impact on other disciplines?

The success of these studies in ovarian cancer have provided a roadmap for similar studies with FTT in breast and prostate cancer. The validation of FTT as a marker of PARP-1 expression in ovarian cancer has provided the impetus similar studies in these other diseases, using similar methodology. Likewise, a static imaging protocol for PET imaging—as opposed to dynamic imaging at 45 minutes to 1 hour—has been adopted in these other disease states. Lastly, the methods developed to test the biomarker potential of FTT has been utilized in the other disease as well. This work in ovarian cancer has been at the leading edge in research in FTT, providing methodology for other disease states. Other PIs have submitted DOD and R01 grants to support their work with FTT in these other disease.

What was the impact on technology transfer?

The validation of FTT as a measure of PARP-1 tissue expression established FTT as a non-invasive marker of PARP-1 drug target expression. This result obviates the need for future tissue correlation studies in certain populations, an expensive and complex endeavor. Additionally, the development of an abbreviated image protocol enables other investigators to avoid time-consuming dynamic imaging studies which hamper recruitment.

What was the impact on society beyond science and technology?

We suspect this work will improve public knowledge and attitude towards precision medicine – that is, in this case, using a non-invasive PET imaging agent to guide targeted therapy. PET-guided treatment has grown in recent years owing to DOTATATE imaging in neuroendocrine tumors and Lutathera therapy, FES imaging of estrogen receptor positive breast cancer to guide endocrine therapy, and PSMA-PET to guide Pluvicto radionuclide therapy. FTT imaging to direct PARPi therapy should add to this growing armamentarium, improve the care of patient.

CHANGES/PROBLEMS:

Changes in approach and reasons for change

Our initial approach to patient enrollment was based on identifying patients that were participating in the GOG3005 clinical trial evaluating chemotherapy +/- veliparib (PARP inhibitor). This trial completed patient accrual nationally earlier than planned. We then identified new trials that were evaluating PARP inhibitor therapy in ovarian cancer. We identified two clinical trials in which patients were either receiving PARP inhibitor monotherapy (LIGHT) or PARP inhibitor combined with a DNA damaging therapy (CAPRI). Patients that are candidates for the LIGHT and CAPRI trial at Penn were well matched to the overall aims of this proposal which was to test whether FTT can predict response to PARP inhibitor therapy. Patients enrolled on the LIGHT and CAPRI were made aware of the FTT study and screened/enrolled if they agree to participate the trial. We have had success in recruiting to our imaging trial using this new strategy. Furthermore, this change better aligned with current treatment strategies with PARPi in ovarian cancer. These changes occurred close to the start of the grant proposal when we were working on Aim 1, allowing us to pivot our studies successfully and increasing the clinical relevance. We also benefitted from the PI of this trial, Dr. Simpkins, also serving as the PI of the multicenter SPORE describe earlier. This evolution also prompted us to study FTT in PDX model (with this research outside the scope of the DOD project, but guided by the results). This has provided a biological underpinning for our studies.

Actual or anticipated problems or delays and actions or plans to resolve them

We encountered several issues with our initial plans that resulted in a slower progression of our timeline than we previously anticipated. As discussed above, we encountered an issue with the clinical trial GOG3005 closing to accrual sooner than expected which required identifying a new clinical trial to enroll patients for the [FTT PET imaging study. This issue was quickly resolved through identifying two different clinical trials that were also evaluating the clinical utility of PARP inhibitors. Lastly, we have had several delays with gaining HRPO approval. We did however finally receive HRPO.

The COVID epidemic also hampered recruitment, as expected. Imaging trials were temporarily halted and upon reopening, recruitment was challenging. We did, though, recruit an adequate number of patients to have sufficient power to study our specific aims.

Changes that had a significant impact on expenditures

Nothing to report.

Significant changes in use or care of human subjects, vertebrate animals, biohazards, and/or select agents

Nothing to report.

Significant changes in use or care of human subjects

Nothing to report.

Significant changes in use or care of vertebrate animals.

Nothing to report.

Significant changes in use of biohazards and/or select agents

Nothing to report.

PRODUCTS

Publications, conference papers, and presentations

Journal publications (all published):

1. Makvandi M, Pantel A, Schwartz L, et al. A PET imaging agent for evaluating PARP-1 expression in ovarian cancer. J Clin Invest. 2018;128:2116-2126.
2. Young AJ, Pantel AR, Viswanath V, et al. Kinetic and Static Analysis of Poly-(Adenosine Diphosphate-Ribose) Polymerase-1-Targeted (18)F-Fluorthanatrace PET Images of Ovarian Cancer. J Nucl Med. 2022;63:44-50.
3. Pantel AR, Gitto SB, Makvandi M, et al. [18F]FluorThanatrace ([18F]FTT) PET Imaging of PARP-Inhibitor Drug-Target Engagement as a Biomarker of Response in Ovarian Cancer, a Pilot Study. Clin Cancer Res. 2023;29:1515-1527.

Books or other non-periodical, one-time publications:

Nothing to reports

Other publications, conference papers, and presentations:

*Mehran Makvandi, Austin Pantel, Lauren E. Schwartz, Kuiying Xu, Chia-Ju Hsieh, Hyoung Kim, Shi-Hong Li, Robert Doot, Sharon Lee, Fiona Simpkins, Roger A. Greenberg, David A. Mankoff, Robert H. Mach, Lilie Lin; Abstract 3716: Exploring the significance of PARP-1 expression for therapy and clinical PET/CT imaging of PARP-1 in ovarian cancer. Cancer Res 1 July 2017; 77 (13_Supplement): 3716. https://doi.org/10.1158/1538-7445.AM2017-3716

*Austin Pantel, Mehran MaKvandi, Robert Doot, Lauren Schwartz, Roger Greenberg, Fiona Simpkins, David Mankoff, Lilie Lin, Robert Mach. A pilot study of a novel poly (ADP-ribose) polymerase-1 (PARP) PET tracer ([18F]FluorThanatrace) in patients with ovarian carcinoma. Journal of Nuclear Medicine May 2017, 58 (supplement 1) 386.

*Mehran Makvandi, Austin Pantel, Michael Farwell, Daniel Pryma, David A Mankoff, Roger A Greenberg, Robert H Mach, Lilie Lin, and Fiona Simpkins. PET imaging of PARP inhibitor target engagement in ovarian cancer. Basser Center for BRCA Annual Symposium. 2018

*Austin Pantel, Mehran Makvandi, Michael Farwell, Daniel Pryma, David A Mankoff, Roger A Greenberg, Robert H Mach, Lilie Lin, and Fiona Simpkins. PET imaging of PARP inhibitor target engagement in ovarian cancer. Basser Center for BRCA Annual Symposium. 2019

*Austin Pantel, Mehran Makvandi, Hyoung Kim, Joanna Weeks, Drew Torigian, Nawar Latif, Lainie Martin, Janos Tanyi, Mark Morgan, Robert Doot, Lilie Lin, David Mankoff, Robert Mach, Fiona Simpkins. PET imaging of PARP-inhibitor drug-target engagement predicts response in ovarian cancer in a pilot study. Journal of Nuclear Medicine June 2022, 63 (supplement 2) 2486.

Joanna Weeks, Austin Pantel, Daniel Pryma, Michael Farwell, Erin Schubert, Robert Mach, Fiona Simpkins, Lilie Lin. Clinical assessment of 18F FTT PET versus 18F FDG PET in characterizing tumor PARP expression in ovarian cancer. Journal of Nuclear Medicine Jun 2022, 63 (supplement 2) 2487;

Sarah B. Gitto, Austin R. Pantel, Mehran Makvandi, Hyoung Kim, Sergey Medvedev, Joanna K. Weeks, Drew A. Torigian, Chia-Ju Hsieh, Benjamin Ferman, Nawar A. Latif, Janos L. Tanyi, Lainie P. Martin, Shannon M. Lanzo, Fang Liu, Quy Cao, Gordon B. Mills, Robert K. Doot, David A. Mankoff, Robert H. Mach, Lilie L. Lin, Fiona Simpkins; Abstract 5610: [^{18}F]FluorThanatrace ([^{18}F]FTT) PET Imaging of PARP-inhibitor drug-target engagement as a biomarker of response in ovarian cancer. *Cancer Res* 1 April 2023; 83 (7_Supplement): 5610. https://doi.org/10.1158/1538-7445.AM2023-5610

- denotes presentation produced a manuscript

Website(s) or other Internet site(s)

A press release was also issued by Penn to increase awareness of the manuscript published in the Journal of Clinical Investigation (*1*):
https://www.pennmedicine.org/news/news-releases/2018/april/parp-1-may-be-key-to-effectiveness-of-parp-inhibitors-and-now-researchers-can-image-it

Technologies or techniques

As discussed, an abbreviated imaging protocol has been validated. The details of this methods are freely available in the associated publication (*2*)

Inventions, patent applications, and/or licenses

Nothing to report.

Other Products

Nothing to report.

PARTICIPANTS & OTHER COLLABORATING ORGANIZATIONS

What individuals have worked on the project?

Name:	*Fiona Simpkins*
Project Role:	Primary-Investigator
Researcher Identifier (e.g. ORCID ID):	
Nearest person month worked:	1.56
Contribution to Project:	Dr. Simpkins is the lead investigator on this trial and oversees the study. She recruits patients and manages patients on trial. She performs data analysis, patient follow up, trial management, and composing scientific literature
Funding Support:	
Name:	Mehran Makvandi
Project Role:	Co-Investigator
Researcher Identifier (e.g. ORCID ID):	Not available
Nearest person month worked:	2.4
Contribution to Project:	Dr. Makvandi primarily advises on the science and rationale of [18F]FTT imaging with secondary roles in coordinating imaging studies, gathering/inputting data, analyzing data, composing scientific literature, and performing in vitro lab assays

Funding Support:	No other current funding
Name:	Cristian Tolento
Project Role:	Research Coordinator
Researcher Identifier (e.g. ORCID ID):	
Nearest person month worked:	2.4
Contribution to Project:	Cristian is a research coordinator in the department of OB-GYN. She screens and enrolls patients on the clinical trial. She communicates with research coordinators in the department of radiology.
Funding Support:	
Name:	Katie Elkins
Project Role:	Study Coordinator
Researcher Identifier (e.g. ORCID ID):	
Nearest person month worked:	2.4
Contribution to Project:	Katie is a research coordinator in the department of obstetrics and gynecology. She screens and enrolls patients on the clinical trial. Jyothy communicates with research coordinators in the department of radiology.
Funding Support:	
Name:	Erin Schubert
Project Role:	Protocol Manager

Researcher Identifier (e.g. ORCID ID):	
Nearest person month worked:	1.2
Contribution to Project:	Ms. Schubert composes and manages the clinical protocols and IRB approval process. In addition, she provides valuable regulatory oversight.
Funding Support:	

Has there been a change in the active other support of the PD/PI(s) or senior/key personnel since the last reporting period?

Nothing to report.

What other organizations were involved as partners?

Nothing to report.

SPECIAL REPORTING REQUIREMENTS

Nothing to report.

APPENDICES

References

1. Makvandi M, Pantel A, Schwartz L, et al. A PET imaging agent for evaluating PARP-1 expression in ovarian cancer. *J Clin Invest.* 2018;128:2116-2126.

2. Young AJ, Pantel AR, Viswanath V, et al. Kinetic and Static Analysis of Poly-(Adenosine Diphosphate-Ribose) Polymerase-1-Targeted (18)F-Fluorthanatrace PET Images of Ovarian Cancer. *J Nucl Med.* 2022;63:44-50.

3. Pantel AR, Gitto SB, Makvandi M, et al. [18F]FluorThanatrace ([18F]FTT) PET Imaging of PARP-Inhibitor Drug-Target Engagement as a Biomarker of Response in Ovarian Cancer, a Pilot Study. *Clin Cancer Res.* 2023;29:1515-1527.

4. Foo T, George A, Banerjee S. PARP inhibitors in ovarian cancer: An overview of the practice-changing trials. *Genes Chromosomes Cancer.* 2021;60:385-397.

5. Liu YL, Zamarin D. Shedding Light on PARP Inhibitor Response through Functional Imaging. *Clin Cancer Res.* 2023;29:1384-1386.

6. Weeks J, Pantel A, Pryma D, et al. Clinical assessment of 18F FTT PET versus 18F FDG PET in characterizing tumor PARP expression in ovarian cancer. *Presented at the Society of Nuclear Medicine Annual Meeting; June 14, 2022; Vancouver, CA.*

[^{18}F]FluorThanatrace ([^{18}F]FTT) PET Imaging of PARP-Inhibitor Drug-Target Engagement as a Biomarker of Response in Ovarian Cancer, a Pilot Study

Austin R. Pantel[1], Sarah B. Gitto[2], Mehran Makvandi[1], Hyoung Kim[3], Sergey Medvedv[3], Joanna K. Weeks[1], Drew A. Torigian[1], Chia-Ju Hsieh[1], Benjamin Ferman[3], Nawar A. Latif[4], Janos L. Tanyi[4], Lainie P. Martin[4], Shannon M. Lanzo[1], Fang Liu[5], Quy Cao[5], Gordon B. Mills[6], Robert K. Doot[1], David A. Mankoff[1], Robert H. Mach[1], Lilie L. Lin[7], and Fiona Simpkins[3,4]

ABSTRACT

Purpose: PARP inhibitors have become the standard-of-care treatment for homologous recombination deficient (HRD) high-grade serous ovarian cancer (HGSOC). However, not all HRD tumors respond to PARPi. Biomarkers to predict response are needed. [^{18}F]FluorThanatrace ([^{18}F]FTT) is a PARPi-analog PET radiotracer that noninvasively measures PARP-1 expression. Herein, we evaluate [^{18}F]FTT as a biomarker to predict response to PARPi in patient-derived xenograft (PDX) models and subjects with HRD HGSOC.

Experimental Design: In PDX models, [^{18}F]FTT-PET was performed before and after PARPi (olaparib), ataxia-telangiectasia inhibitor (ATRi), or both (PARPi-ATRi). Changes in [^{18}F]FTT were correlated with tumor volume changes. Subjects were imaged with [^{18}F]FTT-PET at baseline and after ∼1 week of PARPi. Changes in [^{18}F]FTT-PET uptake were compared with changes in tumor size (RECISTv1.1), CA-125, and progression-free survival (PFS).

Results: A decrease in [^{18}F]FTT tumor uptake after PARPi correlated with response to PARPi, or PARPi-ATRi treatment in PARPi-resistant PDX models ($r = 0.77$–0.81). In subjects ($n = 11$), percent difference in [^{18}F]FTT-PET after ∼7 days of PARPi compared with baseline correlated with best RECIST response ($P = 0.01$), best CA-125 response ($P = 0.033$), and PFS ($P = 0.027$). All subjects with >50% reduction in [^{18}F]FTT uptake had >6-month PFS and >50% reduction in CA-125. Utilizing only baseline [^{18}F]FTT uptake did not predict such responses.

Conclusions: The decline in [^{18}F]FTT uptake shortly after PARPi initiation provides a measure of drug-target engagement and shows promise as a biomarker to guide PARPi therapies in this pilot study. These results support additional preclinical mechanistic and clinical studies in subjects receiving PARPi ± combination therapy.

See related commentary by Liu and Zamarin, p. 1384

Introduction

PARP inhibitors (PARPi) are a newer class of agents that are FDA approved for the treatment of high-grade serous ovarian cancer (HGSOC) in the maintenance and recurrent setting (1–5). PARPi selectively inhibit predominantly PARP-1, PARP-2, and less so PARP-3 enzymes, although the efficacy of these drugs is primarily dependent on PARP-1 inhibition (6).

PARPi have shown efficacy in malignancies with preexisting DNA repair defects, most notably tumors that harbor mutations in homologous recombination DNA repair genes, such as Breast Cancer Susceptibility genes 1 and 2 (*BRCA1/BRCA2*). These homologous recombination deficient (HRD) tumors lacking *BRCA1/2* or other HR-related genes (e.g., *ATM*, *RAD51C/D*, *CHK2*) cannot repair double-stranded DNA breaks that result from PARP inhibition, leading to cell death with less impact on healthy tissue not expressing these mutations (7, 8). This phenomenon, deemed "synthetic lethality," has been leveraged for the selection of patients for treatment with this class of medications. Currently, there are three PARPi with FDA approval in ovarian cancer—olaparib, rucaparib, and niraparib—for patients with known HRD recurrent disease, or for all patients regardless of HRD status as maintenance therapy after response to platinum-based chemotherapy (1, 2, 4, 9–11). The *BRCA1/2* mutation serves as a genomic biomarker that predicts sensitivity to PARPi (1, 2, 4), although increasing evidence supports PARPi sensitivity in non-*BRCA* HRD tumors (12–16).

Despite defined selection criteria, response to PARPi remains variable with not all patients responding to or benefitting from treatment with these agents. For example, in the recurrent setting, overall response rates to olaparib in *BRCA* mutant ($BRCA^{MUT}$) ovarian cancer is 30% to 40% (17, 18). In the maintenance setting, PARPi are used to prevent recurrence and even though a significant benefit has been shown, not all patients benefit (19, 20). Because of suboptimal response, new combination strategies that synergize with PARPi by targeting DNA-damage response mechanisms (e.g., ATR, WEE1, BET), oncogenic pathways (e.g., PI3K/AKT/mTOR and RAS/RAF/MEK), angiogenesis, or by enhancing endogenous immunity are under clinical development (21). Thus, there is a pressing clinical need to

[1]Division of Nuclear Medicine Imaging and Therapy, Department of Radiology, Hospital of the University of Pennsylvania, Philadelphia, Pennsylvania. [2]Department of Pathology and Laboratory Medicine, Perelman School of Medicine, University of Pennsylvania, Philadelphia, Pennsylvania. [3]Penn Ovarian Cancer Research Center, Division of Gynecologic Oncology, Department of Obstetrics and Gynecology, University of Pennsylvania, Philadelphia, Pennsylvania. [4]Division of Gynecologic Oncology, Department of Obstetrics and Gynecology, Perelman School of Medicine at the University of Pennsylvania, Philadelphia, Pennsylvania. [5]Department of Biostatistics, Epidemiology, and Informatics, Perelman School of Medicine, University of Pennsylvania, Philadelphia, Pennsylvania. [6]Department of Cell, Developmental and Cancer Biology, Oregon Health & Science University School of Medicine, Portland, Oregon. [7]The University of Texas, MD Anderson Cancer Center, Houston, Texas.

A.R. Pantel and S.B. Gitto Contributed equally to this article.

Corresponding Author: Fiona Simpkins, Department of Obstetrics and Gynecology, University of Pennsylvania, Philadelphia, PA 19104. E-mail: fiona.simpkins@pennmedicine.upenn.edu

Clin Cancer Res 2023;29:1515–27

doi: 10.1158/1078-0432.CCR-22-1602

©2022 American Association for Cancer Research

Downloaded from http://aacrjournals.org/clincancerres/article-pdf/29/8/1515/3320981/1515.pdf by University of Pennsylvania Libraries user on 06 August 2023

Translational Relevance

PARP inhibitors (PARPi) have proven, but not universal, efficacy in ovarian cancer selected predominately based on homologous recombination deficiency. To more precisely select patients for PARPi treatment, predictive biomarkers are needed. We previously showed that the PET radiotracer [^{18}F]FluorThanatrace ([^{18}F]FTT) measures PARP-1 expression in ovarian cancer. Herein, we demonstrate the potential of [^{18}F]FTT to serve as a noninvasive molecular biomarker to guide PARPi therapy. In patient-derived xenografts, [^{18}F]FTT signal abrogation after PARPi and PARPi-ATRi correlated with anatomic response, suggesting utility for this tool in selecting drug combinations for human translation. In this pilot clinical study, abrogation of [^{18}F]FTT uptake after short-term PARPi therapy as a measure of drug-target engagement correlated with RECIST and CA-125 response, and PFS, suggesting its potential to identify patients likely to benefit from PARPi therapy. These translational studies provide the first evidence of a PARPi radiotracer as a biomarker to guide PARPi therapy warranting further study.

develop additional biomarkers to better select patients with ovarian cancer for treatment with both PARPi monotherapy and combination approaches.

[^{18}F]FluorThanatrace ([^{18}F]FTT) is a radiopharmaceutical for PET imaging that is an analog of rucaparib, with pharmacokinetic properties and PARP-specific binding properties similar to approved PARP-inhibiting drugs (22–26). As such, [^{18}F]FTT provides an *in vivo* radioligand imaging assay of regional PARP expression in tumors (22, 25, 26), predominantly PARP-1 (23). Other PET compounds for PARP imaging are also under preclinical and clinical development (27, 28). We have previously demonstrated that PET uptake of [^{18}F]FTT correlates with PARP-1 expression in ovarian cancer tumor tissue, validating its biologic target (25). Kinetic analysis of dynamic imaging revealed biologic insight into the radiotracer uptake mechanism and supported a static imaging protocol suitable for widespread clinical use (26). As a noninvasive marker of regional drug-target binding amenable to serial measurements, we expect that this PET radiotracer could serve as a noninvasive imaging biomarker of PARPi drug-target engagement to guide therapy (29).

In most clinical trials investigating new targeted agents, response to therapy is typically assessed anatomically by imaging (e.g., using the RECIST1.1 criteria; ref. 30). An effective therapy should lead to a decrease in size of target lesions, indicative of tumor cell death (30). However, such anatomic changes often lag months behind the molecular response (31), hampering the ability to quickly adapt treatment early in the course of therapy to avoid futility and unnecessary toxicity. By imaging the molecular pharmacodynamic response to therapy—including drug-target engagement or downstream molecular sequelae—treatment effects can be revealed sooner, facilitating new treatment paradigms. We hypothesized that PARP-1 expression, measured prior to PARPi treatment, and PARPi drug-target engagement measured after a short exposure to PARPi, can be leveraged as a biomarker to predict response to PARPi therapies.

Herein, we describe pilot translational studies of [^{18}F]FTT as a biomarker of response to PARPi in ovarian cancer. We first explore [^{18}F]FTT in preclinical models of ovarian cancer using patient-derived xenografts (PDX), followed by pilot data from a phase II clinical trial integrated biomarker study in ovarian cancer subjects.

Materials and Methods

Therapeutic agents

Olaparib (PARPi, AZD2281) and ataxia–telangiectasia inhibitor (ATRi, AZD6738) were provided by AstraZeneca. [^{18}F]FTT was produced at the Cyclotron Facility at the PET Center of the University of Pennsylvania (UPENN) as described previously (22). Specific activity ranged from 2,170 to 21,325 mCi/μmol, and radiochemical purity was ≥99.7%.

Preclinical studies

Ovarian cancer PDX studies

NSG mice (NOD/SCID IL2Rγ$^{-/-}$) were purchased from the Stem Cell and Xenograft Core at the UPENN. All mice were housed according to the UPENN Institutional Animal Care and Use Committee. Studies were performed in accordance with approved UPENN IUCAC protocol (#806772). Tumor was obtained from ovarian cancer debulking surgeries conducted at the Hospital of the UPENN and Pennsylvania Hospital (IRB #702679). PDXs were generated by surgically engrafting three to four pieces (2–3 mm each) orthotopically to the mouse fallopian tube/ovary (32). For preclinical studies, cryopreserved tissue was thawed and retransplanted to the fallopian tube/ovary of 6- to 8-week-old female NSG mice for evaluation of *in vivo* drug response and microPET imaging of PARPi drug-target engagement. For PARPi-resistant PDX models, once tumor volume reached 40 to 50 mm^3, animals were pretreated with olaparib (75 mg/kg/day, oral gavage 6 days weekly) and after a 2-fold increase in volume (confirming PARPi resistance), were randomized to treatment arms. For the microPET imaging cohort, a 7-day PARPi washout period occurred prior to continuation with the study.

Preclinical efficacy and microPET/CT imaging

We evaluated the efficacy of olaparib and AZD6738 (ATRi), as single-agents and in combination in a placebo-controlled study. Alongside preclinical efficacy studies, we performed serial [^{18}F]FTT microPET imaging in a cohort of mice with identical treatment groups. Three PDX models were evaluated to compare a PARPi-sensitive model (WO-3, germline *BRCA2*^{MUT} [g*BRCA2*^{MUT}]) to two PARPi-resistant models (WO-33 [g*BRCA1*^{MUT}]; WO-58 [g*BRCA1*^{MUT}, *CCNE1* amplified copy number 7, efficacy studies reported previously; ref. 33]). Once tumor volumes reached 70 to 100 mm^3, animals were randomized to treatment groups. PARPi-resistant models WO-33 and WO-58 were treated at 75 mg/kg olaparib D1–6, 50 mg/kg ATRi D1–5, or combination, whereas WO-3 was treated at 50 mg/kg olaparib D1–6, 25 mg/kg ATRi D1–5, or combination. Body Condition scores evaluating activity level, fur coat, body condition, appearance with score from 1 to 5 (5 being the healthiest) were used to assess for drug toxicity. Weekly ultrasonographic measurements (SonoSite Edge II Ultrasound System), weight assessments, and condition scores were obtained for treatment groups in a blinded manner. Mice in the efficacy cohorts were followed up to 300 days or removed from study due to tumor progression. For the imaging cohort, [^{18}F]FTT microPET was performed at baseline (prior to treatment) and to measure drug-target engagement 7 days from the initiation of therapy, which corresponds to treatment steady state. Primary measures of response were assessed as the percent change in tumor volume from the first microPET study.

PET/CT imaging and analysis of PDX models

Mouse imaging was performed on X-Cube micro-CT and β-Cube PET scanners (Molecubes). The X-Cube micro-CT was used for both anatomic localization of tumors (voxel resolution of up to 0.05 mm)

Downloaded from http://aacrjournals.org/clincancerres/article-pdf/29/8/1515/3320981/1515.pdf by University of Pennsylvania Libraries user on 06 August 2023

and for PET attenuation and scatter corrections (34). The β-Cube PET scanner has a 130 mm × 72 mm field of view, spatial resolution of 1 mm, and absolute peak sensitivity of 12.4%. PET images were acquired for 10 minutes starting 52.5 ± 6.0 minutes (±SD) post-injection of 7.26 ± 1.06 MBq of radiotracer (n = 91 including 47 baseline and 44 posttreatment PET scans). PET images were reconstructed via 3D maximum likelihood expectation maximization (MLEM) reconstruction with 20 iterations and 30 subsets with decay, scatter, and dead time corrections to generate cubic voxels with size 0.4 mm × 0.4 mm × 0.4 mm (34).

PMOD image analysis was used for WO-58 (n = 20), WO-3 (12 baseline and 10 posttreatment), and WO-33 mice (n = 15 baseline and 14 posttreatment; PMOD version 3.7, PMOD Technologies Ltd.). Radiotracer uptake by the tumor, reflected by standardized uptake value peak (SUV_{peak}), was quantified by calculating the average activity concentration in the five highest activity concentration voxels in a hand-drawn tumor volume of interest (VOI). A 5-mm diameter spherical VOI was drawn on normal hind leg muscle on the opposite side of the tumor to calculate tumor-to-background-muscle [^{18}F]FTT uptake ratios (T/M). T/M (vs. SUV) was chosen for the mouse models as it is more robust to variability from mouse injections and has been shown to correlate with SUV results in subjects (26).

Cell lines and primary cells

To infer changes in [^{18}F]FTT uptake seen with drug treatment in the PDX models, similar human cell lines were chosen for *in vitro* assays of PARP-1 expression levels pre- and posttherapy. JHOS4 (*BRCA1*^{MUT}) ovarian cancer cells, representative of PARPi-sensitive tumors, were grown in DMEM/F12 media with 10% FBS, and penicillin/streptomycin. PEO1 PARPi-resistant ovarian cancer cells (PEO1 PR, *BRCA2*^{MUT}) were developed by long-term drug exposure (>12 months; 3 μmol/L of olaparib) and grown in RPMI media with 10% FBS, and penicillin/streptomycin supplemented with olaparib. Prior to *in vitro* studies, PEO1 PR cells were grown without olaparib for 14 days for drug washout. JOSH4 cells and parental PEO1 cells were a generous gift from Dr. Ronny Drapkin, University of Pennsylvania and Dr. Andrew Godwin, University of Kansas, respectively. Cell lines were authenticated by short tandem repeats at the Oncogenomics Core (Wistar Institute) and confirmed mycoplasma negative by end-point PCR (Cell Center Service at UPENN).

RPPA analysis of ovarian cancer cells and PDX tumors

Ovarian cancer JHOS4 and PARPi-resistant PEO1 PR cells and select PDX tumors were evaluated by reverse phase protein array (RPPA) analysis. Cells were seeded and treated with 1 μmol/L PARPi, 1 μmol/L ATRi, or both for 72 hours. The cells were collected and lysed with SDS buffer prior to analysis. To infer PARP-1 expression changes *in vivo*, PARPi-resistant WO-57 [with a *BRCA1* reversion mutation (*BRCA1*^{REV})] PDX tumors harvested and banked from a previously reported preclinical study testing the efficacy of 75 mg/kg PARPi or 40 mg/kg ATRi alone or in combination were also assessed (33). Control and combination treatment samples were collected via biopsy 2 weeks posttreatment initiation. Tumors from control, monotherapy, and combination groups were collected at the survival endpoint. Samples were analyzed by the RPPA platform at the MD Anderson Center RPPA core facility as described (35). Antibodies targeting >300 proteins were included in this assay (see for detailed methods and antibody descriptions: http://www.mdanderson.org/education-and-research/resources-for-professionals/scientific-resources/core-facilities-and-services/functional-proteomics-rppa-core/index.html). The results were reported with normalized data at both linear and Log_2 version.

IHC of PDX tumors

PDX tumors were fixed in 10% buffered formalin then embedded in paraffin. Paraffin blocks were cut into 4- to 6-μm sections and placed onto slides. After deparaffinization and rehydration, antigen retrieval using citrate buffer was performed under pressure. Anti-PARP-1 antibody (RRID:AB_2679240) staining was optimized and set to a titer of 1:600. Slides were incubated with anti-rabbit HRP and developed using 3,3′-diaminobenzidine (DAB) and chromogen. H&E was performed on serial sections using the DAKO Cover-Stainer (Agilent). Sides were imaged at 20× using a Leica DM 2000 microscope.

Statistical analysis

Longitudinal analysis of PDX tumor growth was performed by linear mixed-effect modeling on log pre-processed tumor volumes followed by log transformation using the TumGrowth web tool (https://kroemerlab.shinyapps.io/TumGrowth/; ref. 36). [^{18}F]FTT T/M uptake ratios and percent change posttreatment were calculated for statistical comparisons. Two-tailed Spearman correlation of the percent change in tumor volume compared with the percent change in T/M was performed. Change in T/M across all models were tested for differences between groups using a one-way ANOVA test with a Tukey *post hoc* test, or Fishers least significant difference test (when specified). *In vitro* data were analyzed by ANOVA and Turkey *post hoc* test or two-tailed Mann-Whitney test when appropriate. Statistical significance was set at *<0.05, **<0.01, ***<0.001, and ****<0.0001 (GraphPad Prism v 9.1, RRID:SCR_002798).

Clinical trial

Trial design

This single-center, prospective, cohort study was approved by the UPENN Institutional Review Board (IRB #833685) and registered with the FDA as an expanded investigational new drug (clinical trial identifier: NCT02637934). All subjects provided written informed consent and studies were conducted in accordance with the Declaration of Helsinki statement on ethical biomedical research and the U.S. Common Rule. Women >18 years of age with known or suspected recurrent epithelial ovarian, fallopian tube, or primary peritoneal cancer were eligible for this study. Patients with HGSOC either with germline or somatic mutations in HR genes, or HRD positive tumors by standard CLIA approved assay (e.g., Myriad MyChoice CDx) were selected for enrollment. A baseline [^{18}F]FTT-PET scan prior to starting therapy (e.g., a PARPi) was required. A second [^{18}F]FTT-PET scan 1–21 days after initiation of therapy was requested.

Subjects were recruited through the Division of Gynecology Oncology at UPENN, with particular attention to recruiting subjects enrolled in two trials evaluating PARPi in ovarian cancer: the LIGHT trial and the CAPRI trial, or off trial with plan for treatment with a PARPi. The phase II LIGHT trial (NCT02983799) evaluated olaparib treatment in subjects with platinum-sensitive relapsed ovarian cancer stratified by *BRCA1/2*^{MUT} and HRD tumor status (37). The phase II CAPRI trial (NCT03462342) evaluated the combination of olaparib with an ATRi (AZD6738) in subjects with recurrent ovarian cancer, including platinum-sensitive, platinum-resistant, and platinum sensitive and PARPi resistant cohorts (38). Off trial patients with germline *BRCA1/2* mutations or had tumors positive for HRD (e.g., Myriad My Choice CDx), who were planning to receive treatment with a

Downloaded from http://aacrjournals.org/clincancerres/article-pdf/29/8/1515/3320981/1515.pdf by University of Pennsylvania Libraries user on 06 August 2023

PARPi treatment, were offered participation in the imaging clinical trial. For subjects enrolled on the [^{18}F]FTT imaging and CAPRI trials, posttherapy imaging (if obtained) was planned after the initiation of olaparib (5–7 days), but before the ATRi was initiated. Subjects were also recruited for the [^{18}F]FTT trial, who would be treated with a PARPi as standard-of-care for recurrent ovarian cancer outside of a clinical trial.

Baseline demographic and tumor characteristic data were collected, including germline/somatic alterations (e.g., *BRCA1, BRCA2*, and other homologous recombination repair gene defects). Progression-free survival (PFS) was calculated at the time from starting a PARPi to the time treatment stopped secondary to progression or death, or based on CA-125 levels, as determined by subjects treating physicians.

[^{18}F]FTT PET/CT imaging protocol and analysis

Subjects were imaged with [^{18}F]FTT as described previously (25, 26). Briefly, images were obtained from the skull base to the thighs on an Ingenuity TF scanner (Philips Healthcare) for 3 minutes/bed position for a total imaging time of 20 to 25 minutes, 60 to 90 minutes after intravenous injection with 8 to 12 mCi [^{18}F]FTT. [^{18}F]FTT-PET images were analyzed with MIM v7.1 (MIM Software Inc.) in a blinded manner by a board-certified nuclear medicine physician (ARP) and confirmed by a nuclear radiology fellow (SML). SUV_{max} data, normalized by body weight, were collected for lesions (primary tumors and/or metastases) identified as target lesions by the RECISTv1.1 criteria (30), described below. Only static imaging was used for this analysis, and no correction was made for partial volume correction, noting that SUV_{max} values at 60 minutes post-injection has been validated as a measure of PARP-1 expression (26). For subjects with follow-up PET imaging, percent change [^{18}F]FTT uptake was calculated as the percent difference between the sum of SUV_{max} on follow up compared with the sum at baseline (SUV), akin to RECISTv1.1 calculations (30).

Anatomic imaging evaluation

Anatomic images were evaluated by a board-certified radiologist (DAT) using RECISTv1.1 criteria, blinded to [^{18}F]FTT results. Target lesions (a maximum five total and a maximum two per organ) were selected on pretreatment studies among all lesions present based on a (i) RECISTv1.1 size criteria for measurability (≥15 mm in short-axis for nodal lesions and ≥10 mm in long-axis for nonnodal lesions), as well as with preference towards lesions with (ii) larger size, (iii) noncystic or necrotic appearance, (iv) well-defined boundaries such that accurate measurement at baseline and on follow-up assessments could be ensured as much as possible, and (v) representative sampling distribution among all involved organs/tissues. The changes in the sum of lesion diameters were used to provide an indication of index lesion response to which [^{18}F]FTT-PET results were compared. Best overall response (target plus nontarget tumor burden) was recorded for each subject.

Statistical analysis

Two-tailed Spearman correlation comparing percent change of SUV_{max} from baseline (SUV) measurements, percent change in tumor size (target lesion summed diameter) from CT atomic imaging, PFS, and percent change in CA-125 (baseline to nadir). For PFS, CA-125, and best RECIST response correlation analysis, the two subjects currently active on trial were censored and removed as data points. Blue lines in graphs show the best fit line (linear regression). As seven subjects were off trial, investigator determined PFS was used for analysis unless specified. Two-tailed Mann-Whitney test was performed comparing the PFS, change in CA-125 or change in anatomic imaging to the SUV at ≤ or >50% reduction in radiotracer uptake between scans.

Data availability statement

The data generated in this study are mostly available within the article and its supplemental files. Please contact the corresponding author for additional data requests.

Results

Correlation of [^{18}F]FTT-PET imaging with treatment response in PDX ovarian cancer models

PDX studies were used to (i) investigate changes in [^{18}F]FTT uptake in PDX tumors after treatment with PARPi, ATRi, or combination and (ii) serve as a mechanistic basis for interpreting clinical [^{18}F]FTT-PET studies. Study design for [^{18}F]FTT-PET-PDX experiments is depicted in **Fig. 1A**. For the PARPi-resistant, *BRCA1*^{MUT} WO-33 model, *in vivo* efficacy studies showed the best response in the combination treatment group (75 mg/kg olaparib + 50 mg/kg ATRi) compared with monotherapy ($P \leq 0.0002$, **Fig. 1B**, left). Previously, we reported findings for the PARPi-resistant, *BRCA1*^{MUT}/*CCNE*^{AMP} WO-58 model which showed modest activity with ATRi monotherapy and similar synergistic tumor regression with combination PARPi+ATRi treatment (33). The PARPi-sensitive, *BRCA1*^{MUT} WO-3 model (PARPi treatment naïve model) had a significant reduction in tumor volume with 50 mg/kg olaparib alone and more so when in combination with 25 mg/kg ATRi compared with control and ATRi monotherapy ($P < 0.0001$, **Fig. 1B**, right). Also, there was improvement in duration of tumor response for combination therapy compared with olaparib alone ($P = 0.013$), but there was no significant difference in size between these groups up to 20 weeks, times at which the combination showed clear benefit for the PARPi-resistant PDX models.

PET imaging was performed to assess the impact of PARPi, ATRi, and a combination of both drugs on [^{18}F]FTT uptake as an indication of drug-target engagement and possible predictor for tumor response. Once tumors had grown to about 70 mm^3, PDX models underwent drug wash out (for PARPi-resistant models which were treated with PARPi to confirm resistance), pretherapy PET/CT imaging, and were then randomized to treatment arms. All three PDX models showed PARP-1 expression pretherapy (Supplementary Fig. S1A), allowing for assessment of drug-target engagement with [^{18}F]FTT. In the PET-imaged cohort, the best response for the PARPi-resistant WO-33 and WO-58 models was observed in the combination treatment arm, similar to the efficacy studies; whereas no difference was observed in PARPi-sensitive WO-3. PET imaging with [^{18}F]FTT and representative pre- and posttreatment images are shown (**Fig. 1C**). [^{18}F]FTT tumor/muscle uptake ratios (T/M) were calculated for each animal to normalize for nonspecific uptake, and the % decline in T/M pretherapy and after 7 days of the selected treatment regimen was compared with % change in tumor volume at the same time. Of note, there was no significant antitumor effects seen by any treatment in all groups at this early time point. The majority of tumors actually increased in volume during the treatment week (Supplementary Fig. S1B). In addition, RPPA analysis suggests that there was no significant upregulation in apoptosis markers such as cleaved caspase 3, 7, or 8 in a PARPi-resistant PDX model (WO-57 *BRCA1*^{REV}) after 2 weeks of combination treatment (Supplementary Fig. S1C), indicating that 7-days posttreatment is an appropriate timepoint to measure drug-target engagement with minimal cytotoxic drug effect. The two PARPi-resistant PDX models showed a correlation

Downloaded from http://aacrjournals.org/clincancerres/article-pdf/29/8/1515/3320981/1515.pdf by University of Pennsylvania Libraries user on 06 August 2023

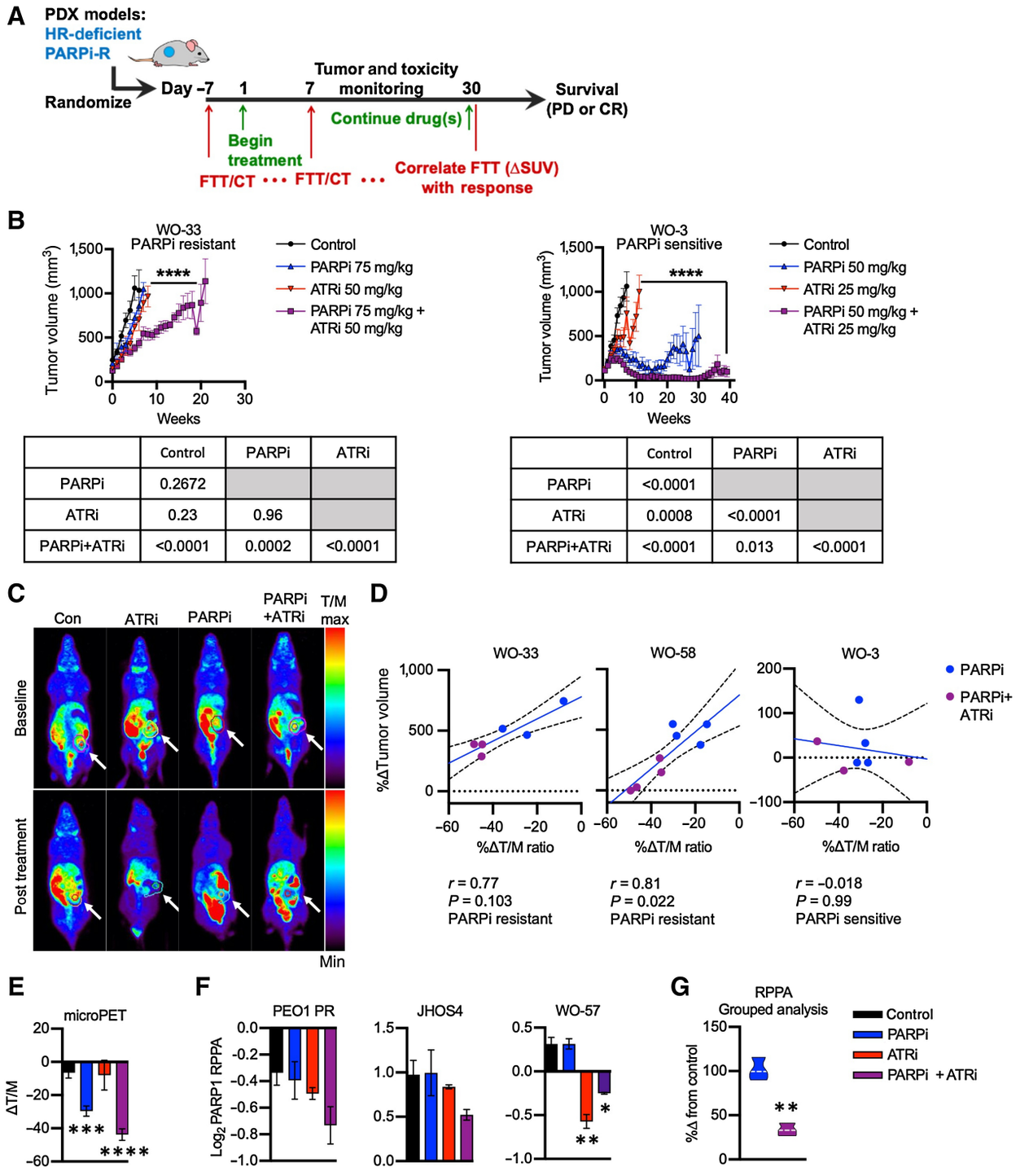

	Control	PARPi	ATRi
PARPi	0.2672		
ATRi	0.23	0.96	
PARPi+ATRi	<0.0001	0.0002	<0.0001

	Control	PARPi	ATRi
PARPi	<0.0001		
ATRi	0.0008	<0.0001	
PARPi+ATRi	<0.0001	0.013	<0.0001

Figure 1.

Preclinical imaging and therapy in PDX ovarian cancer models. **A,** Schema of preclinical *in vivo* efficacy and [^{18}F]FTT-microPET imaging studies. Preclinical HRD or PARPi-resistant PDX models were evaluated for PARPi+ATRi efficacy and the change in [^{18}F]FTT uptake before and after therapy. For the imaging cohort, mice were assessed for uptake of [^{18}F]FTT before drug treatment and 1 week after randomization then normalized by a tumor-to-muscle ration (ΔSUV). ΔSUV ΔT/M ratio was correlated to response measured by tumor volume. CR, complete response; PD, progressive disease. **B,** *In vivo* efficacy studies testing PARPi and ATRi monotherapy or combination in PARPi-resistant WO-33 (left) and PARPi-sensitive WO-3 (right) PDX models. Tumor volume data over time are shown and represented as mean ± SEM (n = 7–20 per group), and statistical analysis is shown. **C–E,** PARPi-1 expression as determined by [^{18}F]FTT PET/CT imaging. **C,** Representative [^{18}F]FTT-PET imaging pre- and post-PARPi (top and bottom, respectively). **D,** Spearman correlation of percent change of tumor volume (%Δ tumor volume) from baseline compared with ΔSUV, expressed as percent change in the tumor/muscle SUV ration (%ΔT/M) for mice treated with PARPi or PARPi+ATRi for 1 week across three PDX models: WO-33 and WO-58 (PARPi-resistant) and WO-3. **E,** Percent change in T/M ratio across all three models (Control, n = 16; ATRi, n = 6; PARPi, n = 11; PARPi+ATRi, n = 10). **F,** RPPA analysis for PARP-1 expression in PEO1 PR (*BRCA2*^{MUT}, PARPi-resistant), JHOS4 (*BRCA1*^{MUT}, PARPi-sensitive) cells and WO-57 (g*BRCA1*^{REV}, PARPi-resistant) PDX tumors. Data are represented as mean ± SD and analyzed by one-way ANOVA. Combined analysis of PARP-1 expression post-PARPi versus post-PARPi-ATRi across all cell lines is shown and analyzed by two-tailed Mann-Whitney test (**G**).

Downloaded from http://aacrjournals.org/clincancerres/article-pdf/29/8/1515/3320981/1515.pdf by University of Pennsylvania Libraries user on 06 August 2023

been % decline in [^{18}F]FTT T/M and % change in tumor size (WO-33, $r = 0.77$, $P = 0.103$; WO-58, $r = 0.81$, $P = 0.022$) when analyzed by PDX model (**Fig. 1D**). A greater decline in the [^{18}F]FTT T/M posttherapy correlated with greater abrogation of tumor growth. The WO-3 model, a PARPi treatment naïve model, which was especially sensitive to olaparib treatment alone, did not show this correlation ($r = -0.018$, $P = 0.99$), indicating that that the change in [^{18}F]FTT T/M with treatment was not simply a result of the impact of the change in tumor size. Lack of correlation in this model was likely secondary to the marked sensitivity of PARPi-monotherapy without an additive or synergistic effect of ATRi treatment.

To better understand the treatment-related changes in [^{18}F]FTT, we compared decreases in [^{18}F]FTT T/M across all models grouped by treatment type (**Fig. 1E**). Percent changes in [^{18}F]FTT T/M after olaparib treatment were significantly different across all models ($P < 0.0001$, ANOVA). *Post hoc* analysis revealed significant reduction in [^{18}F]FTT T/M in PARPi monotherapy and combination PARPi+ARTi compared with control ($P < 0.005$ and $P < 0.0001$, respectively). The improvement in drug-target engagement with the addition of ATRi to PARPi compared with PARPi monotherapy approached significance with correction for multiple comparisons ($P = 0.09$). Without correction for multiple comparisons, this comparison was significant ($P = 0.02$, uncorrected Fisher LSD), suggesting added benefit for these two agents given no significant benefit of ATRi or PARPi alone compared with control in PARPi-resistant models, as studied previously (33). We note, though, that these experiments were not powered to detect all differences between treatment pairs. Thus, although the data are limited by sample size, there appears to be an association between the impact of therapy on [^{18}F]FTT and efficacy in controlling tumor growth, particularly with combination therapy.

Effects of combination treatment on PARP-1 expression

Given [^{18}F]FTT changes with combined DNA damage response (DDR) inhibitor (PARPi-ATRi) treatment, we sought to better characterize the nature of the changes in [^{18}F]FTT uptake before and after treatment in the combination arm compared with olaparib control. We evaluated PARP-1 expression by RPPA using two human ovarian cancer cell lines: PARPi-sensitive JHOS4 (*BRCA2*^{MUT}) and PARPi-resistant PEO1 PR (*BRCA1*^{MUT}) cells, and tumors collected at the survival endpoint of a preclinical efficacy study (PARPi-resistant WO-57, *BRCA1*^{REV}). PARPi treatment did not lead to a decrease in PARP-1 expression in any of the models. Only WO-57 tumors showed a significant decline with ATRi, alone ($P = 0.0019$) and in combination with olaparib ($P = 0.01$), highlighting the effects on PARP-1 expression *in vivo* after therapy (**Fig. 1F**). However, a trending decrease in PARP-1 expression was observed in PEO1 PR and JHOS4 cells with combination PARPi-ATRi treatment after 72 hours. When models were grouped together, there was a clearly significant difference in the impact of PARP-1 expression for PARPi monotherapy (no-change) and combination PARPi-ATRi therapy (significant reduction in PARP-1 expression, $P = 0.0035$; **Fig. 1G**). Comparing the changes in [^{18}F]FTT uptake *in vivo* and PARP-1 expression for PARPi alone versus PARPi-ATRi combination therapy suggests that the decline in [^{18}F]FTT uptake represents the combined effect on [^{18}F]FTT binding by competition for the PARPi binding site with much higher levels of therapeutic PARPi and any reduction in PARPi expression caused by the ATRi combination. This provides an impetus for further study of [^{18}F]FTT as a tool for understanding the pharmacodynamic impact of combination therapy.

Phase 2 clinical trial to evaluate [^{18}F]FTT-PET as a biomarker for PARPi therapy in ovarian cancer

Sixteen subjects with HGSOC are included in the following analysis. Subject details of genetic mutations are provided in **Table 1** and baseline characteristics are summarized in Supplementary Table S1. The subjects' ages ranged from 46 to 72 years, and they had pathogenic or likely pathogenic mutations in HRR genes or had tumors that were HRD by a CLIA approved assay. Of those subjects with genetic testing performed, 31.3% had germline *BRCA1/2* mutations (5 of 16), 18.8% had germline *RAD51C, RAD51D*, or *ATM* mutations (3 of 16). 41.7%

Table 1. Summary of germline, somatic, and HRD testing for subjects on study.

Subject	Germline MPT	Somatic HRR gene alterations	HRD	Additional somatic gene alterations of interest and testing company	
1	*BRCA1*	*BARD1*	NA	*TP53*	Caris
2	*BRCA1*	Negative	Negative	NA	NA
3	Negative	NA	Positive	NA	NA
4	Negative	Negative	Negative	*TP53; ARID1A; CHEK2*	Caris
5	*BRCA2*	NA	NA	NA	NA
6	*BRCA1*	*BRCA1*	Positive	*TP53; ATRX*	Caris
7	*RAD51C*	NA	NA	NA	NA
8	Negative	Negative	Positive	none	Caris
9	Negative	*BRCA1*	NA	*TP53*	Caris
10	Negative	*BRCA1*	Positive	*TP53;* High genomic LOH (28%)	Caris
11	Negative	Negative	Positive	*TP53; PIK3CA*	Caris
12	Negative	*BRCA1*	NA	*TP53*	Caris
13	Negative	*BRCA1*	NA	*TP53; FGFR1* fusion; High genomic LOH (32%); *BRCA1* likely reversion	Caris
14	*ATM*	*ATM*	Positive	*TP53*	Caris
15	*RAD51D*	Negative	NA	*TP53*	Caris
16	*BRCA1*	NA	NA	NA	NA

Abbreviations: MPT, multigene panel testing, including *ATM, BRCA1/2, BRIP1, RAD51C/D, PALB2, MLH1, MSH2, MSH6, PMS2, EPCAM (*deletion/duplication), and Lynch genes; NA, not available.

Downloaded from http://aacrjournals.org/clincancerres/article-pdf/29/8/1515/3320981/1515.pdf by University of Pennsylvania Libraries user on 06 August 2023

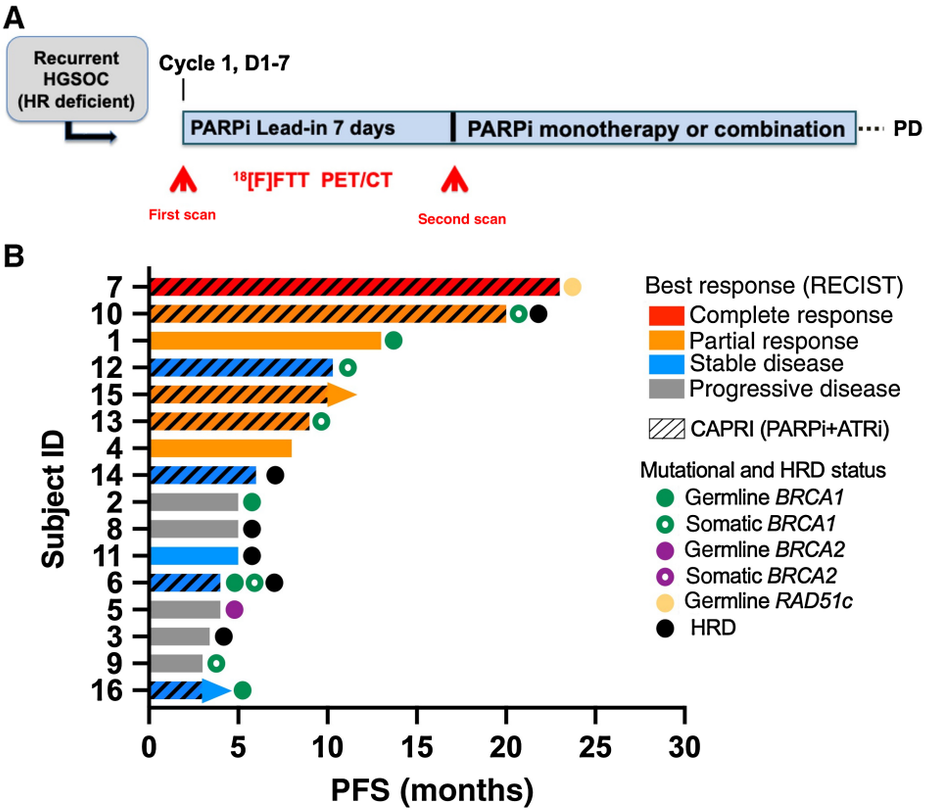

Figure 2.
Clinical trial design and PFS on treatment. **A,** Schematic of the clinical trial design. PD, progressive disease. **B,** Swimmer plot for PFS on treatment. Sixteen subjects were evaluated by RECISTv1.1. All subjects received a PARPi unless indicated for PARPi+ATRi (CAPRI) combination. Somatic and germline mutations of interest and HRD tumor status are indicated. Arrows indicate subjects still on trial and undergoing treatment at the time of analysis.

had somatic *BRCA1/2* mutations (5 of 12). Somatic mutations detected in other HRR genes, included *ATM* and *CHEK2*. Seventy five percent (6 of 8) subjects had HRD tumors by positive assay. The PARPi treatment course and response is delineated per subject in Supplementary Table S2. Eight subjects (50%) enrolled in the FTT trial, received combination PARPi-ATRi, and all others received PARPi alone. Of note, four subjects across both treatment regimens received prior lines of PARPi, namely olaparib or rucaparib.

Clinical trial imaging study design is outlined in **Fig. 2A**. Briefly, all 16 subjects had baseline [^{18}F]FTT-PET imaging prior to starting a PARPi (olaparib), and 13 subjects had paired baseline and second [^{18}F]FTT-PET imaging scans after a short interval after initiation of olaparib, after which they continued olaparib therapy ($n = 5$) or olaparib therapy plus ATRi (ceralsertib; $n = 8$; Supplementary Table S2). The time of the second [^{18}F]FTT-PET after PARPi initiation ranged from 4 to 14 days (median of 7 days and mean of 11 days for all data) with the goal to assess for ability to block uptake of [^{18}F]FTT. A single subject had imaging at 55 days after baseline imaging secondary to scheduling during the COVID pandemic. The time between [^{18}F]FTT-PET scans did not impact the change in SUV uptake between scans (Supplementary Fig. S2A), and low-dose CT imaging obtained (for attenuation correction and anatomic localization and not RECIST measurements) with the PET scan did not show a significant change in tumor volume between scans during this interval between first and second scans (Supplementary Fig. S2B).

Target lesions identified on baseline anatomic imaging per RECIST criteria numbered from 1 to 4 (median 1.5) with 8 subjects having one target lesion with partial volume effects mitigated as lesions were selected based on RECISTv1.1 criteria. Two target lesions in two separate subjects identified anatomically were not well seen on baseline [^{18}F]FTT-PET and excluded from this analysis. Both of these lesions were adjacent to the liver, with physiologic uptake in the liver precluding accurate assessment.

For determination of time-to-progression, the date of the baseline [^{18}F]FTT scan served as day 0 (also the first day of initiation of PARPi). Target lesions were identified on anatomic imaging obtained prior to treatment, ranging from 47 days before [^{18}F]FTT scan to 6 days after (median and mean of 15 and 18 days before, respectively). First anatomic follow-up assessment by RECIST occurred at a median of 68 days and a mean of 93 days (range from 57 to 158 days). Best RECIST measurements occurred at a median of 179 days and a mean of 166 days (range from 57 to 351 days). Baseline SUV ranged from 1.68 to 10.23, and follow-up SUV ranged from 1.36 to 3.1. Representative [^{18}F]FTT-PET/CT imaging for subjects with and without response to PARPi by RECIST are shown (**Fig. 3**).

For study analysis, two subjects were excluded from CA-125 data due to missing data. Also, subjects 15 and 16 were censored and thus excluded from PFS, best CA-125 response, and best RECIST response analysis as these subjects remained on trial at the time of this analysis (note that subjects are responding to treatment; and are denoted in red when graphed). PFS ranged from 3 to 23 months, with a median of 5.5 months and a mean of 8.5 months (SD of 6.2; **Fig. 2B**). Combination therapy was associated with a greater than 6-month PFS, inclusive of a subject still on trial at 10 months ($P = 0.036$, Chi-squared test).

[^{18}F]FTT correlation with anatomic response to PARPi treatment

We first studied the ability of the change in [^{18}F]FTT-PET uptake after PARPi initiation to predict drug response by anatomic/CT

Downloaded from http://aacrjournals.org/clincancerres/article-pdf/29/8/1515/3320981/1515.pdf by University of Pennsylvania Libraries user on 06 August 2023

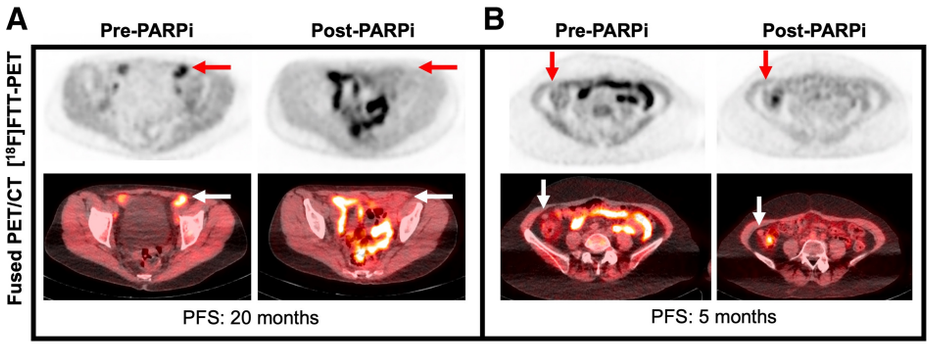

Figure 3.

Representative clinical imaging of [^{18}F]FTT-PET/CT in a PARPi responder and nonresponder. [^{18}F]FTT-PET and fused PET/CT images are shown for a PARPi responder (subject 10, *BRCA1*^{MUT}; PFS = 20 months; **A**) and nonresponder (subject 11, *BRCA1/2*^{WT}, HRD positive; PFS = 5 months; **B**). **A,** Pre-PARPi [^{18}F]FTT-PET/CT demonstrates [^{18}F]FTT uptake in a left external iliac lymph node (SUV_{MAX} of 5.2). Imaging performed 8 days later, and after starting olaparib, demonstrates decreased [^{18}F]FTT uptake (SUV_{MAX} of 2), representing successful receptor targeting of the PARPi. **B,** Pre-PARPi [^{18}F]FTT-PET/CT demonstrates no uptake above background in a right peritoneal implant (SUV_{MAX} of 1.7) suggestive of absent PARP-1 expression and PARPi drug target, thus no therapeutic effect of PARPi. Imaging performed 6 days later, and after starting olaparib, demonstrates no decrease in [^{18}F]FTT uptake (SUV_{MAX} of 2). As expected, this subject had a relatively short PFS.

imaging using RECISTv1.1. A correlation was observed between RECIST response at first evaluation and SUV on a per subject ($r = 0.60$, $P = 0.034$; **Fig. 4A**), but not on a per lesion basis (Supplementary Fig. S3A). When assessing the correlation between SUV (per subject) and the best RECIST response, there was an even greater correlation ($r = 0.75$, $P = 0.01$) demonstrated (**Fig. 4B**). Subjects with a >50% decrease in SUV had a significant reduction in anatomic size with treatment versus those who did not achieve such a ^{18}F]FTT-PET response (**Fig. 4A** and **B**; first response, $P = 0.022$; best response, $P = 0.009$, respectively). Using baseline SUV as opposed to SUV also did not yield associations with first anatomic response (Supplementary Figs. S4A and S4B).

[^{18}F]FTT and correlation with response by CA-125

We next assessed the correlation of FTT imaging with the best response by CA-125, a tumor marker indicative of overall disease burden (percent change in baseline to nadir). [^{18}F]FTT SUV demonstrated a significant correlation with change in CA-125 ($r = 0.73$; $P = 0.033$; **Fig. 4C**). SUV threshold again dichotomized the CA-125 response. Subjects with >50% decrease in SUV all had a >50% decrease in CA-125, whereas subjects who did not experience this degree of SUV uptake decrease, did not achieve a CA-125 response ($P = 0.016$). A threshold of at least a 50% decrease in CA-125 defines a response by the Gynecologic Cancer Intergroup (GCIG), providing clinical relevance for this metric (39). SUV compared with GCIG criteria for response, resulted in a similar trend (Spearman: $r = 0.64$, $P = 0.07$; T test: $P = 0.016$; Supplementary Fig. S5A).

Similar to RECIST results, a correlation was not seen with this outcome measure and baseline SUV only ($r = -0.28$, $P = 0.40$; Supplementary Fig. S4C). These findings again indicate the value of drug-target engagement measured by [^{18}F]FTT over drug-target expression alone. Change in size by first RECIST response (median 58 days) was also not associated with eventual best CA-125 response ($r = 0.58$, $P = 0.11$; Supplementary Fig. S3B), noting that the best CA-125 response could occur anytime during treatment. As expected, the outcome measures of PFS and CA-125 were correlated ($r = -0.92$, $P = 0.0016$; Supplementary Fig. S5B).

Evaluation of [^{18}F]FTT to predict PFS

Next, we studied the ability of [^{18}F]FTT-PET uptake prior to PARPi treatment and/or change in [^{18}F]FTT after initiation of a PARPi compared with baseline to serve as a biomarker predictive of PFS. A significant correlation was seen between provider determined PFS (as imaging not obtained consistently off trial) and percent change in SUV_{max} between baseline and post-PARPi (short interval) imaging (SUV; $r = -0.67$, $P = 0.027$; **Fig. 4D**). As [^{18}F]FTT uptake decreased, indicative of drug-target engagement, PFS increased. All five subjects demonstrating a decline in SUV ≤50% had PFS ≤6 months. Conversely, all six subjects with decline in SUV >50% had >6-month PFS. Dichotomizing subjects by this SUV threshold of 50% (or similarly a PFS of 6 months) yielded significant differences in PFS ($P = 0.004$; **Fig. 4D**). PFS by RECIST had a similar trend ($r = -0.6$, $P = 0.056$) and comparing >/≤ 50% SUV revealed similar results ($P = 0.0087$; Supplementary Fig. S5C). Baseline [^{18}F]FTT uptake alone did not yield a significant correlation with PFS ($r = 0.26$, $P = 0.37$; Supplementary Fig. S4D), suggesting that the level of drug binding to target alone was not sufficient to predict response. PFS and percent change in lesion size by first assessment on CT by subject also demonstrated a significant correlation ($r = -0.65$, $P = 0.035$; Supplementary Fig. S3C), noting that the first RECIST assessment was obtained after the post-PARPi [^{18}F]FTT-PET (median 68 days vs. 7 days, respectively), increasing the clinical relevance of the PET imaging data. Together given RECIST, CA-125, and PFS correlation with [^{18}F]FTT target engagement, [^{18}F]FTT-PET may serve to further identify patients who may benefit clinically from PARPi therapy.

[^{18}F]FTT-PET in PARPi-resistant subjects

Patients with HRD ovarian cancers should receive a PARPi. Most patients benefit but PARPi resistance ultimately often emerges. Two subjects had benefited and then progressed on a PARPi, then underwent assessment with [^{18}F]FTT-PET/CT (prior to enrollment onto CAPRI for combination PARPi-ATRi; NCT03462342). Subject 13 completed olaparib 300 mg twice daily for 14 months prior to progression and underwent subsequent [^{18}F]FTT-PET imaging after drug washout. Subject #16 completed two years of rucaparib therapy nearly 6 years before enrollment

Downloaded from http://aacrjournals.org/clincancerres/article-pdf/29/8/1515/3320981/1515.pdf by University of Pennsylvania Libraries user on 06 August 2023

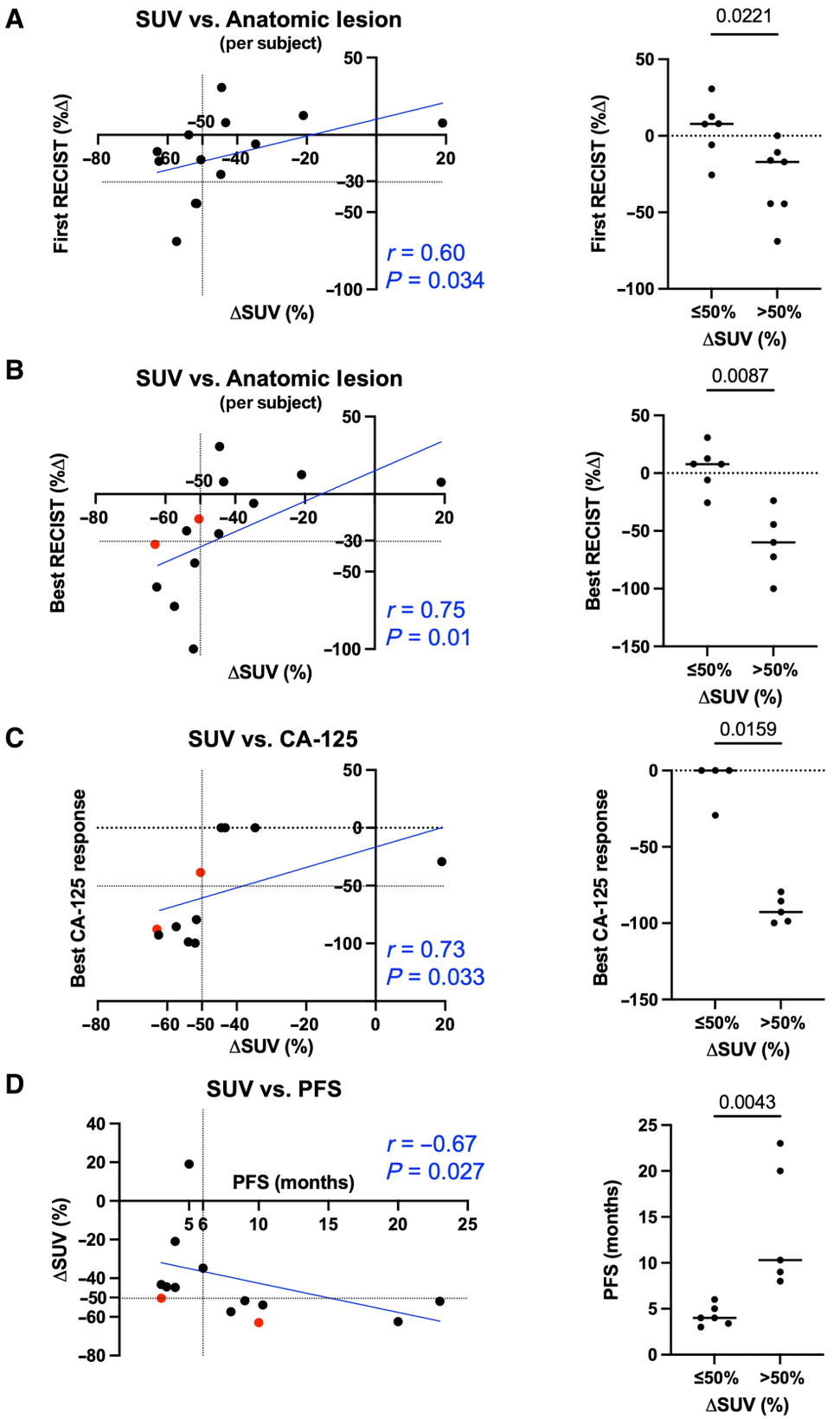

Figure 4.

[^{18}F]FTT imaging to predict PARPi response. **A** and **B,** Spearman correlation [^{18}F]FTT SUV versus the change of lesion size per subject (1–4 target lesions averaged) from anatomic baseline to first RECIST response (obtained 57–158 days after baseline by CT, **A**) or best RECIST response (obtained 57–351 days after baseline by CT, **B**). **C,** Spearman correlation SUV versus the best CA-125 response. **D,** Spearman correlation of change in [^{18}F]FTT SUV from baseline to after starting PARPi therapy (SUV) versus PFS. **A–D**, Two-tailed *T* test of PFS, CA-125 response, and RECIST response at ≤50% and >50% reduction are shown. When appropriate, two subjects (shown in red) were excluded from statistical analyses (Spearman and Mann-Whitney) as these subjects are currently on trial.

Downloaded from http://aacrjournals.org/clincancerres/article-pdf/29/8/1515/3320981/1515.pdf by University of Pennsylvania Libraries user on 06 August 2023

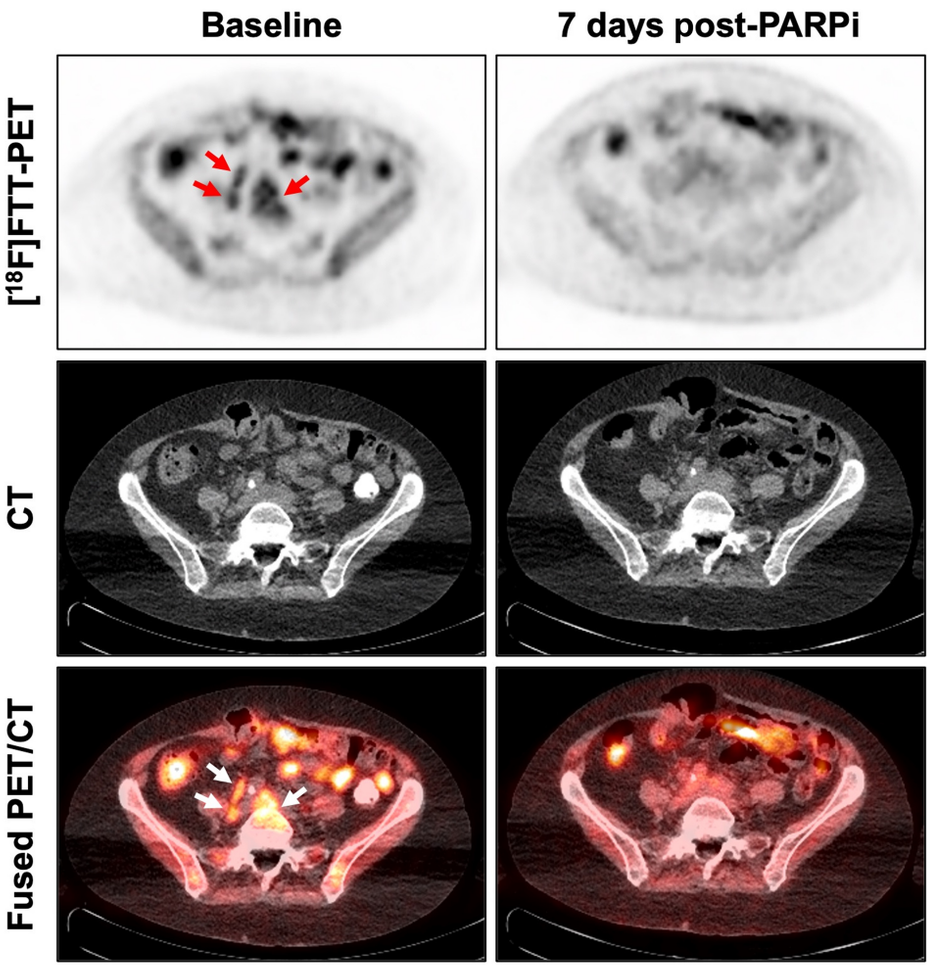

Figure 5.
[^{18}F]FTT-PET on subject previously treated with PARPi. Subject 16 previously progressed on a PARPi nearly 6 years prior to enrolling in the CAPRI trial. [^{18}F]FTT-PET uptake is seen in retroperitoneal lymph nodes at baseline (left), with abrogation of signal on [^{18}F]FTT-PET obtained 7 days after initiating olaparib (right). Findings indicate PARPi drug target expression with subsequent therapeutic effect. This subject remains on trial with an encouraging early response.

on the CAPRI trial, with six cycles of carboplatin/taxol also completed in the interim. Both subjects demonstrated [^{18}F]FTT uptake at baseline followed by abrogation of signal after PARPi run-in (52% and 50% decrease for #13 and #16, respectively) with subject #13 having a relatively long PFS of 9 months. Subject 16 is currently responding to therapy after 3 months and is still on trial. Representative [^{18}F]FTT-PET/CT imaging is shown for both subjects (#13, Supplementary Fig. S6; #16, **Fig. 5**). The constellation of findings suggests continued expression of PARP-1 in these previously resistant tumors and therapeutic effect of PARPi combination, advocating for further study for PARPi retreatment and combined approaches in these tumors and the potential utility of [^{18}F]FTT-PET/CT in PARPi-resistant patients.

Discussion

Because the initial approval of olaparib in 2014, treatment of HGSOC with PARPi is standard of care. Indeed, three PARPi are currently approved—olaparib, rucaparib, and niraparib—with broadening clinical indications from ovarian cancer and including now other malignancies (pancreas, prostate, and breast cancer). Patient selection for these targeted agents, though, leverages associations of drug efficacy with underlying genetic mutations or prior sensitivity to platinum agents, without direct measurement of tumoral drug-target expression or engagement. PARP-1 is the major target of PARPi with PARP-2 and PARP-3 less so (40). A target-specific biomarker has the potential to guide therapy identifying patients who will benefit with the goal to ultimately improve patient outcomes. In this study, we evaluated the utility of a non-invasive PET imaging agent of PARP-1 expression, [^{18}F]FTT, to guide PARPi treatment, both as a biomarker for current agents as well as a tool for future drug development, and in particular, combination DDR inhibitor therapies.

Preclinical human PDX studies support the ability of [^{18}F]FTT to measure the early pharmacodynamic effect of PARPi monotherapy and in combination with ATRi, with PARP-1 protein expression studies providing insight into the molecular mechanism (**Fig. 1**). As expected, PARPi administration led to a decrease in radiotracer uptake as evidence by measuring [^{18}F]FTT T/M. The addition of an ATRi led to a further abrogation of tracer uptake, suggesting an additive effect. PARP-1 protein expression studies provided a plausible molecular mechanism for this phenomenon. Unlike single-agent PARPi therapy, the addition of ATRi decreased PARP-1 expression. The combination of blocking and decreased target expression would therefore be expected to lead to a larger decrease in PET signal compared with blocking alone with PARPi monotherapy. The extent of [^{18}F]FTT signal decrease correlated with anatomic size changes in the two PARPi-resistant tumors after therapy, with clear separation between the effects of PARPi monotherapy and combination PARPi-ATRi. That is, as drug-target engagement increases, either PARPi binding to the PARP-1 binding site or ATRi reduction in PARP-1 expression,

Downloaded from http://aacrjournals.org/clincancerres/article-pdf/29/8/1515/3320981/1515.pdf by University of Pennsylvania Libraries user on 06 August 2023

seen as a decline in [^{18}F]FTT uptake pre- and posttherapy, anatomic growth slowed. In a PARPi-sensitive model, such a correlation was not revealed, likely due the robust sensitivity to PARPi monotherapy where there was no added benefit to combination therapy, underscoring the utility for [^{18}F]FTT in guiding use for combination therapies. Finally, tumor growth curves demonstrated the additive synergistic effects of combination therapy, corroborating prior studies with the xenograft models (33). These results add to the literature investigating the underlying biology of PARPi-ATRi combination therapy (33), a promising therapy to overcome PARPi- and platinum-resistance, and supports the use of [^{18}F]FTT as an investigational tool to facilitate drug development.

This preclinical data support the ability to assess PARPi-target engagement for combinations of PARPi with other relevant DDR agents. Such preclinical investigation could help guide clinical studies by identifying combination effects *in vivo*. Indeed, the Phase II CAPRI clinical trial is underway evaluating the combination of ceralasertib (AZD6738), an ATRi, plus olaparib in subjects with recurrent, platinum sensitive (cohort A) and PARPi-resistant (Cohort C and D) ovarian cancer. Results from the platinum-resistant cohort demonstrate some activity of this combination, particularly in HR-deficient subjects (38). More strikingly, the PARPi-ATRi combination demonstrated efficacy in a cohort of subjects who had previously progressed on prior PARPi, representing human translation of the findings in animal models (41).

In the early human studies with [^{18}F]FTT-PET imaging presented here, the difference of [^{18}F]FTT uptake post-PARPi compared with baseline, indicative of drug-target engagement, appeared to identify patients most likely to benefit from PARPi therapy only ∼1 week after treatment initiation (**Fig. 4**). Most strikingly, SUV and not baseline SUV alone, correlated with first and best response to treatment by RECIST. Moreover, subjects with greater than 50% decrease in [^{18}F]FTT uptake had a PFS greater than 6 months, whereas those who had less than 50% decrease had a PFS less than 6 months. A similar dichotomy was seen with the best CA-125 response: subjects with a greater than 50% decrease in [^{18}F]FTT signal also had a greater than 50% decrease in CA-125, with the converse also true. Change in lesion size by CT (RECIST) correlated with PFS, but not CA-125 response (Supplementary Figs. S3B and S3C), again noting that RECIST assessments took place a median of 2 months after the paired [^{18}F]FTT scans. Importantly, leveraging a PET measure of drug-target engagement to predict response has previously been demonstrated with estrogen receptor imaging agent, [^{18}F]Fluoroestradiol (FES), and targeted estrogen-therapy (42, 43), providing a model for translation of this paradigm. However, the pretherapy [^{18}F]FTT uptake, which provides a measure of PARP-1 expression, alone did not predict response to therapy. This finding deserves further study, but suggest that estimates of drug-target engagement using serial imaging may be important in predicting response to PARPi ± combination therapy.

The preclinical reduction of [^{18}F]FTT-PET signal with the addition of ATRi to PARPi therapy compared with PARPi alone suggests synergistic effects of these agents, which is beginning to be born out in clinical trials (41). Subjects in our human imaging trial treated with combination therapy, though, were imaged after a PARPi run-in and prior to the addition of ATRi, demonstrating predictive value for combined therapy and the identification of patients with preserved PARP-1 expression and tracer uptake blockade with therapeutic PARPi. Future studies at our center will include imaging patients soon after the initiation of PARPi-ATRi combination therapy to study the earlier biomarker application of [^{18}F]FTT to infer the impact of the combined therapy similar to the mouse studies. Future study might evaluate [^{18}F]FTT as a tool to select drug dosages in the development of new PARPi. Dosing to pharmacologic endpoint of complete blockade of [^{18}F]FTT signal, as opposed to intolerable side effects, may prove especially valuable. A similar strategy has been used with FES in the development of new ER-blocking agents (44).

This study has a number of limitations, most noticeably the limited number of mouse models and clinical trial patients. The hypothesis generated here should be studied in larger trials, including multicenter studies. Additional studies should also include [^{18}F]FTT-PET imaging after combination therapies, which were not performed here, but which are supported by preclinical studies. Decrease in [^{18}F]FTT uptake decline could also indicate general cytotoxic drug effect resulting in overall less viable tumor or cleavage of the DNA-binding domain of PARP 1 or 2 during apoptosis by cleaved caspase 3/7 or 8, respectively (45, 46). Evidence from our studies including no change in tumor volume between clinical scans (Supplementary Fig. S2B), supporting that viable tumor has not substantially changed. Tumor growth during initial treatment phase in preclinical studies (Supplementary Fig. S1B), and no significant upregulation of apoptosis markers by RPPA in a PDX model after 2 weeks of treatment (Supplementary Fig. S1C), provide compelling evidence that any apoptosis effects are below biologic levels and not significantly contributing to [^{18}F]FTT uptake decline. Further validation of the lack of cell/tumor dropout as contributing to the decline in [^{18}F]FTT uptake in tumors could be performed by pairing [^{18}F]FTT scans with FDG scans, as was done in a prior study of ER expression using [^{18}F]Fluoroestradiol PET paired FDG-PET (47).

Overall, the preclinical and early human studies described herein provide the first evidence of a PARPi-PET radiotracer to serve as an early biomarker to guide PARP-targeted therapies. Such information, obtained noninvasively and across the burden of disease, has potential to advance precision medicine and improve outcomes with PARPi. Further larger studies are needed to validate these findings.

Authors' Disclosures

A.R. Pantel reports grants from Basser Center for BRCA, NIH KL2TR001879, and DOD OC160269 during the conduct of the study as well as personal fees from Blue Earth Diagnostics and GE and grants and personal fees from Progenics outside the submitted work. D.A. Torigian reports employment with Quantitative Radiology Solutions LLC. L.P. Martin reports personal fees and other support from Sutro Biopharma and ImmunoGen and other support from Mersana and AstraZeneca outside the submitted work. G.B. Mills reports grants, personal fees, nonfinancial support, and other support from Amphista, AstraZeneca, Chrysallis Biotechnology, GSK, ImmunoMET, Ionis, Lilly, PDX Pharmaceuticals, Signalchem Lifesciences, Symphogen, Tarveda, Turbine, Zentalis Pharmaceuticals, Catena, HRD assay to Myriad Genetics DSP to NanoString, Adelson Medical Research Foundation, Breast Cancer Research Foundation, Komen Research Foundation, Ovarian Cancer Research Foundation, Prospect Creek Foundation, NanoString Center of Excellence, Ionis (provision of tool compounds), and Genentech during the conduct of the study as well as grants, personal fees, nonfinancial support, and other support from Amphista, AstraZeneca, Chrysallis Biotechnology, GSK, ImmunoMET, Ionis, Lilly, PDX Pharmaceuticals, Signalchem Lifesciences, Symphogen, Tarveda, Turbine, Zentalis Pharmaceuticals, Catena Pharmaceuticals, HRD assay to Myriad Genetics, DSP to NanoString, Adelson Medical Research Foundation, Breast Cancer Research Foundation, Komen Research Foundation, Ovarian Cancer Research Foundation, Prospect Creek Foundation, NanoString Center of Excellence, Ionis (provision of tool compounds), and Genentech outside the submitted work. R.K. Doot reports grants from PARP-Targeting PET Tracer to Guide DDR Inhibitor Therapy and Department of Defense during the conduct of the study. D.A. Mankoff reports other support from Trevarx outside the submitted work as well as membership on a Trevarx Scientific Advisory Board. R.H. Mach reports other support from Trevarx outside the submitted work; in addition, R.H. Mach has a patent issued

Downloaded from http://aacrjournals.org/clincancerres/article-pdf/29/8/1515/3320981/1515.pdf by University of Pennsylvania Libraries user on 06 August 2023

and licensed to Trevarx and is also the co-founder of Trevarx. L.L. Lin reports other support from Trevarx and grants from AstraZeneca, Pfizer, and Varian outside the submitted work. F. Simpkins reports grants, personal fees, and nonfinancial support from AstraZeneca during the conduct of the study. No disclosures were reported by the other authors.

Authors' Contributions

A.R. Pantel: Conceptualization, resources, data curation, software, formal analysis, supervision, funding acquisition, validation, investigation, visualization, methodology, writing–original draft, project administration, writing–review and editing. **S.B. Gitto:** Data curation, software, formal analysis, investigation, visualization, writing–original draft, writing–review and editing. **M. Makvandi:** Conceptualization, resources, data curation, software, formal analysis, supervision, funding acquisition, validation, investigation, visualization, methodology, writing–original draft, project administration, writing–review and editing. **H. Kim:** Data curation, investigation, methodology, writing–review and editing. **S. Medvedv:** Data curation, investigation, methodology, writing–review and editing. **J.K. Weeks:** Data curation, writing–review and editing. **D.A. Torigian:** Data curation, software, formal analysis, methodology, writing–review and editing. **C.-J. Hsieh:** Data curation, software, formal analysis, investigation, methodology, writing–review and editing. **B. Ferman:** Data curation, investigation, writing–review and editing. **N.A. Latif:** Investigation, writing–review and editing. **J.L. Tanyi:** Investigation, writing–review and editing. **L.P. Martin:** Investigation, writing–review and editing. **S.M. Lanzo:** Resources, validation, writing–review and editing. **F. Liu:** Formal analysis, writing–review and editing. **Q. Cao:** Formal analysis, writing–review and editing. **G.B. Mills:** Resources, investigation, methodology, writing–review and editing. **R.K. Doot:** Data curation, software, formal analysis, investigation, writing–review and editing. **D.A. Mankoff:** Conceptualization, resources, supervision, methodology, project administration, writing–review and editing. **R.H. Mach:** Conceptualization, resources, supervision, methodology, project administration, writing–review and editing. **L.L. Lin:** Conceptualization, resources, supervision, funding acquisition, methodology, project administration, writing–review and editing. **F. Simpkins:** Conceptualization, resources, data curation, formal analysis, supervision, funding acquisition, investigation, visualization, methodology, project administration, writing–review and editing.

Acknowledgments

The authors would like to acknowledge the University of Pennsylvania PET Center and Cyclotron Facility for clinical support and manufacturing of radiopharmaceuticals used in this study. The authors also acknowledge Christina Dulal for assistance with clinical trial documentation, and the kind gift provided by the Miriam and Sheldon Adelson Medical Research Foundation.

DOD OC160269 (F. Simpkins, R.H. Mach, A.R. Pantel, and M. Makvandi); SPORE 1P50CA228991 (F. Simpkins, M. Makvandi); NIH KL2TR001879 (A.R. Pantel); Basser Center Team Science grant (F. Simpkins, A.R. Pantel, M. Makvandi), The BioTrust Collection of the UPENN Translational Center of Excellence in Ovarian Cancer.

The publication costs of this article were defrayed in part by the payment of publication fees. Therefore, and solely to indicate this fact, this article is hereby marked "advertisement" in accordance with 18 USC section 1734.

Note

Supplementary data for this article are available at Clinical Cancer Research Online (http://clincancerres.aacrjournals.org/).

Received June 29, 2022; revised September 26, 2022; accepted November 22, 2022; published first November 28, 2022.

References

1. Moore K, Colombo N, Scambia G, Kim BG, Oaknin A, Friedlander M, et al. Maintenance Olaparib in patients with newly diagnosed advanced ovarian cancer. N Engl J Med 2018;379:2495–505.
2. Poveda A, Floquet A, Ledermann JA, Asher R, Penson RT, Oza AM, et al. Olaparib tablets as maintenance therapy in patients with platinum-sensitive relapsed ovarian cancer and a BRCA1/2 mutation (SOLO2/ENGOT-Ov21): a final analysis of a double-blind, randomised, placebo-controlled, phase 3 trial. Lancet Oncol 2021;22:620–31.
3. Penson RT, Valencia RV, Cibula D, Colombo N, Leath CA 3rd, Bidzinski M, et al. Olaparib Versus Nonplatinum chemotherapy in patients with platinum-sensitive relapsed ovarian cancer and a germline BRCA1/2 mutation (SOLO3): a randomized phase III trial. J Clin Oncol 2020;38:1164–74.
4. Oza AM, Lorusso D, Aghajanian C, Oaknin A, Dean A, Colombo N, et al. Patient-centered outcomes in ARIEL3, a phase III, randomized, placebo-controlled trial of rucaparib maintenance treatment in patients with recurrent ovarian carcinoma. J Clin Oncol 2020;38:3494–505.
5. Swisher EM, Lin KK, Oza AM, Scott CL, Giordano H, Sun J, et al. Rucaparib in relapsed, platinum-sensitive high-grade ovarian carcinoma (ARIEL2 Part 1): an international, multicentre, open-label, phase 2 trial. Lancet Oncol 2017;18:75–87.
6. Helleday T, Petermann E, Lundin C, Hodgson B, Sharma RA. DNA repair pathways as targets for cancer therapy. Nat Rev Cancer 2008;8:193–204.
7. Noordermeer SM, van Attikum H. PARP inhibitor resistance: a tug-of-war in BRCA-mutated cells. Trends Cell Biol 2019;29:820–34.
8. Lord CJ, Ashworth A. PARP inhibitors: synthetic lethality in the clinic. Science 2017;355:1152–8.
9. Gonzalez-Martin A, Pothuri B, Vergote I, DePont Christensen R, Graybill W, Mirza MR, et al. Niraparib in patients with newly diagnosed advanced ovarian cancer. N Engl J Med 2019;381:2391–402.
10. Reiss KA, Mick R, O'Hara MH, Teitelbaum U, Karasic TB, Schneider C, et al. Phase II study of maintenance rucaparib in patients with platinum-sensitive advanced pancreatic cancer and a pathogenic germline or somatic variant in BRCA1, BRCA2, or PALB2. J Clin Oncol 2021;39:2497–505.
11. Tew WP, Lacchetti C, Ellis A, Maxian K, Banerjee S, Bookman M, et al. PARP inhibitors in the management of ovarian cancer: ASCO Guideline. J Clin Oncol 2020;38:3468–93.
12. de Bono J, Mateo J, Fizazi K, Saad F, Shore N, Sandhu S, et al. Olaparib for metastatic castration-resistant prostate cancer. N Engl J Med 2020;382:2091–102.
13. Mirza MR, Monk BJ, Herrstedt J, Oza AM, Mahner S, Redondo A, et al. Niraparib maintenance therapy in platinum-sensitive, recurrent ovarian cancer. N Engl J Med 2016;375:2154–64.
14. Qian B, Leng W, Yan Z, Lu J, Chen S, Yi H, et al. Clinical benefit with PARP inhibitor for pathogenic germline FANCA-mutated relapsed epithelial ovarian cancer: a case report. Front Oncol 2022;12:778545.
15. Poveda A, Lheureux S, Colombo N, Cibula D, Lindemann K, Weberpals J, et al. Olaparib maintenance monotherapy in platinum-sensitive relapsed ovarian cancer patients without a germline BRCA1/BRCA2 mutation: OPINION primary analysis. Gynecol Oncol 2022;164:498–504.
16. Keung MY, Wu Y, Badar F, Vadgama JV. Response of breast cancer cells to PARP inhibitors is independent of BRCA status. J Clin Med 2020;9:940.
17. Kaufman B, Shapira-Frommer R, Schmutzler RK, Audeh MW, Friedlander M, Balmana J, et al. Olaparib monotherapy in patients with advanced cancer and a germline BRCA1/2 mutation. J Clin Oncol 2015;33:244–50.
18. Domchek SM, Aghajanian C, Shapira-Frommer R, Schmutzler RK, Audeh MW, Friedlander M, et al. Efficacy and safety of olaparib monotherapy in germline BRCA1/2 mutation carriers with advanced ovarian cancer and three or more lines of prior therapy. Gynecol Oncol 2016;140:199–203.
19. Wang Y, Ren F, Song Z, Wang X, Zhang C, Ouyang L. PARP inhibitors in patients with newly diagnosed advanced ovarian cancer: a meta-analysis of randomized clinical trials. Front Oncol 2020;10:1204.
20. Pothuri B, O'Cearbhaill R, Eskander R, Armstrong D. Frontline PARP inhibitor maintenance therapy in ovarian cancer: a society of gynecologic oncology practice statement. Gynecol Oncol 2020;159:8–12.
21. Miller RE, El-Shakankery KH, Lee JY. PARP inhibitors in ovarian cancer: overcoming resistance with combination strategies. J Gynecol Oncol 2022;33:e44.

Downloaded from http://aacrjournals.org/clincancerres/article-pdf/29/8/1515/3320981/1515.pdf by University of Pennsylvania Libraries user on 06 August 2023

22. Zhou D, Chu W, Xu J, Jones LA, Peng X, Li S, et al. Synthesis, [(1)(8)F] radiolabeling, and evaluation of poly (ADP-ribose) polymerase-1 (PARP-1) inhibitors for *in vivo* imaging of PARP-1 using positron emission tomography. Bioorg Med Chem 2014;22:1700–7.
23. Edmonds CE, Makvandi M, Lieberman BP, Xu K, Zeng C, Li S, et al. [(18) F]FluorThanatrace uptake as a marker of PARP1 expression and activity in breast cancer. Am J Nucl Med Mol Imaging 2016;6:94–101.
24. Michel LS, Dyroff S, Brooks FJ, Spayd KJ, Lim S, Engle JT, et al. PET of poly (ADP-Ribose) polymerase activity in cancer: preclinical assessment and first in-human studies. Radiology 2017;282:453–63.
25. Makvandi M, Pantel A, Schwartz L, Schubert E, Xu K, Hsieh CJ, et al. A PET imaging agent for evaluating PARP-1 expression in ovarian cancer. J Clin Invest 2018;128:2116–26.
26. Young AJ, Pantel AR, Viswanath V, Dominguez TL, Makvandi M, Lee H, et al. Kinetic and static analysis of poly-(Adenosine Diphosphate-Ribose) polymerase-1-targeted (18)F-fluorthanatrace PET images of ovarian cancer. J Nucl Med 2022;63:44–50.
27. Stotz S, Kinzler J, Nies AT, Schwab M, Maurer A. Two experts and a newbie: [(18) F]PARPi vs [(18)F]FTT vs [(18)F]FPyPARP—a comparison of PARP imaging agents. Eur J Nucl Med Mol Imaging 2022;49:834–46.
28. Schoder H, Franca PDS, Nakajima R, Burnazi E, Roberts S, Brand C, et al. Safety and feasibility of PARP1/2 imaging with (18)F-PARPi in patients with head and neck cancer. Clin Cancer Res 2020;26:3110–6.
29. McDonald ES, Pantel AR, Shah PD, Farwell MD, Clark AS, Doot RK, et al. *In vivo* visualization of PARP inhibitor pharmacodynamics. JCI Insight 2021;6:e146592.
30. Eisenhauer EA, Therasse P, Bogaerts J, Schwartz LH, Sargent D, Ford R, et al. New response evaluation criteria in solid tumours: revised RECIST guideline (version 1.1). Eur J Cancer 2009;45:228–47.
31. Wahl RL, Jacene H, Kasamon Y, Lodge MA. From RECIST to PERCIST: Evolving considerations for PET response criteria in solid tumors. J Nucl Med 2009;50:122S–50S.
32. Gitto SB, George E, Medvedev S, Simpkins F, Powell DJ. Humanized patient-derived xenograft models of ovarian cancer. In: Kreeger PK, editor. Ovarian Cancer: Methods and Protocols. New York, NY: Springer US; 2022. p 255–74.
33. Kim H, Xu H, George E, Hallberg D, Kumar S, Jagannathan V, et al. Combining PARP with ATR inhibition overcomes PARP inhibitor and platinum resistance in ovarian cancer models. Nat Commun 2020;11:3726.
34. Krishnamoorthy S, Blankemeyer E, Mollet P, Surti S, Van Holen R, Karp JS. Performance evaluation of the MOLECUBES beta-CUBE-a high spatial resolution and high sensitivity small animal PET scanner utilizing monolithic LYSO scintillation detectors. Phys Med Biol 2018;63:155013.
35. Tibes R, Qiu Y, Lu Y, Hennessy B, Andreeff M, Mills GB, et al. Reverse phase protein array: validation of a novel proteomic technology and utility for analysis of primary leukemia specimens and hematopoietic stem cells. Mol Cancer Ther 2006;5:2512–21.
36. Enot DP, Vacchelli E, Jacquelot N, Zitvogel L, Kroemer G. TumGrowth: an open-access web tool for the statistical analysis of tumor growth curves. Oncoimmunology 2018;7:e1462431.
37. Cadoo KA, Simpkins F, Mathews CA, Kabil N, Bennett J, Aghajanian C. Olaparib treatment in patients (pts) with platinum-sensitive relapsed (PSR) ovarian cancer (OC) by BRCA mutation (BRCAm) and homologous recombination deficiency (HRD) status: phase II LIGHT study. J Clin Oncol 2020; 38:6013.
38. Shah PD, Wethington SL, Pagan C, Latif N, Tanyi J, Martin LP, et al. Combination ATR and PARP Inhibitor (CAPRI): a phase 2 study of ceralasertib plus olaparib in patients with recurrent, platinum-resistant epithelial ovarian cancer. Gynecol Oncol 2021;163:246–53.
39. Rustin GJ, Quinn M, Thigpen T, du Bois A, Pujade-Lauraine E, Jakobsen A, et al. Re: New guidelines to evaluate the response to treatment in solid tumors (ovarian cancer). J Natl Cancer Inst 2004;96:487–8.
40. Antolin AA, Ameratunga M, Banerji U, Clarke PA, Workman P, Al-Lazikani B. The kinase polypharmacology landscape of clinical PARP inhibitors. Sci Rep 2020;10:2585.
41. Wethington SL, Shah PD, Martin LP, Tanyi JL, Latif NA, Morgan MA, et al. Combination of PARP and ATR inhibitors (olaparib and ceralasertib) shows clinical activity in acquired PARP inhibitor-resistant recurrent ovarian cancer. J Clin Oncol 2021;39:5516.
42. Mortimer JE, Dehdashti F, Siegel BA, Trinkaus K, Katzenellenbogen JA, Welch MJ. Metabolic flare: indicator of hormone responsiveness in advanced breast cancer. J Clin Oncol 2001;19:2797–803.
43. van Kruchten M, de Vries EG, Glaudemans AW, van Lanschot MC, van Faassen M, Kema IP, et al. Measuring residual estrogen receptor availability during fulvestrant therapy in patients with metastatic breast cancer. Cancer Discov 2015;5:72–81.
44. Wang Y, Ayres KL, Goldman DA, Dickler MN, Bardia A, Mayer IA, et al. (18)F-fluoroestradiol PET/CT measurement of estrogen receptor suppression during a phase I trial of the novel estrogen receptor-targeted therapeutic GDC-0810: using an imaging biomarker to guide drug dosage in subsequent trials. Clin Cancer Res 2017;23:3053–60.
45. Benchoua A, Couriaud C, Guegan C, Tartier L, Couvert P, Friocourt G, et al. Active caspase-8 translocates into the nucleus of apoptotic cells to inactivate poly (ADP-ribose) polymerase-2. J Biol Chem 2002;277:34217–22.
46. Salvesen GS, Dixit VM. Caspases: intracellular signaling by proteolysis. Cell 1997; 91:443–6.
47. Peterson LM, Kurland BF, Yan F, Jiresova AN, Gadi VK, Specht JM, et al. (18)F-fluoroestradiol PET imaging in a phase II trial of vorinostat to restore endocrine sensitivity in ER+/HER2- metastatic breast cancer. J Nucl Med 2021;62:184–90.

Downloaded from http://aacrjournals.org/clincancerres/article-pdf/29/8/1515/3320981/1515.pdf by University of Pennsylvania Libraries user on 06 August 2023

JCI The Journal of Clinical Investigation

A PET imaging agent for evaluating PARP-1 expression in ovarian cancer

Mehran Makvandi, … , Robert H. Mach, Lilie L. Lin

J Clin Invest. 2018;128(5):2116-2126. https://doi.org/10.1172/JCI97992.

Clinical Medicine | Oncology | Therapeutics

BACKGROUND. Poly(ADP-ribose) polymerase (PARP) inhibitors are effective in a broad population of patients with ovarian cancer; however, resistance caused by low enzyme expression of the drug target PARP-1 remains to be clinically evaluated in this context. We hypothesize that PARP-1 expression is variable in ovarian cancer and can be quantified in primary and metastatic disease using a novel PET imaging agent.

METHODS. We used a translational approach to describe the significance of PET imaging of PARP-1 in ovarian cancer. First, we produced *PARP1*-KO ovarian cancer cell lines using CRISPR/Cas9 gene editing to test the loss of PARP-1 as a resistance mechanism to all clinically used PARP inhibitors. Next, we performed preclinical microPET imaging studies using ovarian cancer patient–derived xenografts in mouse models. Finally, in a phase I PET imaging clinical trial we explored PET imaging as a regional marker of PARP-1 expression in primary and metastatic disease through correlative tissue histology.

RESULTS. We found that deletion of *PARP1* causes resistance to all PARP inhibitors in vitro, and microPET imaging provides proof of concept as an approach to quantify PARP-1 in vivo. Clinically, we observed a spectrum of standard uptake values […]

Find the latest version:

https://jci.me/97992/pdf

A PET imaging agent for evaluating PARP-1 expression in ovarian cancer

Mehran Makvandi,[1] Austin Pantel,[1] Lauren Schwartz,[2] Erin Schubert,[1] Kuiying Xu,[1] Chia-Ju Hsieh,[1] Catherine Hou,[1] Hyoung Kim,[3] Chi-Chang Weng,[1] Harrison Winters,[4] Robert Doot,[1] Michael D. Farwell,[1] Daniel A. Pryma,[1] Roger A. Greenberg,[4] David A. Mankoff,[1] Fiona Simpkins,[3] Robert H. Mach,[1] and Lilie L. Lin[5]

[1]Department of Radiology, Division of Nuclear Medicine and Molecular Imaging, University of Pennsylvania, Perelman School of Medicine, Philadelphia, Pennsylvania, USA. [2]Department of Pathology, Hospital of the University of Pennsylvania, Philadelphia, Pennsylvania, USA. [3]Department of OBGYN, Division of Gynecology and Oncology, [4]Department of Cancer Biology, and [5]Department of Radiation Oncology, University of Pennsylvania, Perelman School of Medicine, Philadelphia, Pennsylvania, USA.

BACKGROUND. Poly(ADP-ribose) polymerase (PARP) inhibitors are effective in a broad population of patients with ovarian cancer; however, resistance caused by low enzyme expression of the drug target PARP-1 remains to be clinically evaluated in this context. We hypothesize that PARP-1 expression is variable in ovarian cancer and can be quantified in primary and metastatic disease using a novel PET imaging agent.

METHODS. We used a translational approach to describe the significance of PET imaging of PARP-1 in ovarian cancer. First, we produced *PARP1*-KO ovarian cancer cell lines using CRISPR/Cas9 gene editing to test the loss of PARP-1 as a resistance mechanism to all clinically used PARP inhibitors. Next, we performed preclinical microPET imaging studies using ovarian cancer patient–derived xenografts in mouse models. Finally, in a phase I PET imaging clinical trial we explored PET imaging as a regional marker of PARP-1 expression in primary and metastatic disease through correlative tissue histology.

RESULTS. We found that deletion of *PARP1* causes resistance to all PARP inhibitors in vitro, and microPET imaging provides proof of concept as an approach to quantify PARP-1 in vivo. Clinically, we observed a spectrum of standard uptake values (SUVs) ranging from 2–12 for PARP-1 in tumors. In addition, we found a positive correlation between PET SUVs and fluorescent immunohistochemistry for PARP-1 ($r^2 = 0.60$).

CONCLUSION. This work confirms the translational potential of a PARP-1 PET imaging agent and supports future clinical trials to test PARP-1 expression as a method to stratify patients for PARP inhibitor therapy.

TRIAL REGISTRATION. Clinicaltrials.gov NCT02637934.

FUNDING. Research reported in this publication was supported by the Department of Defense OC160269, a Basser Center team science grant, NIH National Cancer Institute R01CA174904, a Department of Energy training grant DE-SC0012476, Abramson Cancer Center Radiation Oncology pilot grants, the Marsha Rivkin Foundation, Kaleidoscope of Hope Foundation, and Paul Calabresi K12 Career Development Award 5K12CA076931.

Introduction

Epithelial ovarian cancer (EOC) is the fifth deadliest malignancy in women, with more than 70% of patients presenting with advanced disease (1). Until the recent emergence of targeted therapeutics, treatment has relied heavily on cytoreductive surgery and platinum/taxane-based chemotherapy (2). Poly(ADP-ribose) polymerase inhibitors (PARPis) have emerged as promising drug candidates for the treatment of EOC. In current clinical practice, patients are commonly selected for PARPi therapy by testing positive for genetic mutations in genes encoding DNA repair proteins that result in homologous recombination deficiency (HRD), most notably mutations in breast and ovarian cancer susceptibility genes 1 and 2 (*BRCA1* and *BRCA2*) (3, 4). However, only approximately 50% of patients with HRD respond to PARPi therapy (3). Moreover, patients without known HRD have also shown a clinical benefit from PARPis, as seen in recent trials assessing niraparib, olaparib, or rucaparib, as maintenance therapy in platinum-sensitive recurrent ovarian cancer (5–8). Given that not all patients will respond to PARPi therapy, improved clinical tools for predicting which patients will respond are urgently needed.

Numerous clinical trials have led to FDA approval of 3 PARPis since 2014 and there is continued development of 2 additional drugs within this class (9–13). Despite growth in the

▶ Related Commentary: p. 1727

Conflict of interest: The authors have declared that no conflict of interest exists.
Submitted: October 11, 2017; **Accepted:** February 28, 2018.
Reference information: *J Clin Invest*. 2018;128(5):2116–2126.
https://doi.org/10.1172/JCI97992.

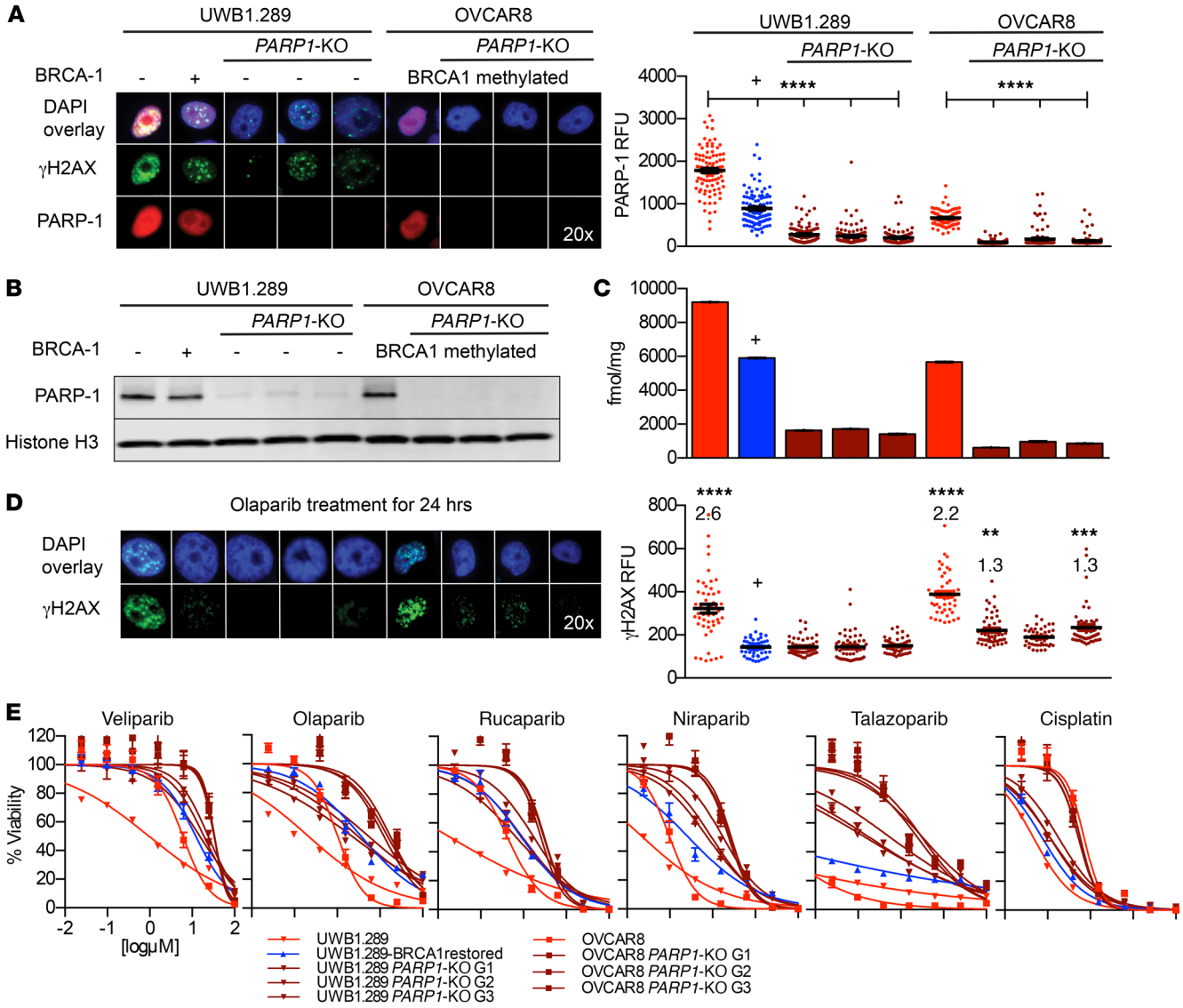

Figure 1. The characterization of *PARP1*-KO ovarian cancer cell lines and in vitro evaluation of PARP inhibitor efficacy. (**A**) Immunofluorescence showed PARP-1 was absent in more than 90% of single cells in *PARP1*-KO polyclonal populations (ANOVA, $^{****}P < 0.0001$) and was reduced in *BRCA1*-restored cells compared with parent control (ANOVA, $^{****}P < 0.0001$). (**B**) Polyclonal populations of *PARP1*-KO cell lines had reduced PARP-1 by Western blot compared with parent control. (**C**) [^{125}I]KX1 radioligand binding assays showed a significant reduction in radiotracer binding in *PARP1*-KO and UWB1.289 *BRCA1*-restored cell lines compared with parent control (ANOVA, $P < 0.0001$). (**D**) Immunofluorescence of olaparib-treated UWB1.289 *PARP1*-KO and UWB1.289 *BRCA1*-restored cells showed no increase in γH2AX compared with DMSO controls. Olaparib-treated OVCAR8 *PARP1*-KO G1 and G3 cells showed a 1.3 times increase (ANOVA, $^{**}P < 0.01$ and $^{***}P < 0.001$, respectively) in γH2AX from DMSO controls. This was in contrast to olaparib-treated UWB1.289 and OVCAR8 cells that showed a 2.6 times (ANOVA, $^{****}P < 0.0001$) and 2.2 times (ANOVA, $^{****}P < 0.0001$) increase in γH2AX from DMSO controls. (**E**) Cell viability assays showed that *PARP1*-KO cells were equally resistant to olaparib compared with *BRCA1*-restored cells and all clinical PARP inhibitors required PARP-1 for maximum efficacy. Loss of *PARP1* caused the greatest change in efficacy for niraparib and talazoparib. Cisplatin sensitivity was used as a positive control and remained unchanged after loss of *PARP1*. All in vitro experiments were completed 3 independent times. Cell lines shown in **A**–**D**, from left to right, are: UWB1.289, UWB1.289 *BRCA1* restored, UWB1.289 *PARP1*-KO G1, UWB1.289 *PARP1*-KO G2, UWB1.289 *PARP1*-KO G3, OVCAR8, OVCAR8 *PARP1*-KO G1, OVCAR8 *PARP1*-KO G2, and OVCAR8 *PARP1*-KO G3. –, *BRCA1* mutant. +, *BRCA1* restored.

development and application of PARPis, the primary drug target poly(ADP-ribose) polymerase 1 (PARP-1) has never been evaluated in vivo, even though loss of expression in vitro is a well-characterized resistance mechanism (3, 14–19). It was first hypothesized that PARPis work primarily through a synthetic lethality pathway where loss of *BRCA1* or *BRCA2* combined with chemical inhibition of PARP-1 results in cell death (20, 21). However, it was later shown that deletion of *PARP1* did not result in enhanced sensitivity to a DNA alkylating agent in WT cells, suggesting that loss of catalytic function could not be the only reason for PARPi efficacy (17–19). Next, Murai et al. demonstrated that all clinically used PARPis have differential abilities to trap PARP-1 on DNA, but equally lack cytotoxicity in *PARP1*-KO$^{-/-}$ cells (22, 23). While some PARPis are potent PARP-1 trappers, all PARPis target the PARP-1 enzyme, making it a potential prerequisite biomarker for efficacy (22–24). Furthermore, PARP-1 has been

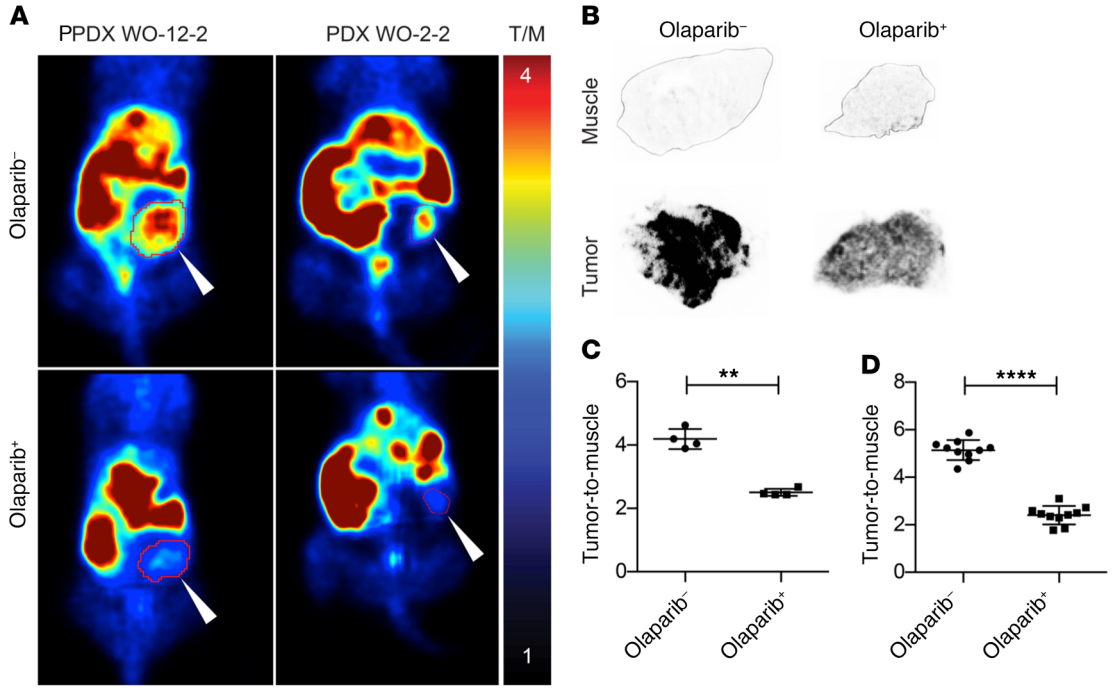

Figure 2. In vivo [^{18}F]FTT microPET imaging and ex vivo autoradiography of 2 xenografts derived from patients with ovarian cancer. (**A**) Tumor-bearing mice underwent microPET imaging with [^{18}F]FTT before (top images) and after (bottom images) olaparib treatment. White arrows point to patient-derived xenograft tumors. (**B**) Ex vivo autoradiographs of tumor and muscle from untreated (–) versus olaparib-treated (+) mice. (**C**) Significant differences were observed in the tumor-to-muscle ratios calculated before and after olaparib treatment from microPET images (4.2 ± 0.32 vs. 2.5 ± 0.11, parametric paired *t* test, $^{**}P < 0.0025$, $n = 4$). (**D**) Ex vivo autoradiographs of untreated (–) versus olaparib-treated (+) mice shown in **B** also showed a statistically significant difference between groups (5.14 ± 0.13 vs. 2.41 ± 0.18, $n = 2$, 10 sections/tumor, parametric unpaired *t* test, $^{****}P < 0.0001$).

shown by immunohistochemistry (IHC) to be highly variable in patients with ovarian (25–28), breast (29), and prostate cancer (30), irrespective of *BRCA* status. Together these studies demonstrate the need for a biomarker technology capable of quantitatively assessing PARP-1 in vivo that could enable patient selection for PARPi therapy.

Current methods to determine PARP-1 expression in clinical tumor specimens are limited and based on immunohistological methods that require invasive procedures such as biopsy or surgery. Association studies of PARP-1 expression by IHC with prognosis and outcome have demonstrated mixed results, suggesting inconsistency of staining procedures and antibodies (25–28). Indeed, there lacks a validated clinical IHC staining protocol for PARP-1 that can be widely and robustly applied in clinical practice (28). Furthermore, approaches based on tissue sampling inadequately assess the potential heterogeneity of PARP-1 expression in disseminated EOC, a stage of disease highly relevant to PARPi therapy.

Radiotracer technology for the noninvasive imaging of PARP-1 could theoretically overcome the limitations of IHC by quantitatively assessing global PARP-1 expression in primary and disseminated disease (31, 32). [^{18}F]FluorThanatrace ([^{18}F]FTT) is a radiolabeled small-molecule PARPi that is currently approved for clinical use under an investigational new drug application at the University of Pennsylvania (Philadelphia Pennsylvania, USA) and Washington University (St. Louis, Missouri, USA) (33, 34). [^{18}F]FTT and its iodinated analogue [^{125}I]KX1 have been shown to correlate with PARP-1 expression through a receptor-ligand effect that stems from their primary pharmacological mechanism of action (16, 35). As such, [^{18}F]FTT and [^{125}I]KX1 quantify PARP-1 expression and have the ability to measure drug-target engagement of clinical PARPis by competing with one another for the NAD^+ binding pocket on the catalytic subdomain of PARP-1. Contrary to current methodologies that measure the biochemical product of PARP-1, poly(ADP-ribose) (PAR), this is a direct measurement of drug-target engagement.

In this work, we validate the preclinical rationale for measuring PARP-1 expression as a predictive biomarker of response to PARPis and report the first clinical trial studying PARP-1 expression with [^{18}F]FTT PET in EOC.

Results

CRISPR/Cas9 deletion of PARP1 in ovarian cancer cells. Using CRISPR/Cas9 gene editing, we mediated the deletion of *PARP1* in 2 ovarian cancer cell lines, one with a *BRCA1* mutation and another with *BRCA1* promoter methylation (UWB1.289 and OVCAR8). OVCAR8 cells have been previously shown to have reduced BRCA-1 expression attributed to promoter methylation and are sensitive to DNA-damaging agents (36–38). Strikingly, the genetic deletion of *PARP1* in EOC cells with a *BRCA1* mutation or *BRCA1* promoter methylation did not result in synthetic lethality, in that the cells were viable and grew in culture (21, 39). Identifying the mechanism of viability was beyond the scope of this work, but is being pursued. Using this system for *PARP1* deletion, we achieved more than 90% reduction of PARP-1 expression in polyclonal populations of *BRCA1* mutant (UWB1.289) and *BRCA1* methyl-

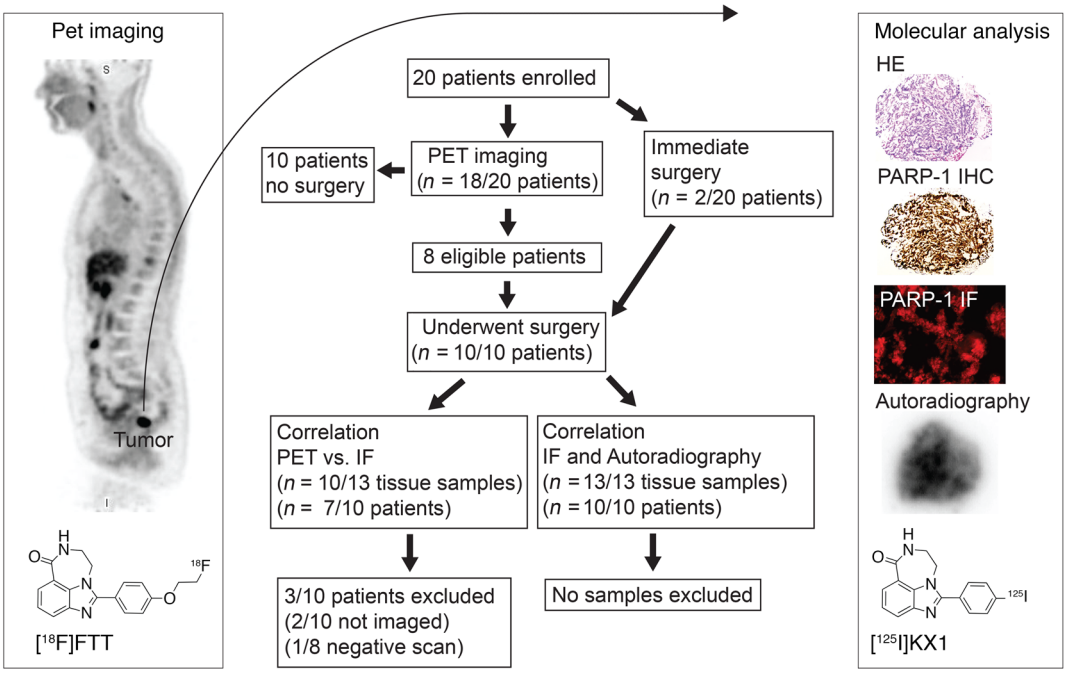

Figure 3. Diagram overview and flow chart of the pilot clinical trial of [18F]FTT PET/CT imaging in ovarian cancer. Ten patients who were enrolled and underwent PET imaging were excluded from this subanalysis due to lack of clinical tissue samples available for correlative studies.

ated (OVCAR8) ovarian cancer cells as measured by immunofluorescence (IF) and Western blot analysis (Figure 1, A and B, and Supplemental Figure 1, A and B; supplemental material available online with this article; https://doi.org/10.1172/JCI97992DS1). Cell microscopy studies showed that PARP-1 was indeed absent at the single-cell level in polyclonal populations (Figure 1A and Supplemental Figure 1A). We also examined PARP-2 and PARP-3 expression by Western blot to investigate off-target effects of single-guide RNAs. We found no differences from control for PARP-2 or PARP-3 expression by Western blot analysis (Supplemental Figure 1B). Lastly, to determine whether PARP-1 expression varies among ovarian cell lines with and without BRCA dysfunction (Supplemental Table 1), we measured PARP-1 in multiple cell lines and demonstrated a dynamic range of expression (Supplemental Figure 2, A and B, and Supplemental Table 2).

[125I]KX1 radioligand binding measures differences in PARP-1 expression. Using the *PARP1*-KO cell lines along with several nonmodified EOC cell lines, we showed significant differences in the radioligand binding of [125I]KX1 relative to PARP-1 expression (Figure 1C, Supplemental Figure 2C, and Supplemental Table 2). Most notably, the deletion of *PARP1* reduced radioligand binding of [125I]KX1 in both models. Furthermore, we observed that the radioligand binding of [125I]KX1 was reduced in BRCA functional versus dysfunctional cells (Figure 1C, Supplemental Figure 2C, and Supplemental Table 2). The restoration of *BRCA1* in UWB1.289 cells resulted in lower radioligand binding and corresponded to lower PARP-1 expression by IF and Western blot (Figure 1, A–C, and Supplemental Figure 2, A–C). These data support in vitro radioligand binding with [125I]KX1 as a method to assay PARP-1 expression.

Loss of PARP1 blunts PARPi efficacy in ovarian cancer cell lines in vitro. The genetic deletion of *PARP1* resulted in reduced DNA damage and sensitivity to PARPis in vitro. First, we examined isogenic UWB1.289 cells by IF after treatment with olaparib for 24 hours. We found no change in DNA damage measured by γH2AX foci formation following olaparib treatment in both *BRCA1*-restored and *PARP1*-KO cells compared with DMSO controls. In contrast, γH2AX levels increased 2.6 times in olaparib-treated UWB1.289 cells compared with DMSO controls (Figure 1D). Similarly, the same effect was observed in OVCAR8 cells (Figure 1D). Next, the cytotoxicity evaluated for clinically used PARPis showed that the loss of *PARP1* resulted in equal or greater resistance compared with restoring *BRCA1* in UWB1.289 cells (Figure 1E, Supplemental Figure 2D, and Supplemental Table 3, A and B). Strikingly, a greater resistance in *PARP1*-KO cells compared with *BRCA1*-restored cells from parent controls was observed for the potent PARP trappers, niraparib and talazoparib. The loss of *PARP1* resulted in greater than a 1,000-fold decrease in sensitivity to talazoparib, whereas restoring *BRCA1* had a lesser effect in UWB1.289 cells. OVCAR8 cells also became resistant to PARPis after loss of *PARP1*. No differences in sensitivity to cisplatin were observed in cell lines after loss of *PARP1*, indicating there was no change in overall sensitivity to DNA-damaging drugs. These data provide direct support for PARP-1 expression as a requirement for PARPi sensitivity in vitro.

Preclinical imaging of PARP-1 expression. The aforementioned findings demonstrate the need for dynamic, noninvasive, and quantitative monitoring of PARP-1 expression in patients selected for PARP inhibitor therapy. To this end, proof-of-concept studies were conducted in preclinical mouse patient-derived xenograft (PDX) models to confirm the in vitro radioligand binding studies and demonstrate the specificity of [18F]FTT for in vivo quantitative imaging of PARP-1. Significant differences were observed in radiotracer uptake in tumors before and after treatment with

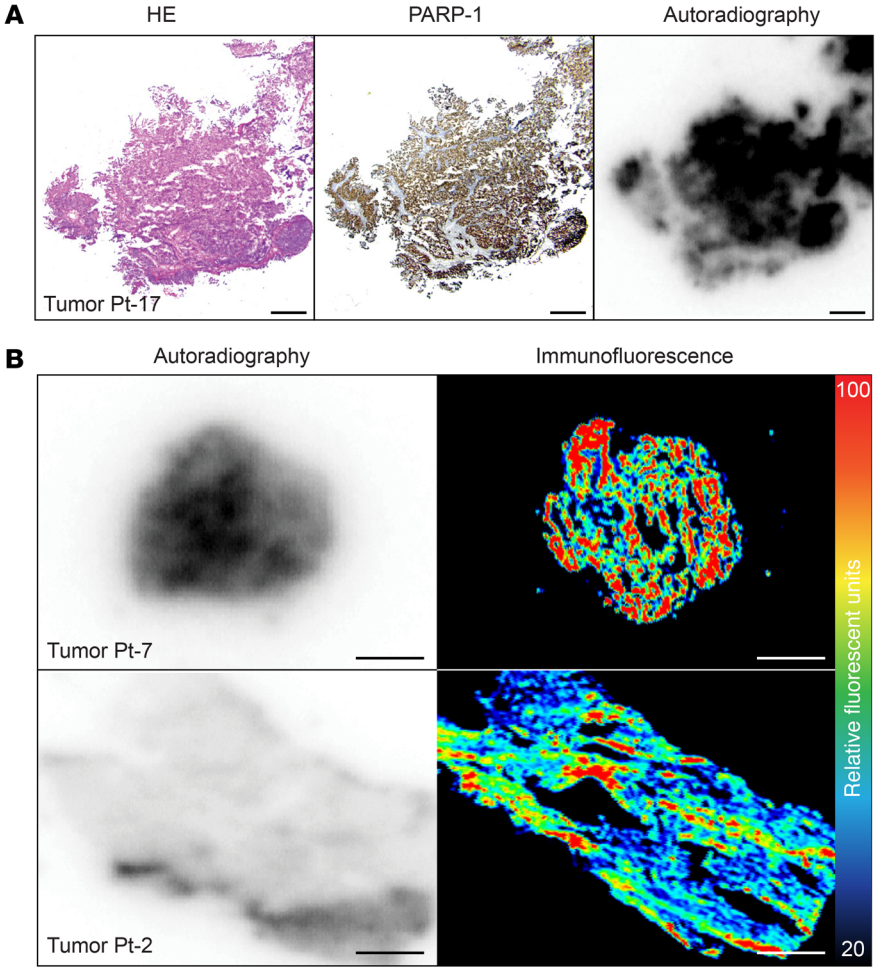

Figure 4. Immunohistochemistry and autoradiography analysis on clinical tissue. Distance bars represent 275 μM. (**A**) HE, PARP-1, and [^{125}I]KX-1 autoradiograph on adjacent tissue sections showed colocalization between [^{125}I]KX1 and PARP-1 c-IHC. (**B**) In vitro autoradiography showed a difference in PARP-1 expression that was also confirmed by PARP-1 f-IHC. Max intensity by autoradiograph was 0.28 vs. 0.20 μCi/mg and fluorescent intensity of PARP-1 from whole-section f-IHC was 9.6 vs. 6.7 RFU.

olaparib. By administering olaparib (50 mg/kg) we observed a reduction in [^{18}F]FTT tumor-to-muscle ratios, a semiquantitative measure of tracer binding in vivo (Figure 2A and Supplemental Figure 3A). In addition, tumor tissue analyzed from untreated and olaparib-treated mice by ex vivo autoradiography was used to confirm microPET findings (Figure 2B and Supplemental Figure 3B). Results between microPET imaging and ex vivo autoradiography were similar. Tumor-to-muscle ratios from microPET imaging before and after olaparib treatment were 4.2 ± 0.32 vs. 2.5 ± 0.11 (paired *t* test, $P < 0.0025$, $n = 4$) (Figure 2C). In agreement with microPET results, ex vivo autoradiographs showed a significant difference between untreated and olaparib-treated groups (5.14 ± 0.13 vs. 2.41 ± 0.18, unpaired *t* test, $P < 0.0001$, $n = 2$, 10 sections/tumor) (Figure 2D). Autoradiographs also showed significant differences in tumor and muscle of untreated and olaparib-treated groups (unpaired *t* test, $P < 0.0001$) (Supplemental Figure 3C).

Clinical trial enrollment. In this trial, 20 patients were enrolled and 10 patients who underwent surgical debulking or biopsy were included in the study. From the 10 patients, 13 tissue specimens were collected for in vitro analysis. Of the 10 patients included in the study, 8 underwent PET/CT imaging (Figure 3). One of the 8 patients had a negative [^{18}F]FTT scan and was excluded from the [^{18}F]FTT PET versus PARP-1 IF correlation.

PARP-1 immunohistochemistry and autoradiography on clinical specimens. Radioligand binding with [^{125}I]KX1 was found to colocalize with PARP-1 colormetric IHC (c-IHC) (Figure 4A) on adjacent tissue sections, supporting the specificity of the iodinated radiotracer for PARP-1. In addition, a spectrum of PARP-1 expression was observed by fluorescent IHC (f-IHC) and autoradiography (Figure 4B and Supplemental Figure 4), providing direct evidence for the wide range of PARP-1 expression in ovarian cancer. Interestingly, PARP-1 colocalized with both tumor cells and lymphocytes in the tumor microenvironment (Supplemental Table 4 and Supplemental Figure 5). PARP-1 expression was also positive in 2 lymph node samples, with residual disease on pathology, and costained with γH2AX. Finally, positive staining for PARP-1 and p53 co-occurred in 77% (10/13) of tissue samples, whereas positive staining for PARP-1 and γH2AX had 100% (13/13) co-occurrence (Supplemental Table 4 and Supplemental Figure 5).

Clinical observations with [^{18}F]FTT PET imaging. PET imaging demonstrated [^{18}F]FTT localized to areas of known EOC based on clinical [^{18}F]FDG PET/CT imaging with low bladder uptake, allowing for clear visualization of lesions within the pelvic region (Figure 5). Despite hepatobiliary excretion, [^{18}F]FTT uptake was discernible in omental disease in the abdomen (Figure 6). Differences in radiotracer uptake were seen between [^{18}F]FTT and [^{18}F]FDG PET, which is commonly used for evaluating tumor response and recurrence in EOC as well as identifying extrapelvic metastases and diagnosis. (40) Such differences suggest these radiotracers provide different and complementary information, concordant with their distinct molecular targets. For example, patient 2, who had completed 4 cycles of carboplatin and paclitaxel 2 weeks prior to imaging, showed multiple omental lesions by [^{18}F]FTT PET imaging with maximum SUVs ranging from 5–8 that were low on [^{18}F]FDG PET (Figure 6A, Figure 6B, and Supplemental Table 5). In follow-up, patient 2 showed disease progression within 4 months of therapy and was platinum resistant. In contrast, patient 11 had a *BRCA1* mutation and showed low uptake on both [^{18}F]FTT and [^{18}F]FDG PET after 4 cycles of therapy (carboplatin and paclitaxel) and was platinum sensitive (Figure 6, C and D). These results suggest that [^{18}F]FTT PET provides unique molecular information as a biomarker of viable tumor tissue and could be used in the future to guide clinical management in addition to current biomarkers

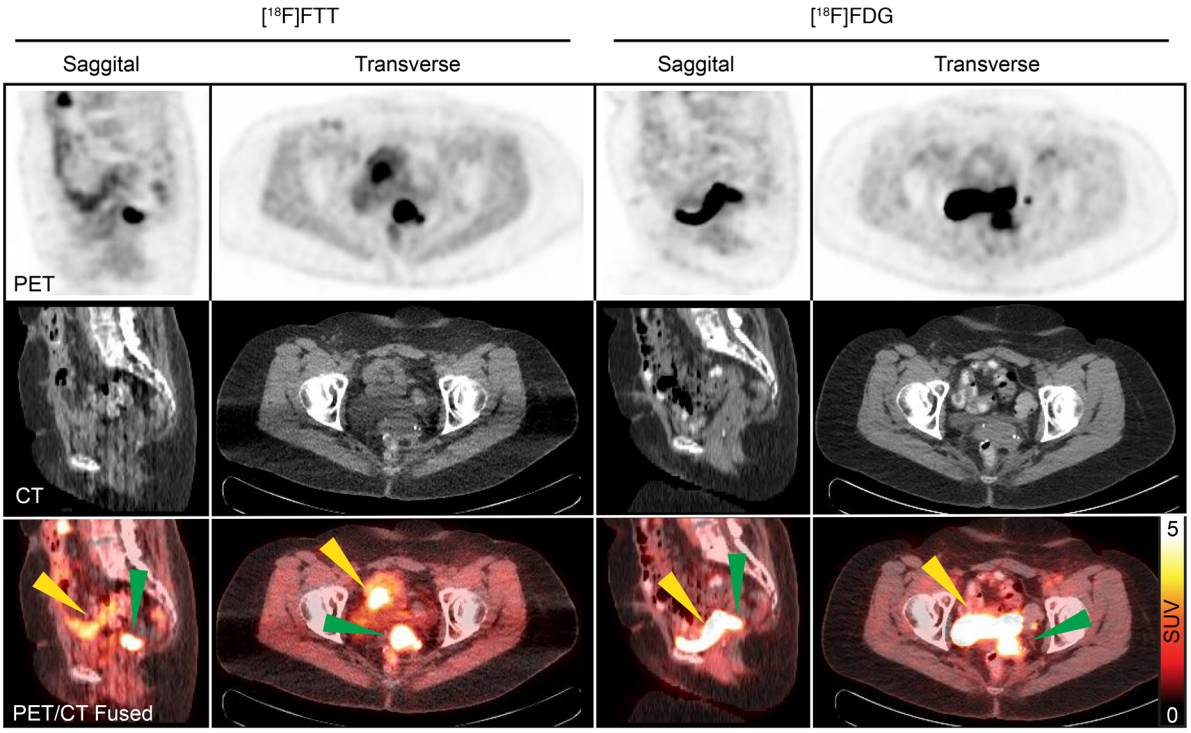

Figure 5. Clinical [18F]FTT and [18F]FDG PET/CT images of a patient with ovarian cancer with vaginal cuff lesion. Minimal radiotracer in the urinary bladder with [18F]FTT PET allowed for clear visualization of the lesion (green arrow) with no interference, despite some bowel uptake (yellow arrow on [18F]FTT image). Note excreted radiotracer in the bladder on [18F]FDG PET (yellow arrow on [18F]FDG PET).

of metabolic activity. Intertumor heterogeneity of [18F]FTT was observed in patients (Supplemental Figure 6), further emphasizing a beneficial role of PET imaging compared with standard biopsy approaches for quantifying PARP-1 in local and disseminated disease.

Clinical [18F]FTT PET imaging positively correlates with PARP-1 expression in patient tumors. A spectrum of [18F]FTT uptake was seen in tumors, indicative of varying levels of PARP-1 expression (Supplemental Table 5). Maximum SUVs of tumors ranged from as low as 2 (background) to as high as 12 and a similar range of PARP-1 expression was also observed by immunofluorescence and autoradiography (Figure 7, A and B, and Supplemental Table 5). Since [18F]FTT uptake is a marker of PARP-1 expression, this could translate to some tumors expressing up to 6 times as much PARP-1 as other tumors, with consequently higher drug-target densities for PARPis (Figure 7A). Further characterizing [18F]FTT as a measurement of PARP-1 expression, we found positive correlations between PARP-1 f-IHC and [18F]FTT PET imaging using linear regression analysis and calculating Pearson coefficients, in addition to PARP-1 f-IHC and [125I]KX1 autoradiography (r^2 = 0.60, 0.79, r = 0.77, 0.89) (Figure 7B and Supplemental Table 5). As expected, there was no correlation observed among PARP-1 f-IHC, [18F]FTT, or [125I]KX1 autoradiography with [18F]FDG, supporting distinct molecular imaging targets for [18F]FTT and [18F]FDG.

Discussion

This translational work further supports PARP-1 as the primary target for PARPis and describes the development of [18F]FTT as a noninvasive measure of regional tumor PARP-1 expression in patients with ovarian cancer. In vitro radioligand binding of [125I]KX1, the radio-iodinated analog of [18F]FTT, was previously reported (16) as a method to assay PARP-1 expression and was further confirmed in the present work. The genetic deletion of *PARP1* was explored as a mechanism of PARPi resistance in a *BRCA1* mutant and a *BRCA1* methylated ovarian cancer cell line, and our findings support the notion that PARP-1 expression is necessary for PARPi sensitivity in vitro. Preclinical imaging of PARP-1 in mice with [18F]FTT demonstrated the specificity of the radiotracer for its molecular target. Lastly, [18F]FTT was studied in patients with EOC involved in a phase I trial. [18F]FTT demonstrated a wide dynamic range of uptake correlating with in vitro measures of PARP-1 expression and the absence of correlation with [18F]FDG. In addition, we confirmed the feasibility of [18F]FTT as a practical radiotracer to image lesions in disseminated omental disease despite bowel uptake. Given our small sample size, it is too early to remark on imaging nodal disease involvement with [18F]FTT although a recent preclinical study suggests uptake in malignant nodes is greater than normal lymph nodes in a diffuse large B cell lymphoma model (41). It is difficult to extrapolate between diseases, but we did observe a single case that showed nodal uptake on [18F]FDG but not [18F]FTT and was negative on pathology, which is consistent with inflammation. Together, these data are important first steps in establishing [18F]FTT as a novel noninvasive biomarker of PARP-1 expression and lay the foundation for future testing of [18F]FTT PET in parallel with PARPi clinical trials.

We explored the loss of drug-target expression as a mechanism of PARPi resistance by studying the effects of the genetic deletion of *PARP1* in *BRCA1* mutant and *BRCA1* methylated cell

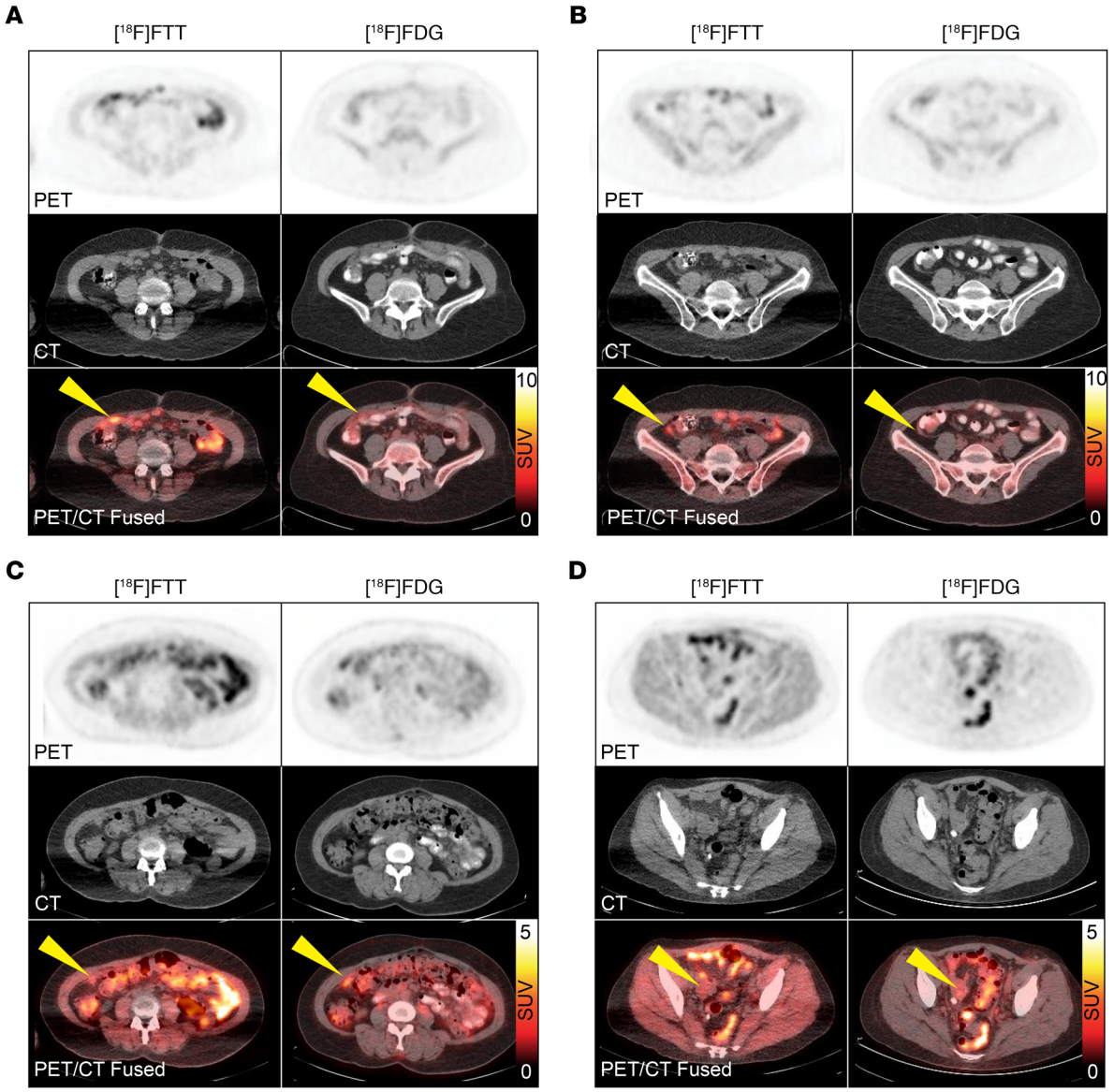

Figure 6. Patients 2 and 11 underwent [18F]FTT PET/CT imaging within 2 weeks of completing 4 cycles of carboplatin and paclitaxel. Omental metastases in patient 2 showed higher uptake of [18F]FTT than [18F]FDG with maximum SUVs of (**A**) 7.8 vs. 3.4 and (**B**) 5.1 vs. 2.0. Patient 2 was platinum resistant and relapsed within 4 months of therapy. Patient 11 showed low uptake on both [18F]FTT and [18F]FDG with maximum SUVs of (**C**) 2.4 vs. 3.7 and (**D**) 2.3 vs. 2.9. Patient 11 received 2 additional cycles of chemotherapy and was platinum sensitive. Yellow arrows indicate sites of disease.

lines. While loss of *PARP1* in *BRCA1* mutant or *BRCA1* methylated cell lines has the potential to be synthetically lethal, we found that stable deletion of *PARP1* by CRISPR/Cas9 resulted in polyclonal populations of cells in which more than 90% of clones lacked PARP-1 expression and grew in culture. It has been recently shown that OVCAR8 cells are capable of forming RAD51 foci, indicating functional homologous recombination, which could explain why loss of *PARP1* was not synthetically lethal in this cell line (42). The observed viability with UWB1.289 cells is most likely due to the biological redundancy between PARP-1 and PARP-2 or PARP-3. Future studies are ongoing to assess *PARP1/PARP2*-KO and *PARP1/PARP3*-KO models to test this hypothesis. In addition, we intend to evaluate loss of *PARP1* in isogenic *BRCA2* mutants with and without reversion mutations, such as the PEO1/PEO4 cell lines, to test whether similar results are found. We also found that lack of PARP-1 expression prevented PARPis from inducing DNA damage, as measured by γH2AX. These results are consistent with previous reports (17–19, 22, 23). Loss of *PARP1* most likely prevents the DNA damage caused by PARPi-induced PARP-1 trapping. This mechanistic understanding is highly relevant to PARPi therapy and our findings are consistent with what has been previously reported, showing PARP-1 as the primary target for PARPi-induced DNA damage (3, 14, 15, 17–19, 23).

In further support, we also observed a greater reduction in PARPi sensitivity with loss of PARP-1 expression compared with *BRCA1* restoration in the UWB1.289 isogenic cell lines when treated with the potent PARP trappers, niraparib and talazoparib. This observation may have translational implications, since olaparib, rucaparib, and niraparib were recently approved by the FDA as maintenance therapy in platinum-sensitive patients, regard-

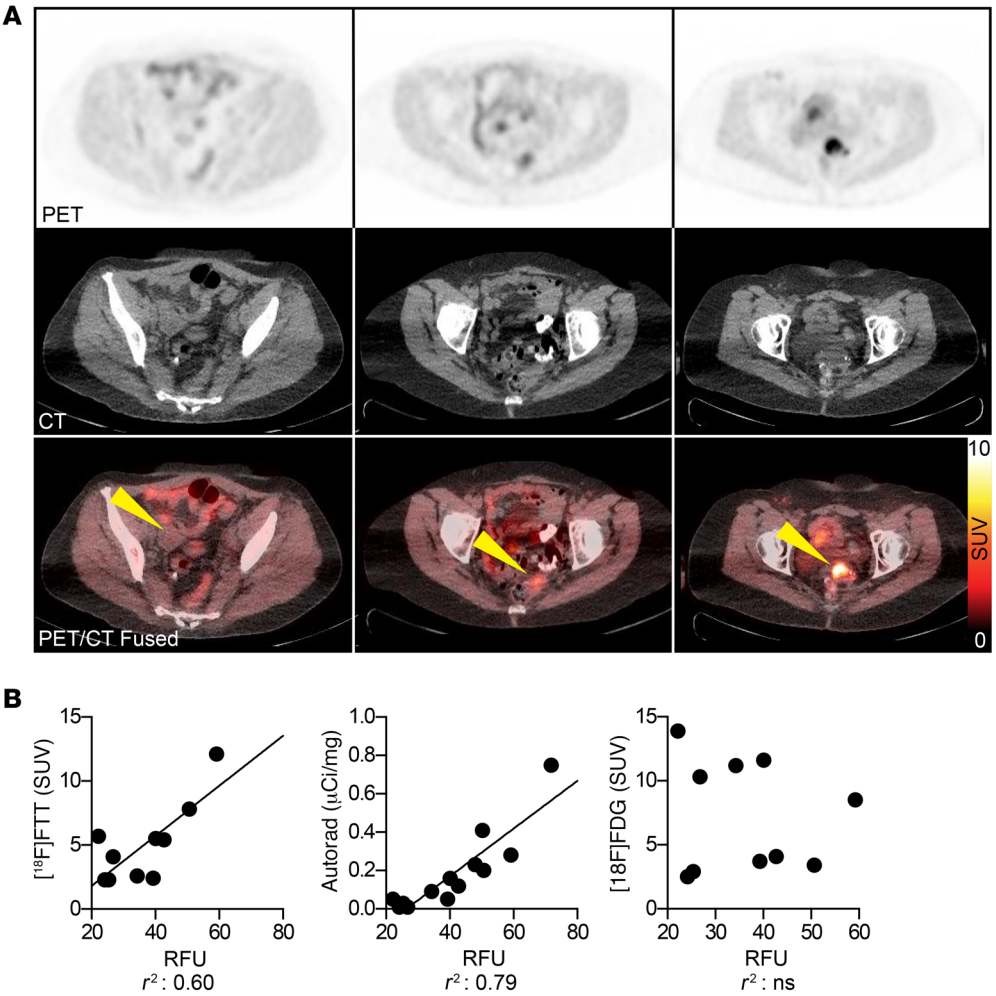

Figure 7. [18F]FTT PET imaging of PARP-1 in ovarian cancer patients and tissue correlates. (**A**) The spectrum of PARP-1 expression as determined by [18F]FTT PET/CT imaging with maximum SUVs ranging from approximately 2 to 12. Yellow arrows indicate sites of disease. (**B**) We found a positive correlation between PARP-1 immunofluorescence versus [18F]FTT PET or [125I]KX1 autoradiography (linear regression, r^2 = 0.60, 0.79). No associations were observed between PARP-1 immunofluorescence, [18F]FTT imaging, or [125I]KX1 autoradiography and [18F]FDG.

less of BRCA mutation status (6–8). These clinical reports suggest there is a need for predictive biomarkers for PARPi therapy that go beyond BRCA mutation and HRD testing. The direct measurement of the PARPi target, PARP-1 expression, described in this work offers a complementary approach that could strengthen genomic testing for predicting patient response to PARPi therapy.

We demonstrated that in addition to using radioligand binding as an in vitro assay of PARP-1 expression, the use of PET radiopharmaceuticals as an in vivo assay for PARP-1 is feasible in patients. This work reports the first clinical imaging trial in EOC using a PARP-1 radiotracer, [18F]FTT, and preliminarily establishes [18F]FTT as a noninvasive biomarker of PARP-1. We found a wide spectrum of PARP-1 expression in EOC measured by [18F]FTT PET, with some tumors showing SUVs as high as 12 and as low as 2. Regardless of the exact mechanism in which PARPis induce anticancer effects, all current models require the drug target PARP-1 (15, 16, 23, 24). This signifies the importance of quantitatively assessing the target of PARPis directly at the site of action by measuring intratumoral PARP-1 in primary and metastatic disease. We have shown in preclinical imaging studies that [18F]FTT is capable of quantifying intratumoral PARPi–PARP-1 drug-target engagement. This is the only biomarker technology capable of noninvasively measuring PARP-1 and PARPi drug-target engagement directly in tumors, in contrast to surrogate assays such as peripheral blood test (43).

PARP-1 expression may also play a role in predicting inherent or incurred DNA damage burden to identify DNA repair deficiencies or even treatment response as a functional biomarker of HRD (44, 45). We are currently entering several clinical trials in both breast and ovarian cancer at the University of Pennsylvania to directly evaluate [18F]FTT as a predictive and pharmacodynamic biomarker of PARPi therapy and other DNA-damaging chemotherapy. These studies should provide the impetus for multicenter clinical trials to fully evaluate the importance of PARP-1 expression as a biomarker for cancer therapy and the technological advantages of [18F]FTT for measuring intratumoral and intertumoral PARP-1 expression versus conventional IHC approaches.

Methods

Study design. The objective of this study was to highlight the significance of PARP-1 expression for PARP inhibitor therapy using preclinical models of ovarian cancer and perform the first PET imaging study of PARP-1 in ovarian cancer using [18F]FTT with histological correlates to confirm radiotracer uptake as a biomarker of PARP-1 expression. This goal was addressed by using CRISPR/Cas9 to delete *PARP1* in models of ovarian cancer, which were then used to test PARPi efficacy in vitro. In addition, we used patient-derived orthotopic xenograft models of ovarian cancer to show proof of concept for [18F]FTT microPET imaging of PARP-1 and PARPi drug-target engagement in

vivo. [18F]FTT PET imaging of PARP-1 was performed in patients with ovarian cancer, and tumor specimens were retrieved at surgical debulking or biopsy for in vitro correlative analysis of PARP-1 using [125I]KX1 autoradiography and PARP-1 f-IHC.

All in vitro experiments were carried out using a standard cell culture technique and repeated 3 independent times. The deletion of *PARP1* with CRISPR/Cas9 was performed in 2 ovarian cancer cell lines. In addition, 3 unique guide RNAs were used to mediate the deletion of *PARP1*. Polyclonal populations of *PARP1*-KO cell lines were used to test PARPi efficacy in vitro. A sample size of 4 was selected for preclinical imaging studies to prevent bias greater than 10% for interpreting and analyzing microPET image results. No data from preclinical models was excluded from analyses.

For the clinical portion of this study, 20 patients with EOC were enrolled, 10 of whom had tissue available for in vitro analysis. Eight of those 10 underwent [18F]FTT imaging prior to subsequent standard clinical management (Figure 3). One of the 8 patients who underwent [18F]FTT had a negative PET image and was excluded from correlative analysis. A total of 13 tissue specimens was available from the 10 patients and these specimens were used for in vitro assays including PARP-1 f-IHC and [125I]KX1 autoradiography (Supplemental Table 5). All tissue specimens from patients who underwent [18F]FTT PET imaging were included in correlations among [18F]FTT PET, [18F]FDG, [125I]KX1 autoradiography, and PARP-1 f-IHC. All tissue specimens collected from consenting patients were included in correlations between [125I]KX1 and PARP-1 f-IHC. Patients with and without *BRCA1* mutations were enrolled in this study (Supplemental Table 6). All experimental procedures for preclinical and clinical work are described in detail in the supplemental information.

CRISPR/Cas9 deletion of PARP1 in ovarian cancer cells. OVCAR8 cells were a gift from David M. Livingston (Dana Farber Cancer Institute, Boston, Massachusetts, USA). All other cell lines were available through ATCC or the Basser Center for BRCA (University of Pennsylvania, Philadelphia, Pennsylvania, USA) (Supplemental Table 1). *PARP1* was deleted in UWB1.289 and OVCAR8 EOC cell lines that have reduced BRCA-1 expression through a deleterious mutation (UWB1.289) or promoter methylation (OVCAR8). These mutations are characterized elsewhere in the literature (46, 47). Using 3 unique guide RNAs (Supplemental Material), *PARP1* deletion was mediated by Cas9 in both cell lines, effectively producing 3 unique polyclonal *PARP1*-KO cell lines for each. Loss of PARP-1 expression was confirmed by IF cell microscopy and Western blot in each polyclonal population. Polyclonal populations were used in all experiments.

[125I]KX1 radioligand binding measures differences in PARP-1 expression. Using multiple ovarian cancer cell lines, we performed in vitro pharmacological PARP-1 saturation radioligand binding studies to quantify PARP-1 expression. [125I]KX1 was synthesized and in vitro radioligand binding studies were performed as previously described (16). Briefly, increasing concentrations of [125I]KX1 from 0.01–10 nM were added to a 96-well plate in quadruplicate for each respective cell line and experiments were completed in triplicate.

Loss of PARP1 promotes PARPi resistance in ovarian cancer cell lines. Immunofluorescence was used to determine DNA damage induced by olaparib or DMSO control in ovarian cancer cell lines. Using 5 clinically used PARPis, we performed in vitro cell viability assays to determine changes in drug sensitivity based on loss of PARP-1 expression. The experimental procedures were adopted from previous work (16). Cisplatin was also examined as a control to evaluate changes in sensitivity of DNA-damaging agents that occur after loss of *PARP1*. Cell viability was assessed using CellTiterGlo (Promega). Experiments were completed in duplicate 3 independent times.

Preclinical microPET imaging of PARP-1. Through serial [18F]FTT PET imaging studies, we evaluated PARP-1 drug-target engagement using the FDA-approved PARPi olaparib. PET imaging of PARP-1 drug-target engagement is a noninvasive methodology to directly assess PARP inhibition. Using 2 ovarian cancer patient–derived xenograft models in 15- to 18-week-old female NOD SCID mice provided from the Simpkins laboratory at the University of Pennsylvania (48), including a *BRCA1* mutant and WT, we performed microPET imaging on a Phillips Medical Systems scanner (n = 4 mice). Mice were imaged on day 1 and then olaparib was orally administered daily by gavage at a dose of 50 mg/kg. Mice were then reimaged on day 4, 1 hour after the fourth dose of olaparib. A total of 4 doses of olaparib was administered between imaging studies to achieve steady state. Ex vivo autoradiography studies were performed on mice from PDX model WO-12-2 with and without olaparib treatment (n = 6). The differences in tumor-to-muscle ratios were measured and were representative of the percentage of PARPi drug-target engagement.

PARP-1 immunohistochemistry and autoradiography on clinical specimens. Colormetric immunohistochemistry was performed at the University of Pennsylvania Pathology Core for H&E and biomarkers, including PARP-1, γH2AX, p53, LCA, and AE1/3. These biomarkers were chosen due to their relevance to EOC. AE1/3 is a keratin marker and was used to identify tumor cells by c-IHC. In order to determine where in the tumor microenvironment PARP-1 was expressed, we costained with LCA, which is a pan lymphocyte marker. In addition, we analyzed common biomarkers present in high-grade serous EOC, including p53 and γH2AX. Lastly, PARP-1 was evaluated by f-IHC and [125I]KX1 autoradiography on adjacent sections to determine whether the 2 methods colocalize.

Clinical [18F]FTT PET imaging. The clinical trial included 2 imaging cohorts: a biodistribution cohort and a dynamic cohort. The patients included in this trial with pathologic correlates were all enrolled in the dynamic cohort. As such, only that protocol is reported in this section. Dynamic scanning was performed for approximately 60 minutes from the time of injection with a field-of-view over the abdomen/pelvis or to include a known site of tumor involvement. Static images from the skull base to mid-thigh were performed starting approximately 90 and 180 minutes after [18F]FTT injection; these static scans were optional at the discretion of the investigator or study physician. Static images obtained at approximately 90 minutes were used in the analysis. [18F]FTT PET/CT imaging was performed on a Phillips Ingenuity PET/CT scanner (Phillips Medical Systems). Images were reconstructed using standard reconstruction techniques and interpreted by trained radiology readers. Lesions were first located on a contemporaneous clinical [18F]FDG PET/CT and then located on the [18F]FTT PET/CT. The maximum SUV was recorded for each scan.

Statistics. Data presented are mean ± SEM unless otherwise noted. All graphs were produced and statistically analyzed using Prism version 6.0, GraphPad. The maximum number of PARP binding sites (B_{max}) was calculated by an exponential nonlinear curve–fit 1-site binding hyperbola function. All statistical tests comparing the mean of 2 groups were 2-sided. The comparisons of the means from more than 2 groups were performed using 1-way ordinary ANOVA.

Dose-response curves were fitted using a nonlinear sigmoidal dose-response curve, and effective calculations for 50% reduction in cell viability were calculated. Image analysis was performed using PMOD software, and tumor-to-muscle ratios were calculated. Preclinical microPET imaging studies comparing tumor uptake of radiotracer were analyzed using a paired, 2-tailed *t* test. Autoradiography studies were analyzed using an unpaired 2-tailed *t* test. We chose an α of 0.05 (95% confidence interval) and data were deemed significant if $P < 0.05$. For correlations, the Pearson correlation coefficient was calculated and the data were considered statistically significant if $P < 0.05$. To determine the ability of [^{18}F]FTT PET maximum SUV to predict PARP-1 expression measured by f-IHC, we used a linear regression and results were considered statistically significant if different from zero.

Study approval. All animal studies were performed under protocols approved by the University of Pennsylvania Institutional Animal Care and Use Committee, Philadelphia, Pennsylvania, USA. Studies were conducted under guidelines for animal welfare provided by the NIH. This was an open-label, phase I trial of [^{18}F]FTT PET conducted under an approved IRB at the University of Pennsylvania, Philadelphia, PA, USA, and registered with the FDA as an expanded investigational new drug (clinical trial identifier: NCT02637934). All subjects consented to PET imaging and providing clinical tissue specimens for in vitro analysis.

Author contributions

MM designed experiments, performed experiments, collected data, analyzed data, and composed the manuscript. AP read PET scans, determined SUV values in lesions for PET tracers, analyzed data, and composed the manuscript. LS interpreted tissue histology and evaluated biomarker positivity. ES wrote the clinical protocol. KX synthesized precursors for radiotracers used. CJH analyzed preclinical PET imaging data. CH performed in vivo preclinical PET imaging studies. HK developed and produced patient-derived xenograft models. CCW performed ex vivo autoradiography studies and analyzed data. HW designed CRISPR/Cas9 guides for PARP-1 and performed in vitro *PARP1*-KO experiments. RD analyzed clinical PET images. MDF administered the radiotracer to patients and interpreted PET images. DAP administered the radiotracer to patients and interpreted PET images. RAG designed in vitro experiments and composed the manuscript. DAM administered the radiotracer to patients, designed experiments, interpreted the data, and composed the manuscript. FS designed patient-derived xenograft models, recruited patients, performed surgeries and biopsies, and composed the manuscript. RHM designed radiotracers and experiments and composed the manuscript. LLL designed experiments, analyzed data, recruited patients, lead the clinical trial, and composed the manuscript.

Acknowledgments

The authors would like to acknowledge the University of Pennsylvania PET center and cyclotron facility for clinical support and manufacturing of radiopharmaceuticals used in this study. The authors would like to specifically thank Mark A. Sellmyer and Elizabeth S. McDonald (Perelman School of Medicine, University of Pennsylvania) for their input regarding this work.

Address correspondence to: Mehran Makvandi, Division of Nuclear Medicine and Clinical Molecular Imaging, Department of Radiology, Perelman School of Medicine University of Pennsylvania, 231 South 34th Street, Philadelphia, Pennsylvania 19104, USA. Phone: 267.572.0621; Email: makvandi@pennmedicine.upenn.edu. Or to: Lilie L. Lin, Department of Radiation Oncology, University of Texas, MD Anderson Cancer Center, 1515 Holcombe Boulevard, Unit 1422, Houston, Texas 77030, USA. Phone: 713.563.2300; Email: lllin@mdanderson.org.

LLL's present address is: Department of Radiation Oncology, University of Texas, MD Anderson Cancer Center, Houston, Texas, USA.

1. Siegel RL, Miller KD, Jemal A. Cancer statistics, 2016. *CA Cancer J Clin*. 2016;66(1):7–30.
2. Herzog TJ. The current treatment of recurrent ovarian cancer. *Curr Oncol Rep*. 2006;8(6):448–454.
3. Lord CJ, Ashworth A. PARP inhibitors: synthetic lethality in the clinic. *Science*. 2017;355(6330):1152–1158.
4. Konstantinopoulos PA, Ceccaldi R, Shapiro GI, D'Andrea AD. Homologous recombination deficiency: exploiting the fundamental vulnerability of ovarian cancer. *Cancer Discov*. 2015;5(11):1137–1154.
5. Mirza MR, Matulonis UA. Niraparib in recurrent ovarian cancer. *N Engl J Med*. 2017;376(8):801–802.
6. Mirza MR, et al. Niraparib maintenance therapy in platinum-sensitive, recurrent ovarian cancer. *N Engl J Med*. 2016;375(22):2154–2164.
7. Coleman RL, et al. Rucaparib maintenance treatment for recurrent ovarian carcinoma after response to platinum therapy (ARIEL3): a randomised, double-blind, placebo-controlled, phase 3 trial. *Lancet*. 2017;390(10106):1949–1961.
8. Pujade-Lauraine E, et al. Olaparib tablets as maintenance therapy in patients with platinum-sensitive, relapsed ovarian cancer and a BRCA1/2 mutation (SOLO2/ENGOT-Ov21): a double-blind, randomised, placebo-controlled, phase 3 trial. *Lancet Oncol*. 2017;18(9):1274–1284.
9. Tutt A, et al. Oral poly(ADP-ribose) polymerase inhibitor olaparib in patients with BRCA1 or BRCA2 mutations and advanced breast cancer: a proof-of-concept trial. *Lancet*. 2010;376(9737):235–244.
10. Tutt AN, et al. Exploiting the DNA repair defect in BRCA mutant cells in the design of new therapeutic strategies for cancer. *Cold Spring Harb Symp Quant Biol*. 2005;70:139–148.
11. Swisher EM, et al. Rucaparib in relapsed, platinum-sensitive high-grade ovarian carcinoma (ARIEL2 Part 1): an international, multicentre, open-label, phase 2 trial. *Lancet Oncol*. 2017;18(1):75–87.
12. Somlo G, et al. Efficacy of the PARP inhibitor veliparib with carboplatin or as a single agent in patients with germline BRCA1- or BRCA2-associated metastatic breast cancer: California Cancer Consortium Trial NCT01149083. *Clin Cancer Res*. 2017;23(15):4066–4076.
13. de Bono J, et al. Phase I, dose-escalation, two-part trial of the PARP inhibitor talazoparib in patients with advanced germline BRCA1/2 mutations and selected sporadic cancers. *Cancer Discov*. 2017;7(6):620–629.
14. Pommier Y, O'Connor MJ, de Bono J. Laying a trap to kill cancer cells: PARP inhibitors and their mechanisms of action. *Sci Transl Med*. 2016;8(362):362ps17.
15. Pettitt SJ, et al. A genetic screen using the PiggyBac transposon in haploid cells identifies Parp1 as a mediator of olaparib toxicity. *PLoS One*. 2013;8(4):e61520.
16. Makvandi M, et al. A radiotracer strategy to quantify PARP-1 expression in vivo provides a biomarker that can enable patient selection for PARP inhibitor therapy. *Cancer Res*. 2016;76(15):4516–4524.
17. Ha HC, Snyder SH. Poly(ADP-ribose) polymerase is a mediator of necrotic cell death by ATP depletion. *Proc Natl Acad Sci U S A*. 1999;96(24):13978–13982.

18. Heacock ML, Stefanick DF, Horton JK, Wilson SH. Alkylation DNA damage in combination with PARP inhibition results in formation of S-phase-dependent double-strand breaks. *DNA Repair (Amst)*. 2010;9(8):929–936.
19. Horton JK, Stefanick DF, Naron JM, Kedar PS, Wilson SH. Poly(ADP-ribose) polymerase activity prevents signaling pathways for cell cycle arrest after DNA methylating agent exposure. *J Biol Chem*. 2005;280(16):15773–15785.
20. Bryant HE, et al. Specific killing of BRCA2-deficient tumours with inhibitors of poly(ADP-ribose) polymerase. *Nature*. 2005;434(7035):913–917.
21. Farmer H, et al. Targeting the DNA repair defect in BRCA mutant cells as a therapeutic strategy. *Nature*. 2005;434(7035):917–921.
22. Murai J, et al. Trapping of PARP1 and PARP2 by Clinical PARP Inhibitors. *Cancer Res*. 2012;72(21):5588–5599.
23. Murai J, et al. Stereospecific PARP trapping by BMN 673 and comparison with olaparib and rucaparib. *Mol Cancer Ther*. 2014;13(2):433–443.
24. Hopkins TA, et al. Mechanistic dissection of PARP1 trapping and the impact on in vivo tolerability and efficacy of PARP inhibitors. *Mol Cancer Res*. 2015;13(11):1465–1477.
25. Godoy H, Mhawech-Fauceglia P, Beck A, Miller A, Lele S, Odunsi K. Expression of poly (adenosine diphosphate-ribose) polymerase and p53 in epithelial ovarian cancer and their role in prognosis and disease outcome. *Int J Gynecol Pathol*. 2011;30(2):139–144.
26. Brustmann H. Poly(adenosine diphosphate-ribose) polymerase expression in serous ovarian carcinoma: correlation with p53, MIB-1, and outcome. *Int J Gynecol Pathol*. 2007;26(2):147–153.
27. Gan A, Green AR, Nolan CC, Martin S, Deen S. Poly(adenosine diphosphate-ribose) polymerase expression in BRCA-proficient ovarian high-grade serous carcinoma; association with patient survival. *Hum Pathol*. 2013;44(8):1638–1647.
28. Hjortkjær M, Waldstrøm M, Jakobsen A, Kanstrup H, Søgaard-Andersen E, Dahl Steffensen K. The prognostic value of BRCA1 and PARP expression in epithelial ovarian carcinoma: immunohistochemical detection. *Int J Gynecol Pathol*. 2017;36(2):180–189.
29. Mazzotta A, Partipilo G, De Summa S, Giotta F, Simone G, Mangia A. Nuclear PARP1 expression and its prognostic significance in breast cancer patients. *Tumour Biol*. 2016;37(5):6143–6153.
30. Wu W, et al. Expression of PARP-1 and its active polymer PAR in prostate cancer and benign prostatic hyperplasia in Chinese patients. *Int Urol Nephrol*. 2014;46(7):1345–1349.
31. Knight JC, Koustoulidou S, Cornelissen B. Imaging the DNA damage response with PET and SPECT. *Eur J Nucl Med Mol Imaging*. 2017;44(6):1065–1078.
32. Carney B, Kossatz S, Reiner T. Molecular imaging of PARP. *J Nucl Med*. 2017;58(7):1025–1030.
33. Zhou D, et al. Synthesis, [^{18}F] radiolabeling, and evaluation of poly (ADP-ribose) polymerase-1 (PARP-1) inhibitors for in vivo imaging of PARP-1 using positron emission tomography. *Bioorg Med Chem*. 2014;22(5):1700–1707.
34. Michel LS, et al. PET of poly (ADP-Ribose) polymerase activity in cancer: preclinical assessment and first in-human studies. *Radiology*. 2017;282(2):453–463.
35. Edmonds CE, et al. [(18)F]FluorThanatrace uptake as a marker of PARP1 expression and activity in breast cancer. *Am J Nucl Med Mol Imaging*. 2016;6(1):94–101.
36. Busschots S, O'Toole S, O'Leary JJ, Stordal B. Carboplatin and taxol resistance develops more rapidly in functional BRCA1 compared to dysfunctional BRCA1 ovarian cancer cells. *Exp Cell Res*. 2015;336(1):1–14.
37. Stordal B, et al. BRCA1/2 mutation analysis in 41 ovarian cell lines reveals only one functionally deleterious BRCA1 mutation. *Mol Oncol*. 2013;7(3):567–579.
38. Choi YE, et al. Sublethal concentrations of 17-AAG suppress homologous recombination DNA repair and enhance sensitivity to carboplatin and olaparib in HR proficient ovarian cancer cells. *Oncotarget*. 2014;5(9):2678–2687.
39. Ding X, et al. Synthetic viability by BRCA2 and PARP1/ARTD1 deficiencies. *Nat Commun*. 2016;7:12425.
40. Khiewvan B, et al. An update on the role of PET/CT and PET/MRI in ovarian cancer. *Eur J Nucl Med Mol Imaging*. 2017;44(6):1079–1091.
41. Tang J, et al. Targeted PET imaging strategy to differentiate malignant from inflamed lymph nodes in diffuse large B-cell lymphoma. *Proc Natl Acad Sci U S A*. 2017;114(36):E7441–E7449.
42. Kondrashova O, et al. Secondary somatic mutations restoring RAD51C and RAD51D associated with acquired resistance to the PARP inhibitor rucaparib in high-grade ovarian carcinoma. *Cancer Discov*. 2017;7(9):984–998.
43. Rodler ET, et al. Phase I study of veliparib (ABT-888) combined with Cisplatin and Vinorelbine in advanced triple-negative breast cancer and/or BRCA mutation-associated breast cancer. *Clin Cancer Res*. 2016;22(12):2855–2864.
44. Li D, et al. A novel crosstalk between BRCA1 and poly (ADP-ribose) polymerase 1 in breast cancer. *Cell Cycle*. 2014;13(21):3442–3449.
45. Wu X, et al. FASN regulates cellular response to genotoxic treatments by increasing PARP-1 expression DNA repair activity via NF-κB SP1 [published online ahead of print October 24, 2016]. *Proc Natl Acad Sci U S A*. doi: 10.1073/pnas.1609934113.
46. Mitra AK, et al. In vivo tumor growth of high-grade serous ovarian cancer cell lines. *Gynecol Oncol*. 2015;138(2):372–377.
47. DelloRusso C, Welcsh PL, Wang W, Garcia RL, King MC, Swisher EM. Functional characterization of a novel BRCA1-null ovarian cancer cell line in response to ionizing radiation. *Mol Cancer Res*. 2007;5(1):35–45.
48. George E, et al. A patient-derived-xenograft platform to study BRCA-deficient ovarian cancers. *JCI Insight*. 2017;2(1):e89760.

Kinetic and Static Analysis of Poly-(Adenosine Diphosphate-Ribose) Polymerase-1–Targeted ^{18}F-Fluorthanatrace PET Images of Ovarian Cancer

Anthony J. Young[1], Austin R. Pantel[1], Varsha Viswanath[1], Tiffany L. Dominguez[1], Mehran Makvandi[1], Hsiaoju Lee[1], Shihong Li[1], Erin K. Schubert[1], Daniel A. Pryma[1], Michael D. Farwell[1], Robert H. Mach[1], Fiona Simpkins[2], Lilie L. Lin[3], David A. Mankoff[1], and Robert K. Doot[1]

[1]*Department of Radiology, Perelman School of Medicine, University of Pennsylvania, Philadelphia, Pennsylvania;* [2]*Division of Gynecology and Oncology, Department of OBGYN, Perelman School of Medicine, University of Pennsylvania, Philadelphia, Pennsylvania; and* [3]*Department of Radiation Oncology, University of Texas MD Anderson Cancer Center, Houston, Texas*

The poly-(adenosine diphosphate-ribose) polymerase (PARP) family of proteins participates in numerous functions, most notably the DNA damage response. Cancer vulnerability to DNA damage has led to development of several PARP inhibitors (PARPi). This class of drugs has demonstrated therapeutic efficacy in ovarian, breast, and prostate cancers, but with variable response. Consequently, clinics need to select patients likely to benefit from these targeted therapies. In vivo imaging of ^{18}F-fluorthanatrace uptake has been shown to correspond to PARP-1 expression in tissue. This study characterized the pharmacokinetics of ^{18}F-fluorthanatrace and tested kinetic and static models to guide metric selection in future studies assessing ^{18}F-fluorthanatrace as a biomarker of response to PARPi therapy. **Methods:** Fourteen prospectively enrolled ovarian cancer patients were injected with ^{18}F-fluorthanatrace and imaged dynamically for 60 min after injection followed by up to 2 whole-body scans, with venous blood activity and metabolite measurements. SUV_{max} and SUV_{peak} were extracted from dynamic images and whole-body scans. Kinetic parameter estimates and SUVs were assessed for correlations with tissue PARP-1 immunofluorescence ($n = 7$). Simulations of population kinetic parameters enabled estimation of measurement bias and precision in parameter estimates. **Results:** ^{18}F-fluorthanatrace blood clearance was variable, but labeled metabolite profiles were similar across patients, supporting use of a population parent fraction curve. The total distribution volume from a reversible 2-tissue-compartment model and Logan reference tissue distribution volume ratio (DVR) from the first hour of PET acquisition correlated with tumor PARP-1 expression by immunofluorescence ($r = 0.76$ and 0.83, respectively; $P < 0.05$). DVR bias and precision estimates were 6.4% and 29.1%, respectively. SUV_{max} and SUV_{peak} acquired from images with midpoints of 57.5, 110 ± 3, and 199 ± 4 min highly correlated with PARP-1 expression (mean ± SD, $r \geq 0.79$; $P < 0.05$). **Conclusion:** Tumor SUV_{max} and SUV_{peak} at 55–60 min after injection and later and DVR from at least 60 min appear to be robust noninvasive measures of PARP-1 binding. ^{18}F-fluorthanatrace uptake in ovarian cancer was best described by models of reversible binding. However, pharmacokinetic patterns of tracer uptake were somewhat variable, especially at later time points.

Key Words: PET; ^{18}F-fluorthanatrace; PARP inhibitor; ovarian cancer; radiotracer tissue pharmacokinetics

Received Jan. 1, 2021; revision accepted Mar. 26, 2021.

For correspondence or reprints, contact Robert K. Doot (robdoot@pennmedicine.upenn.edu).

Published online Apr. 16, 2021.

COPYRIGHT © 2022 by the Society of Nuclear Medicine and Molecular Imaging.

J Nucl Med 2022; 63:44–50
DOI: 10.2967/jnumed.121.261894

Poly-adenosine diphosphate-ribose polymerase inhibitors (PARPis) have demonstrated efficacy in a variety of cancers. Three PARPis (olaparib, rucaparib, and niraparib) are currently approved by the Food and Drug Administration for selected indications for ovarian cancers, and one, talazoparib, is approved for women with locally advanced or metastatic breast cancer with germline breast cancer gene mutations. The PARPi olaparib was initially approved in 2014 for advanced ovarian cancer patients with deleterious or suspected deleterious germline breast cancer gene mutations after treatment with 3 or more lines of chemotherapy. Since then, additional indications have included patients with a response to platinum-based chemotherapy, another marker for DNA repair defects (*1*). However, PARPi efficacy for approved ovarian cancer indications is variable, providing the impetus to develop noninvasive biomarkers to measure the entire burden of disease and better guide selection of targeted therapies containing PARPis (*2*). With this goal, the PET radiotracer ^{18}F-fluorthanatrace has been developed as a noninvasive in vivo measure of PARP-1 expression (*3*,*4*).

^{18}F-fluorthanatrace has been evaluated in preclinical models (*3*) and cancer patients (*4*). The human ovarian cancer study of Makvandi et al. demonstrated a correlation between static PET uptake measures and PARP-1 expression in tissue as measured by immunohistochemistry and autoradiography (*5*). A wide range of ^{18}F-fluorthanatrace uptake was seen in ovarian cancer patients, from a background voxel SUV_{max} of 2 to above 12 g/mL (*5*). Similar studies are under way in other cancers, including breast (*6*), pancreatic, prostate, and glioblastoma (*2*).

In this companion study, we analyzed the pharmacokinetics of ^{18}F-fluorthanatrace PET uptake in 14 ovarian cancer patients by expanding PET data from the single static PET scan reported in Makvandi et al. (*5*) to include a 1-h dynamic acquisition and an optional second static scan for up to 3 same-day PET scans per subject. Our results include 7 previously reported SUVs from the parent study (*5*). Kinetic parameters derived from graphical and compartmental models were compared with tissue PARPi expression assays to inform selection of imaging metrics and timing for PET image acquisition. Computer simulations were used to study model

behavior under typical conditions. Static SUVs and SUV–to–normal-tissue ratios were compared with kinetic parameters to guide selection of clinic-friendly imaging protocols.

MATERIALS AND METHODS

Clinical Trial

Women with known or suspected recurrent or metastatic epithelial ovarian cancer were enrolled and gave written informed consent for a University of Pennsylvania Institutional Review Board–approved prospective clinical trial of ^{18}F-fluorthanatrace PET/CT imaging (NCT02637934) between January 2016 and January 2017 at the Hospital of the University of Pennsylvania. The study protocol is described at clinicaltrials.gov. Surgical or biopsy samples were analyzed for PARP-1 expression using immunofluorescence assays. A detailed description of this clinical trial and tissue analysis methods can be found in a previous publication by Makvandi et al., including supplemental materials (*5*). Patients were separated into dynamic and dosimetry imaging cohorts.

Imaging Protocol

Synthesis of ^{18}F-fluorthanatrace was described previously (*3*). PET/CT imaging was performed on an Ingenuity TF scanner (Philips Healthcare) (*7*) over 1 field of view for 60 min after injection of ^{18}F-fluorthanatrace (387 ± 39 MBq). Up to 2 whole-body scans were acquired, beginning 90 and 180 min after injection. Dynamic PET acquisitions were reconstructed (*7*) into 50 frames: 24 of 5-s duration, 6 of 10-s duration, 3 of 20-s duration, 2 of 30-s duration, 5 of 60-s duration, and 10 of 300-s duration.

Venous Blood Sampling and Analysis

Venous blood was sampled at approximately 2, 5, 10, 30, 60, and 240 min after injection to measure radiometabolites. Activity concentrations in whole blood and plasma were counted using a WIZARD^2 2480 γ-counter (Perkin Elmer). Acetonitrile-treated plasma supernatant was analyzed in a 1260 Infinity Series (Agilent Technologies) high-performance liquid chromatology system using an Agilent ZORBAX StableBond C18 column via a mobile phase of 51% methanol and 49% 0.1 M ammonium formate buffer. A sample radiochromatogram is shown in Supplemental Figure 1 (supplemental materials are available at http://jnm.snmjournals.org).

Image Analysis

PET images were processed using MIM, version 6.9 (MIM Software Inc.), with spheric volumes of interest (VOIs) drawn around tumor and background regions; a board-certified nuclear medicine physician verified placement. Time–activity curves for tumor SUV_{max} and SUV_{peak} with and without partial-volume correction were used for kinetic analysis. SUV_{peak} was automatically positioned as the 1-cm^3 volume with the greatest mean activity for each image frame (*8*). Partial-volume correction of SUV measures was performed as previously described (*9*), using a normal-muscle background region. Image blood pool SUV_{peak} was measured in the iliac artery for 10 patients with abdominal imaging or in the descending aorta for 4 patients with thoracic imaging. Background muscle activity was estimated using a 20-mm-diameter VOI in the gluteal or paraspinal musculature. Tumor–to–normal-muscle activity ratios were calculated by dividing tumor activity by average background. Whole-body scan data were added to dynamic data after correcting for timing of the 2–3 bed positions covering a VOI.

Kinetic Analysis

Kinetic analysis of radiotracer uptake was performed using PMOD, version 3.7 (PMOD Technologies Ltd.). Individual parent fraction data were corrected for plasma protein binding, averaged between patients, and fitted sigmoidally, creating a population ^{18}F-fluorthanatrace parent fraction function to correct blood inputs for labeled metabolites. Tumor blood volume fractions were assumed to vary within 0.01–0.40, with the upper bound being based on literature values for malignant ovarian cancer (*10*) and the lower bound being a minimal physiologically relevant value.

Image-extracted blood input curves were fitted to triexponential functions and corrected for population-averaged plasma partitioning. The initial parameters and bounds were selected to encompass expected parameter ranges (Supplemental Table 1). Compartmental models were initially fit using data from the dynamic and both static scans. For comparison, models were fit with the dynamic plus the first whole-body scan, the 0- to 60-min dynamic dataset, and the truncated 0- to 30-min dataset. Reported results are from the 0- to 60-min dynamic dataset unless stated otherwise.

Tumor kinetics were analyzed using reversible models of ^{18}F-fluorthanatrace binding: a 2-tissue-compartment model with reversible binding (2CR) and a reversible graphical method. The graphical technique of Logan et al. (*11*) was used to estimate the tumor distribution volume ratio (DVR) without needing blood activity or metabolite measurements and to compensate for possible low-level nonspecific uptake. Since the initial equilibration time t* for the population was 40 min, this model was not evaluated on 0- to 30-min data. The positive efflux rate term k_2' for transfer from muscle to plasma was averaged and used for all patients via a multilinear reference tissue model (*12*).

Statistics

Comparisons between kinetic model complexity and effectiveness were evaluated via a PMOD-calculated Akaike information criterion (*13*).

Static tumor SUV, tumor–to–normal-muscle ratios, 2CR distribution volume (V_T), and Logan reference model DVR estimations were each tested for a correlation with 7 PARP-1 tumor immunofluorescence values, using the immunofluorescence methods reported in the supplemental materials of Makvandi et al. (*5*).

The 2-tailed Pearson r was calculated in SPSS25 (IBM Armonk) and used to assess correlations between tissue immunofluorescence and imaging data; correlations with a P value of at least 0.05 were considered significant against the null hypothesis of $r = 0$.

Kinetic Model Performance

Sensitivity curves were calculated as percentage change in model output corresponding to a 1% change in each parameter. The repeatability of kinetic parameter estimation was analyzed using simulated data based on ranges of individual kinetic parameters via methods of Viswanath et al. (*14*). Bias was averaged across each of 100 noise realizations, and averaged across 200 runs. Precision for each run was calculated as the average SD across all noise realizations, divided by the true value.

RESULTS

Twenty women with recurrent or metastatic epithelial ovarian cancer, and ranging in age from 21 to 70 y, were enrolled. A trial diagram overview was published previously (*5*). Eighteen patients were imaged with ^{18}F-fluorthanatrace PET/CT, and 16 completed venous blood sampling with no reported adverse events.

Of the 18 patients, a dynamic imaging cohort of 14 was scanned for 60 min after injection, followed by scanning at 90 and 180 min after injection, from the skull base to the mid thigh (whole body static scans). Blood data from 4 subjects in the dosimetry cohort were included in population blood results. Tumors were visible in dynamic fields of view for 10 patients, 7 of whom had surgical tumor tissue samples and accompanying PARP-1 immunofluorescence assays. Static scans measured tumor activity at 110 ± 3 min (mean ± SD) and 199 ± 4 min after injection. Representative PET and PET/CT images are in Figure 1.

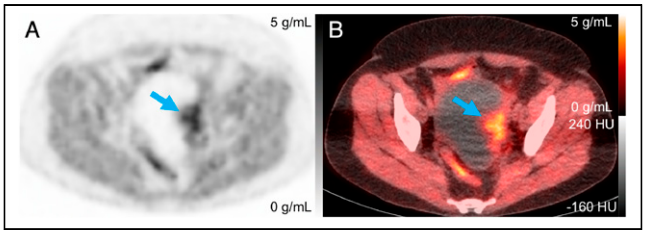

FIGURE 1. PET (A) and PET/CT (B) images of patient 4 at 108 min after injection, with arrow indicating tumor with SUV_{max} of 5.6 g/mL.

Tumor ^{18}F-fluorthanatrace uptake, as measured by SUV_{max} and SUV_{peak}, generally increased over the 60-min dynamic scan and the subsequent static scans, with more variable behavior after 60 min (Fig. 2). SUV_{max} at 55–60 min after injection was 4.2 ± 2.0 g/mL, and SUV_{peak} was 3.4 ± 1.6 g/mL. Normal-muscle, bone, and blood pool activities (representative patient in Fig. 3) were fairly stable over time and were used for kinetic modeling and SUV ratios. Tumor–to–normal-muscle SUV ratios were 2.6 ± 1.1 for SUV_{max} and 2.1 ± 0.9 for SUV_{peak}. Partial-volume corrections based on tumor size and normal-muscle background uptake resulted in SUV increases (Supplemental Table 2).

Blood sampling and processing were performed on 16 patients. Results from samples at 240 min after injection were omitted because of high error from low counts. ^{18}F-fluorthanatrace blood inputs demonstrated some variability between patients. There were also noted differences based on the location of the blood

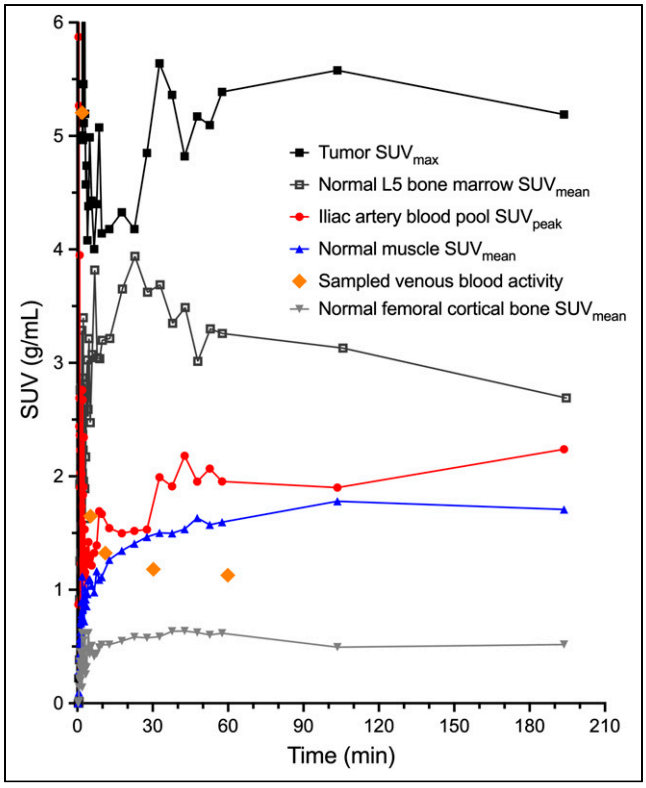

FIGURE 3. Patient 4 time–activity curves for 1-h dynamic acquisition after injection and 2 subsequent whole-body PET/CT scans.

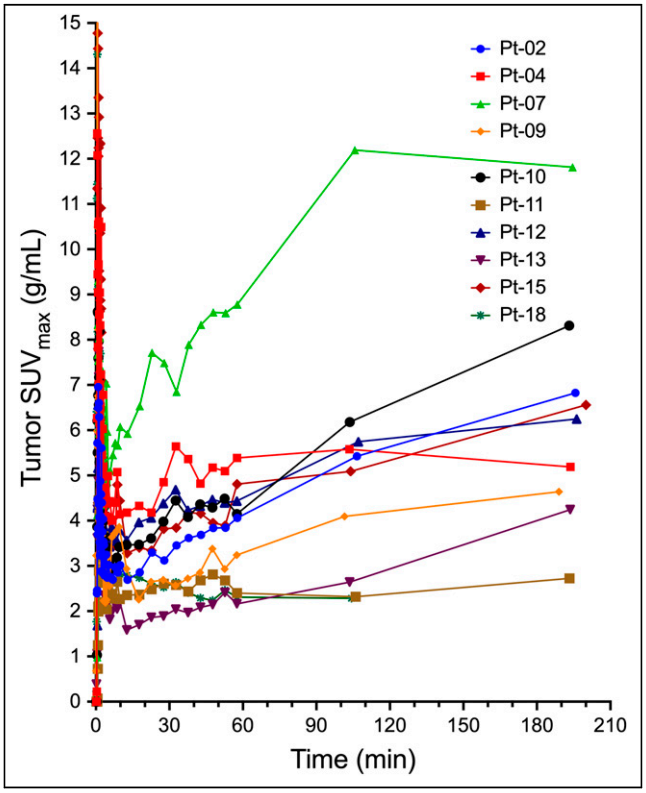

FIGURE 2. ^{18}F-fluorthanatrace index lesion maximum uptake over time for 10 subjects. First 60 min of scanning are from dynamic acquisition, followed by static scan tumor measurements at 110 ± 3 and 199 ± 4 min from 2 subsequent whole-body PET scans. Pt = patient.

pool VOI, related to partial-volume effects and dispersion of tracer from the larger aorta to the iliac arteries (Fig. 4; Supplemental Fig. 2). Plasma–to–whole-blood partitioning was stable throughout imaging, at a ratio of 1.26 ± 0.02 (Supplemental Fig. 3), and between patients, at a ratio of 1.26 ± 0.08 ($n = 16$), and was input into kinetic models as a constant parameter. ^{18}F-fluorthanatrace was metabolized, reaching an average parent percentage of $59\% \pm 10\%$ at 60 min as seen in Figure 5. The resulting population parent fraction curve was used to correct image-derived, individual blood input function for metabolites before kinetic analyses. Metabolites were not included in the model tissue compartments, assuming there was no specific uptake of polar metabolites.

Model-fit Akaike information criterion values (*13*) were 273 ± 24 for the 2CR model, 292 ± 18 for the 2-tissue compartment model with irreversible binding ($k_4 = 0$), and 340 ± 34 for the 1-tissue-compartment model. Example fits for model curves in a representative tumor are provided in Figure 6. In 33 of 39 cases, 2CR outperformed the irreversible model and had lower Akaike information criterion values than the 1-tissue-compartment model in every case. 2CR was therefore used for all subsequent compartmental analysis.

Sensitivity curves for 2CR parameters are provided in Supplemental Figure 4. Blood volume fraction and K_1 exhibited an early influence, followed by K_1/k_2, k_3, and k_4.

When the model parameters V_T and DVR of the fitted tumor SUV_{max} and SUV_{peak} time–activity curves with and without partial-volume correction were compared with the reference standard PARP-1 immunofluorescence, SUV_{peak}-based kinetics

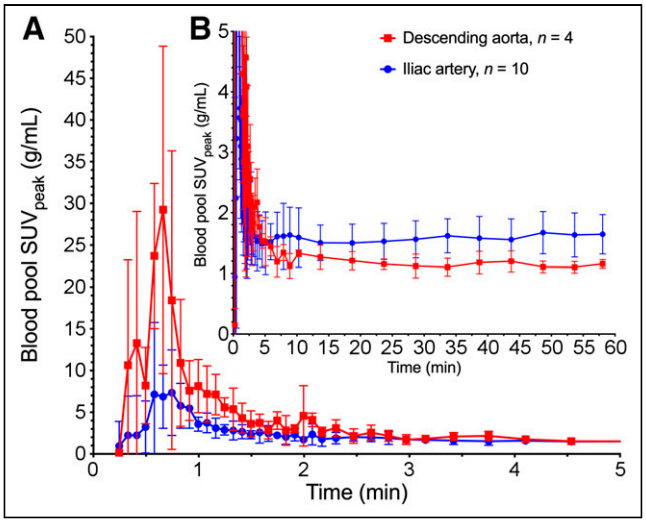

FIGURE 4. Population-averaged blood input functions for descending aorta ($n = 4$) and iliac artery ($n = 10$). Values are mean ± SD. A is from 0 to 5 min after injection and scaled to highlight initial bolus. B is from 0 to 60 min and scaled to show late activity.

correlations were slightly higher; therefore, reported kinetic analyses and simulations used SUV_{peak}.

The Logan reference tissue model with normal muscle was tested as a graphical model of reversible tracer binding that does not require blood sampling. The population k_2' value applied in Logan reference tissue modeling was 0.022 ± 0.022 min^{-1} using positive k_2' values from 7 patients. Logan normal-muscle DVR was 2.2 ± 1.2 ($n = 9$, excluding 1 patient with excessive motion).

Associations between PARP-1 immunofluorescence and tumor uptake, with both static uptake measures and kinetic parameters, were examined. Associations between static measures of tumor uptake and PARP-1 immunofluorescence varied with image timing. SUV_{max} and SUV_{peak} obtained after 55 min (57.5, ~110, and ~119 min) demonstrated statistically significant correlations (Table 1). Partial-volume corrections did not substantially change correlations. Tumor–to–normal-muscle uptake ratios showed similar or slightly decreased associations with PARP-1 expression, as compared with uncorrected SUVs (Table 1). V_T significantly correlated with tissue PARP-1 immunofluorescence for only the 1-h dynamic dataset ($r = 0.76$, $P < 0.05$; Table 2; Fig. 7A). DVR using normal muscle correlated significantly with tissue immunofluorescence ($r = 0.83$, $P < 0.05$, $n = 7$) but not with SUVs at 55–60 min ($r = 0.41$, $P > 0.05$, $n = 10$), until after dynamic acquisition input data were expanded to include measures from 1 or 2 subsequent whole-body scans ($r \geq 0.81$, $P < 0.05$, $n = 10$) (Table 3; Fig. 7B).

Bias and precision estimates from simulations in Table 4 found that Logan DVR had the lowest bias, 6%, and the best precision, 29%.

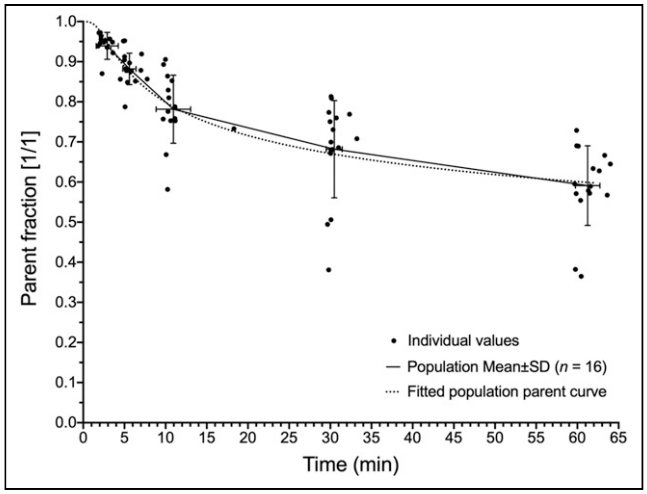

FIGURE 5. ^{18}F-fluorthanatrace population parent fraction curve. Fitting was performed on population mean values, using sigmoidal function. Fitted equation was used for parent fraction corrections for all kinetic modeling blood input curves and was of form $[(1 - t^3/(t^3 + 10^A))]^B + C)/(1 + C)$, where A = 6.504, B = 0.053, and C = 1×10^{-8}, with time after injection, t (in seconds).

DISCUSSION

We studied several PET measures of ^{18}F-fluorthanatrace uptake in ovarian cancer to inform recommendations on metrics and imaging protocols for measuring PARP-1 expression. SUVs and kinetic parameters from dynamic imaging analysis correlated with PARP-1 immunofluorescence pathology measures. However, additional ^{18}F-fluorthanatrace imaging studies of patients participating in PARPi treatment trials will be required to determine whether ^{18}F-fluorthanatrace imaging can serve as a biomarker for response to PARPi therapy.

The superior fit for 2CR to patients' tumors (Fig. 6), superior Akaike information criterion values versus other compartmental models, and high association of reversible model tumor DVR with PARP-1 immunofluorescence support characterization of ^{18}F-fluorthanatrace as having substantial reversible binding in vivo during the imaging session. Makvandi et al. reported a correlation ($r^2 = 0.60$; $n = 10$ lesions) between PARP-1 immunofluorescence and SUV_{max} (*5*). Our corresponding r^2 of 0.64 (or equivalently, $r = 0.80$ in Table 1) is slightly different because of our smaller n (7, only including cancerous lesions within fields of view for the dynamic scans). More clinic-friendly SUV_{max} and SUV_{peak} measures' high correlation with PARP-1 expression supports their use as potentially robust and repeatable metrics for measurement of in vivo PARP-1, with the benefit that SUVs do not require assumptions of reversible or irreversible binding.

Although best described by a reversible model, late uptake of ^{18}F-fluorthanatrace also suggests a degree of irreversible binding, possibly indicative of PARP trapping, as many patients' time–activity curves showed increases in uptake on static scans at 110 and 199 min (Fig. 2). The impact of this variability on the accuracy of kinetic estimates of tracer binding may be complicated by model and input function source selections, as the compartmental model was more sensitive to k_3 and k_4 parameters at later times (Supplemental Fig. 4) when variable uptake of metabolites or issues with the image-derived input functions could interfere with parameter estimates. Without prior dynamic data in humans or preclinically based models to provide physiologic bounds on model fitting, these parameters were highly variable within this patient population. Simulations, Table 4, and Supplemental Figure 5 show the potential for large errors in fitted

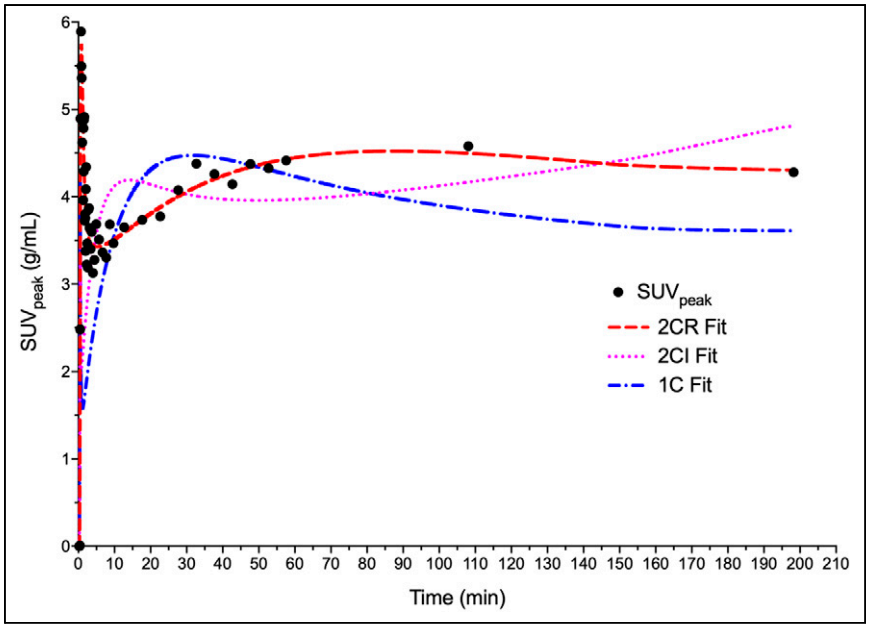

FIGURE 6. Patient 4–modeled time–activity curves with 1-tissue-compartment reversible, 2CR, and 2-tissue compartment irreversible model fits. Akaike information criterion values were 432, 336, and 401 for 1-tissue-compartment reversible, 2CR, and 2-tissue-compartment irreversible models, respectively. 1C = 1-tissue-compartment reversible; 2CI = 2-tissue-compartment irreversible.

2CR V_T. This dataset is not sufficient to rule out an element of irreversible binding of ^{18}F-fluorthanatrace to PARP-1 within the time frame of 200 min after injection.

Although both DVR measures from 0–60 min uptake and SUVs from 55–60 min summed uptake correlated with PARP-1 immunofluorescence tissue assay results, these measures did not correlate with each other. Adding late uptake time points from whole-body scan measures to the dynamic dataset, however, resulted in a significant correlation between DVR and SUVs ($r > 0.81$, $P < 0.01$). Conversely, adding static scans to the dynamic dataset for the 2CR model resulted in decreased correlations between V_T and both PARP-1 immunofluorescence and SUVs (Table 3). DVR's better correlations to SUV when using longer-duration datasets could be due to the fact that the DVR graphical reference technique did not require metabolite corrections. It is also possible that DVRs are better able to account for some nonselective, irreversible parent or metabolite binding at later time points via use of a reference region. Another possibility is the existence of an inflection point in the binding characteristics that is not captured with the gap in imaging between 60 and about 110 min, which may impact V_T estimations.

Metabolism, plasma–to–whole-blood partitioning, and plasma protein binding of ^{18}F-fluorthanatrace were similar within this population, supporting use of averaged population values and functions for kinetic analyses (Fig. 5; Supplemental Fig. 3). Our reported ^{18}F-fluorthanatrace plasma–to–whole-blood partitioning ratio of 1.26 in Supplemental Figure 3 was similar to a ratio of 1.28 (reported as a 0.781 blood-to-plasma ratio) for another rucaparib analog radiotracer, ^{14}C-rucaparib, in a cohort of 6 patients with confirmed advanced solid tumor (*15*). This ^{14}C-rucaparib study (*15*) also used mass spectrometry to determine that 64% ± 13.7% of the labeled components was the parent radiotracer in pooled plasma samples from 1 to 24 h after injection, which was similar to our reported average parent ^{18}F-fluorthanatrace percentage of 59% ± 10% at 1 h. We have not identified these metabolites or their binding properties, except that they are more polar than ^{18}F-fluorthanatrace, similarly to rucaparib metabolites, which are carboxylated at the n-methyl substituent.

Individual image-derived blood input curves were influenced by VOI positioning, suggesting that partial-volume effects may influence our blood pool measurements in the lower torso. This is most apparent in later time points, when the blood pool approaches the

TABLE 1
Correlations Between ^{18}F-Fluorthanatrace SUVs (g/mL) and Unitless SUV Ratios at Different Mid-Bin Times Against PARP-1 Immunofluorescence (n = 7)

	PARP-1 immunofluorescence versus …			
Parameter	32.5 min*	57.5 min*	110 ± 3 min	199 ± 4 min
SUV$_{max}$	0.656	0.796†	0.800†	0.819†
SUV$_{peak}$	0.686	0.787†	0.855†	0.825†
PVC SUV$_{max}$	0.657	0.795†	0.799†	0.818†
PVC SUV$_{peak}$	0.684	0.786†	0.854†	0.823†
SUV$_{max}$/NM	0.445	0.696	0.741	0.706
SUV$_{peak}$/NM	0.512	0.707	0.808†	0.734
PVC SUV$_{max}$/NM	0.454	0.700	0.318	0.531
PVC SUV$_{peak}$/NM	0.515	0.710	0.808†	0.737

*Duration of dynamic frame was 5 min.
†$P < 0.05$.
PVC = partial-volume correction; NM = normal-muscle reference tissue.

TABLE 2
Kinetic Measures from Different Total Duration Input Data Correlations with PARP-1 Immunofluorescence

	PARP-1 immunofluorescence versus …			
Parameter	0–30 min	0–60 min	0–60 + 110 min	0–60 + 110 + 199 min
2CR* V_T (mL/cm^3)	0.415	0.758†	0.407	0.555
Logan NM DVR‡	—	0.825†	0.869†	0.822†

*$k_4 > 0$.
†$P < 0.05$.
‡Graphical methods not performed for 0- to 30-min dataset.
NM = normal-muscle reference tissue.

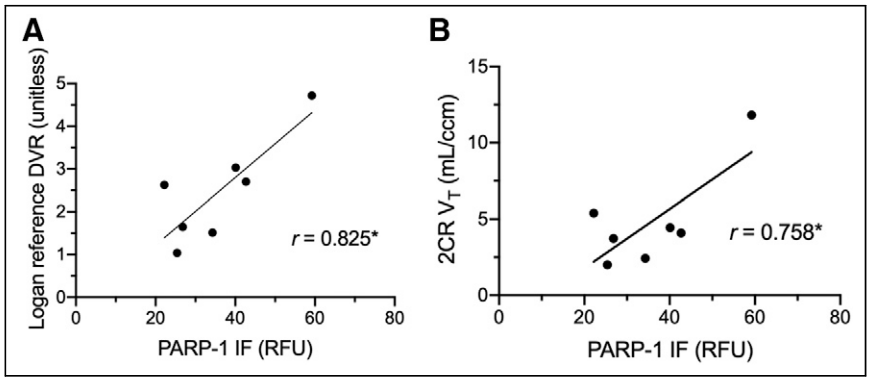

FIGURE 7. Correlation plots between kinetic parameters and PARP-1 immunofluoresence ($n = 7$) in relative fluorescence units (RFU) for Logan reference tissue DVR (A) and 2CR V_T (B). *$P < 0.05$.

activity level of the surrounding tissue and remains above the sampled blood activity (Figs. 3 and 4). Decreased adjacent background activity (spillover) for VOIs in the descending aorta, as compared with VOIs in the iliac arteries, potentially biased measured activity based on differences in the arterial internal diameters. A reduced artery size contributes to increased partial-volume effects, and the 1-cm^3, or 12.4-mm diameter, peak VOIs used for calculating blood activity are above the luminal diameter of the common iliac artery, reported to be 8.8 ± 1.2 mm in women (*16*), and thus more impacted than the larger descending aorta at 13.7 ± 1.9 to 16.6 ± 3.0 mm. The full-width-at-half-maximum resolution of the Ingenuity PET scanner, 4.8 mm (*7*), also limits the ability to use significantly smaller VOIs within small vessels. Using venous blood sampling instead of arterial sampling also limits our ability to verify the arterial blood input function extracted from image blood pools.

Variable levels of background uptake in surrounding tissue support use of background corrections to quantitate ^{18}F-fluorthanatrace uptake. In this study of ovarian cancer, however, partial-volume corrections had little impact on correlations with tissue PARP-1 expression, in contrast to work in breast cancer imaging of ^{18}F-fluorthanatrace uptake (*6*), potentially because of very low levels of background uptake in breast tissue in comparison to higher background uptake in muscle surrounding most ovarian lesions. Partial-volume correction of tumor–to–normal-muscle ratios similarly did not have a substantial effect on correlations with PARP-1 immunofluorescence (Table 1).

We found somewhat variable tumor kinetics late after tracer injection, potentially resulting from the variable trapping of the PARPi analog, ^{18}F-fluorthanatrace, or tissue uptake of metabolites, which account for 30%–50% of circulating blood radioactivity at 60 min. This concern and the good correlation between the 57.5-min ^{18}F-fluorthanatrace SUV_{max} and SUV_{peak} measures with PARP-1 immunofluorescence tissue assay results support a recommendation for imaging at 60 min after injection for static uptake measures. To better inform image quantification and kinetic analysis methods, additional studies with longer dynamic acquisitions of at least 90 min, with arterial blood sampling and a higher percentage of tumors receiving ex vivo assays of PARP-1 expression, would be helpful. However, it may prove difficult to recruit sufficient cancer patients who could tolerate longer imaging times and accept more invasive arterial blood sampling. Preclinical experiments to assess the degree to which ^{18}F-fluorthanatrace binding within cells is reversible during the first 2 h of ^{18}F-fluorthanatrace uptake would inform future selection of kinetic analysis techniques and possibly the ideal postinjection time range for static SUV measures of tumor uptake.

TABLE 3
Kinetic Measure Correlations with SUV_{peak} ($n = 10$)

Parameter	57.5 min SUV_{peak}	110 ± 3 min SUV_{peak}	199 ± 4 min SUV_{peak}
2CR* V_T (0–60 min)	0.929†	0.974†	0.940†
2CR* V_T (0–60 + 110 min)	0.082	0.259	0.365
2CR* V_T (0–60 + 110 + 199 min)	0.548	0.722†	0.781†
Logan NM DVR (0–60 min)	0.410	0.265	0.083
Logan NM DVR (0–60 + 110 min)	0.879†	0.976†	0.969†
Logan NM DVR (0–60 + 110 + 199 min)	0.806†	0.915†	0.974†

*$k_4 > 0$.
†$P < 0.05$.
NM = normal-muscle reference tissue.

TABLE 4
Estimates of Kinetic Model Parameter Bias and Precision

Parameter	Bias	Precision
2CR V_T (mL/cm^3)	250%	635%
2CR K_1 (mL/cm^3/min)	−8%	54%
Logan DVR (unitless)	6%	29%

CONCLUSION

Pharmacokinetics of ovarian cancer uptake of ^{18}F-fluorthanatrace suggest that SUVs from whole-body PET scans acquired 60 min after injection are a robust metric for noninvasively quantifying PARP-1 expression in vivo. Although the Logan normal-muscle reference tissue model is a promising kinetic analysis technique for quantitating ^{18}F-fluorthanatrace uptake, there is not yet sufficient evidence that kinetic estimates or tumor–to–normal-muscle SUV ratios represent substantial enough improvements over more clinic-friendly SUV_{max} or SUV_{peak} tumor measures to justify dynamic scanning for larger-scale trials of ^{18}F-fluorthanatrace PET. More preclinical and human ^{18}F-fluorthanatrace studies would be valuable to elucidate underlying reversible and irreversible ^{18}F-fluorthanatrace binding mechanisms and guide future ^{18}F-fluorthanatrace studies, especially in the study of PARPi dosing and pharmacodynamics and utility as a biomarker.

DISCLOSURE

Robert Mach and David Mankoff (spouse) declare financial conflicts of interest related to ownership in Trevarx Biomedical, Inc., which holds a license for ^{18}F-fluorthanatrace. Erin Schubert and Robert Doot (spouse) have been paid consultants for Trevarx Biomedical, Inc. Lilie Lin has received funds from Astrazenca for travel to meetings and to support an investigator-initiated clinical trial of immunotherapy combined with radiotherapy. This research was supported by the USA National Cancer Institute (P30CA016520), the National Institute on Drug Abuse (K01DA040023 [Robert Doot]), and the National Center for Advancing Translational Sciences (KL2TR001879 [Austin Pantel] and UL1TR000003) of the National Institutes of Health and by the Kaleidoscope of Hope Foundation, Marsha Rivkin Foundation, University of Pennsylvania (Penn) Institute for Translational Medicine and Therapeutics, and Penn Radiology Department. Lilie Lin is supported by the Kaleidoscope of Hope Foundation and the Marsha Rivkin Foundation. This research was also sponsored by the National Center for Research Resources. No other potential conflict of interest relevant to this article was reported.

ACKNOWLEDGMENTS

We thank Elizabeth S. McDonald for helpful discussions on ^{18}F-fluorthanatrace uptake in breast cancer, Regan Sheffer for protocol development and data collection, Jenny Cai and Matthew A. Fillare for research coordination, Kuiying Xu for synthesis of radiotracer precursors, Chia-Ju Hsieh for help in blood data collection, the University of Pennsylvania cyclotron facility for radiotracer manufacture, and the Nuclear Medicine–Advanced Image Analysis Laboratory for providing workstations and software used for image analyses.

KEY POINTS

QUESTION: Can characterization of the pharmacokinetics of ovarian cancer uptake of ^{18}F-fluorthanatrace inform selection of uptake quantitation methods and postinjection timing of PET acquisitions?

PERTINENT FINDINGS: Prospective clinical trial of human ovarian cancer patients found SUV and DVR quantitation of ^{18}F-fluorthanatrace tumor uptake to be significantly correlated with PARP-1 expression.

IMPLICATIONS FOR PATIENT CARE: ^{18}F-fluorthanatrace scans may one day select patients likely to benefit from PARPi therapy and serve as a tool to monitor response.

REFERENCES

1. Franzese E, Centonze S, Diana A, et al. PARP inhibitors in ovarian cancer. *Cancer Treat Rev.* 2019;73:1–9.
2. Ambur Sankaranarayanan R, Kossatz S, Weber W, Beheshti M, Morgenroth A, Mottaghy FM. Advancements in PARP1 targeted nuclear imaging and theranostic probes. *J Clin Med.* 2020;9:2130.
3. Zhou D, Chu W, Xu J, et al. Synthesis, [^{18}F] radiolabeling, and evaluation of poly (ADP-ribose) polymerase-1 (PARP-1) inhibitors for in vivo imaging of PARP-1 using positron emission tomography. *Bioorg Med Chem.* 2014;22:1700–1707.
4. Michel LS, Dyroff S, Brooks FJ, et al. PET of poly (ADP-ribose) polymerase activity in cancer: preclinical assessment and first in-human studies. *Radiology.* 2017;282:453–463.
5. Makvandi M, Pantel A, Schwartz L, et al. A PET imaging agent for evaluating PARP-1 expression in ovarian cancer. *J Clin Invest.* 2018;128:2116–2126.
6. McDonald ES, Doot RK, Pantel AR, et al. Positron emission tomography imaging of poly–(adenosine diphosphate–ribose) polymerase 1 expression in breast cancer: a nonrandomized clinical trial. *JAMA Oncol.* 2020;6:921–923.
7. Kolthammer JA, Su K-H, Grover A, Narayanan M, Jordan DW, Muzic RF. Performance evaluation of the Ingenuity TF PET/CT scanner with a focus on high count-rate conditions. *Phys Med Biol.* 2014;59:3843–3859.
8. Wahl RL, Jacene H, Kasamon Y, Lodge MA. From RECIST to PERCIST: evolving considerations for PET response criteria in solid tumors. *J Nucl Med.* 2009;50(suppl 1):122S–150S.
9. Peterson LM, Mankoff DA, Lawton T, et al. Quantitative imaging of estrogen receptor expression in breast cancer with PET and ^{18}F-fluoroestradiol. *J Nucl Med.* 2008;49:367–374.
10. Thomassin-Naggara I, Balvay D, Aubert E, et al. Quantitative dynamic contrast-enhanced MR imaging analysis of complex adnexal masses: a preliminary study. *Eur Radiol.* 2012;22:738–745.
11. Logan J, Fowler JS, Volkow ND, Wang GJ, Ding YS, Alexoff DL. Distribution volume ratios without blood sampling from graphical analysis of PET data. *J Cereb Blood Flow Metab.* 1996;16:834–840.
12. Ichise M, Liow JS, Lu JQ, et al. Linearized reference tissue parametric imaging methods: application to [^{11}C]DASB positron emission tomography studies of the serotonin transporter in human brain. *J Cereb Blood Flow Metab.* 2003;23:1096–1112.
13. Akaike H. A new look at the statistical model identification. *IEEE Trans Automat Contr.* 1974;19:716–723.
14. Viswanath V, Zhou R, Lee H, et al. Kinetic modeling of 18F-(2S,4R)4-fluoroglutamine in mouse models of breast cancer to estimate glutamine pool size as an indicator of tumor glutamine metabolism. *J Nucl Med.* 2021;62:1154–1162.
15. Liao M, Watkins S, Nash E, et al. Evaluation of absorption, distribution, metabolism, and excretion of [^{14}C]-rucaparib, a poly(ADP-ribose) polymerase inhibitor, in patients with advanced solid tumors. *Invest New Drugs.* 2020;38:765–775.
16. Pedersen OM, Aslaksen A, Vik-Mo H. Ultrasound measurement of the luminal diameter of the abdominal aorta and iliac arteries in patients without vascular disease. *J Vasc Surg.* 1993;17:596–601.